UNIVERSITÁ DEGLI STUDI DI NAPOLI FEDERICO II

DIPARTIMENTO DI INGEGNERIA CHIMICA, DEI MATERIALI E DELLA PRODUZIONE INDUSTRIALE

TESI DI DOTTORATO
IN
INGEGNERIA DEI MATERIALI E DELLE STRUTTURE
XXVII CICLO

BIODEGRADABLE PLA COMPOSITES WITH DIFFERENT FILLERS FOR FOOD PACKAGING APPLICATION

RELATORE

Dott.^{ssa} VERONICA AMBROGI

CANDIDATA

ANTONELLA MARRA

CORRELATORE

Dott.^{ssa} DONATELLA DURACCIO

Anno Accademico 2014/2015

The most beautiful thing we can experience is the mysterious.
It is the source of all true art and science.

Albert Einstein

Abstract

The food packaging initially born as a "container" of food for the sale of quantities defined in adequate conditions of hygiene, then had to perform the function of "protection" of the food in respect of environment. Today, in fact, the most important function of the packaging, when it comes to preservation technology, is to prevent deterioration of the food, to extend the duration of use of a food and to maintain and /or to increase its quality and integrity. So the main purpose of food packaging is to protect food from bacterial and chemical contamination and, where necessary, from oxygen, water vapour and light keeping the product fresh until use.

The aim of this work is, therefore, to develop new film based on PLA for applications in the food packaging with improved properties such as barrier properties, mechanical, UV properties, antibacterial activity using TiO_2 nanoparticles (modified by plasma treatment, and not modified), micro-particles of ZnO (obtained by a process of spray pyrolysis) and nanoparticles of MMT (modified by dimethyl dihydrogenated tallow ammonium). In a first step structural and morphological characterizations were performed, and then a particular study was made on the degradation of PLA composites. The incorporation of particles is an effective tool to control the degradation process in various media, so it was evaluated the UV, hydrolytic, enzymatic and thermal degradation of the PLA with the addition of different fillers (TiO_2 , ZnO and MMT). In conclusion, the results are surely satisfactory because it is found that biodegradable PLA based composites can be used for food packaging application.

CONTENTS

CHAPTER 2-MORPHOLOGY AND STRUCTURE…….45

INTRODUCTION

The food packaging sector is extremely important for the development of world society and it is constantly expanding. It must continually respond to new and urgent demands of the market and try to solve logistical problems and storage of food products in the respect of environment, energy resources and human health. The food packaging initially born as a "container" of food for the sale of quantities defined in adequate conditions of hygiene, then had to perform the function of "protection" of the food in respect of environment. Today, in fact, the most important function of the packaging, when it comes to preservation technology, is to prevent deterioration of the food, to extend the duration of use of a food and to maintain and /or to increase its quality and integrity. So the main purpose of food packaging is to protect food from bacterial and chemical contamination and, where necessary, from oxygen, water vapour and light [1] keeping the product fresh until use.

In recent decades, the use of polymers as materials for food packaging has increased tremendously due to the many advantages that they have over other traditional materials, such as glass and tin [2-4]. The overall market for polymers, whose production has increased from 5 million tons in 1950 to 100 million tons in 2011, is covered by 42% from the packaging (Figure 1).
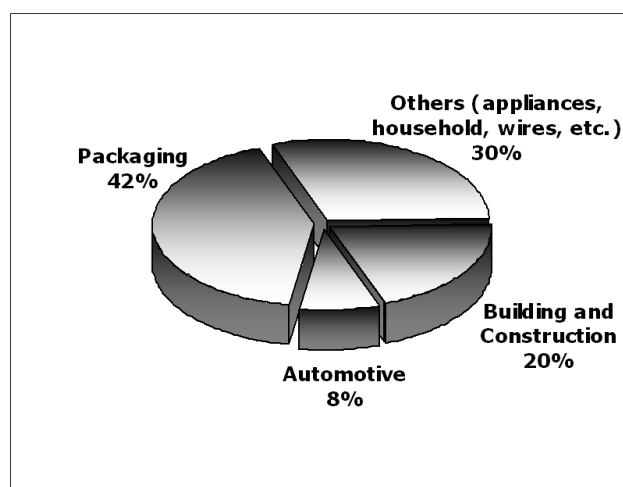
Figure 1. *Pie chart showing the application fields of polymers*

Thanks to plastic, a wide range of products and drinks, can be transported over long distances and stored safely, without compromising the quality and reducing product loss. Plastics enable the production of both rigid and flexible packaging, maintain their characteristics even for very long periods and possess generally satisfactory barrier properties, which reduce the penetration of gas and help prevent the loss of the organoleptic characteristics of food. A great advantage of the plastic lies in the possibility to use a wide range of materials of different compositions and capable of providing the most convenient design according to the specific needs required by each product.

Today, polymers and materials used for food packaging consist of a variety of petrochemical-based polymers, metals, glass, paper, and board, or combinations hereof. The durability and degradability of packaging materials are two contradictory subjects; the 1st is desirable for packaging stability and protection for its contents during shelf life and the 2nd for its rapid degradation in the environment [5,6].

Advantages of petrochemical-based polymers, which encouraged industries to use them, are: (a) low cost and high-speed production; (b) high mechanical performance; (c) good barrier properties; and (d) good heat sealability. On the other hand, several disadvantages include: (a) declining oil and gas resources; (b) increasing oil and gas prices during recent decades; (c) environmental concerns for their degradation or incineration and global warming; (d) uneconomical costs and cross-contaminations in their recycling; and (e) consumer toxicity risks about their monomers or oligomers migrating to edible materials [7-10].

Mechanical recycling (segregated plastics, mixed plastics), biological recycling (sewage, compost, soil), and energy recovery (incineration, pyrolysis) are three alternative ways for plastics waste management, with

each having some advantages and disadvantages as to economical, processing, and technological aspects [11].

The above-mentioned concerns are negligible for biopolymers concerning the biodegradation process that takes place in nature. Biodegradation is defined as the degradation of a polymer in natural environments that includes changes in chemical structure, loss of mechanical and structural properties, and finally, changing into other compounds like water, carbon dioxide, minerals, and intermediate products like biomass and humid materials. The natural environments contain chemical, biological, and physical forces with impinging factors like temperature, humidity, pH, O_2 presence, and so on, which determine the rate and products of the biodegradation process [12].

Biopolymers are produced from natural resources and crude oil. Four categories of biopolymers are recognized: (a) extracted directly from natural raw materials, such as polysaccharides like starch and cellulose; proteins like gelatin, casein, and silk; and marine prokaryotes; (b) produced by chemical synthesis from bio-derived monomers such as poly(lactic acid) (PLA), see Figure 2; (c) produced by microorganisms or genetically modified bacteria such as polyhydroxyalkanoates (PHA), polyhydroxybutyrate (PHB), poly hydroxyl-valerate (PHV), bacterial cellulose, xanthan, and pullan; and (d) produced from crude oil like aliphatic and aromatic polyesters, polyvinyl alcohol, and modified polyolefins, which are sensitive to temperature and light [13,14].

PLA was discovered in 1932 by Carothers (at DuPont). He was only able to produce a low molecular weight PLA by heating lactic acid under vacuum while removing the condensed water. The problem at that time was to increase the molecular weight of the products; and, finally, by ring-opening polymerization of the lactide, high-molecular weight PLA was synthesized. PLA was first used in combination with polyglycolic acid (PGA) as suture material and sold under the name Vicryl in the U.S.A. in 1974 [15].
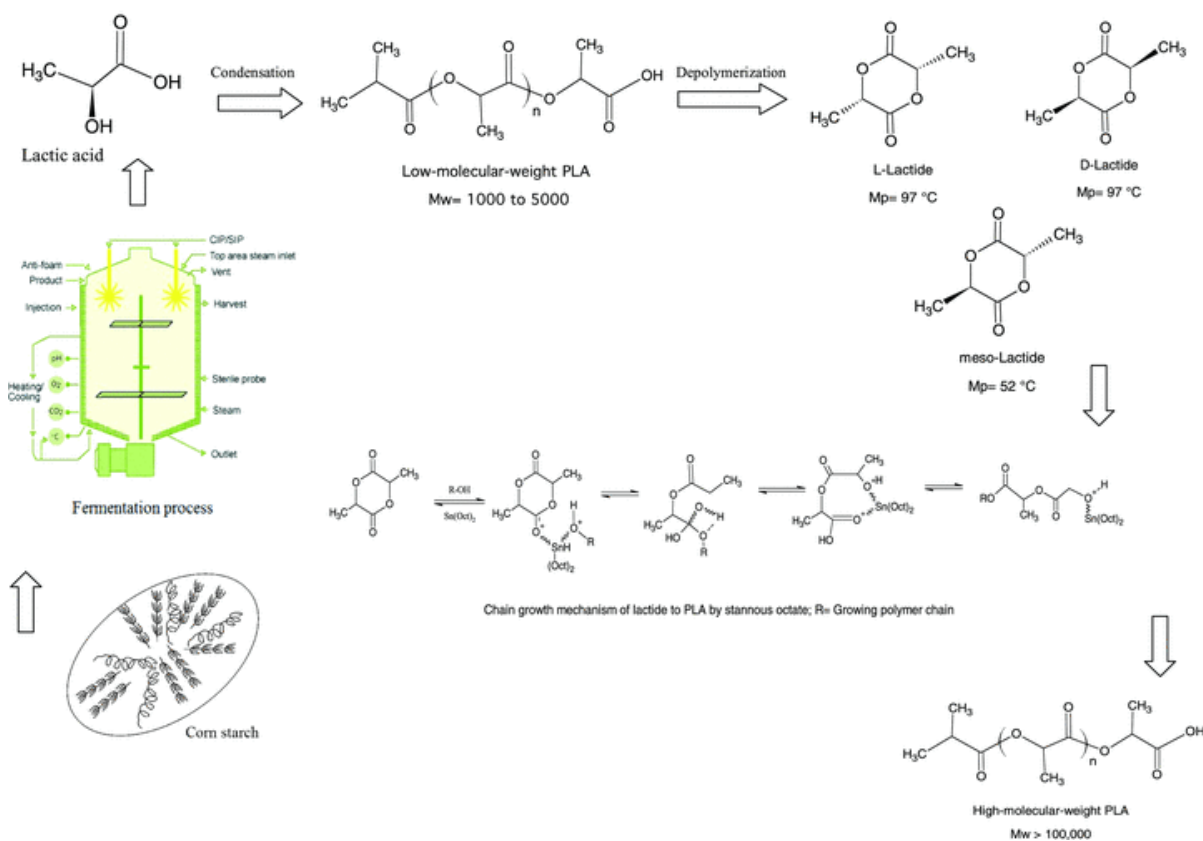
Figure 2. *PLA production steps by ring-opening polymerization using stannous octoate as an initiator[22]*

In comparison to other biopolymers, the production of PLA has numerous advantages including: (a) production of the lactide monomer from lactic acid, which is produced by fermentation of a renewable agricultural source corn; (b) fixation of significant quantities of carbon dioxide via corn (maize) production by the corn plant; (c) significant energy savings; (d) the ability to recycle back to lactic acid by hydrolysis or alcoholysis; (e) the capability of producing hybrid paper-plastic packaging that is compostable; (f) reduction of landfill volumes; (g) improvement of the agricultural economy; and (h) the all-important ability to tailor physical properties through material modifications [16].

Briefly, PLA is based on agricultural (crop growing), biological (fermentation), and chemical (polymerization) sciences and technologies. It

is classified as generally recognized as safe (GRAS) by the United State Food and Drug Administration (FDA) and is safe for all food packaging applications [17,18].

 The continuous questions and demanding food market demand to vary the intrinsic and technological properties of processing, to increase the functionality of packaging improving technical features such as weldability, printability, mechanical and barrier properties. In particular, the industries also tend to produce very thin films, in order to reduce the environmental impact in the disposal of used packaging both energy consumption and thus the costs. The research is oriented to develop new composite materials to help avoid in food development of rancidity, colour loss or change, loss of nutrients, dehydration, microbial growth, gas production, development of odours and senescence. Nanotechnology has potential applications in all aspects of food chain including food processing, food quality monitoring, food packaging and storage [19,20]. Major areas of food industry which could benefit from nanotechnology are [20] development of new functional materials for food packaging, [21] microscale and nanoscale processing, [22] product development and [23] methods and instrumentation design for improved food safety and biosecurity [21]. Application of nanotechnology in food packaging is considered highly promising since this technology could improve safety and quality of food while reducing the use of valuable raw materials and the generation of packaging waste. Nanotechnology is applicable in food packaging to improve packaging performances such as gas, moisture, UV and volatile barriers, mechanical strength, heat resistance and flame retardancy and its weight [22,23]. Nanotechnology can provide shelf life extension via active packaging, product condition monitoring through intelligent packaging, and delivery and controlled release of nutraceuticals. Barrier properties, mechanical and oxidation stability and biodegradability of conventional polymer materials could be improved by nanotechnology.

Poor barrier and mechanical properties of biodegradable films could be improved by using nanoparticles so that the use of these materials in food industry could be expanded. The use of biodegradable nanocomposites will help to reduce packaging waste while extending shelf life of processed foods. Bioactive compounds nanoencapsulated into the packaging are a promising approach due to controlled release of these compounds into the food product. Another potential application of nanotechnology in smart packaging is the use of nanosensors embedded in the packaging to monitor product condition, to detect food spoilage and to alert the consumer when food is spoiled [24,25].

The research is oriented to materials with reduced permeability, so as the literature [26-28] shows, the dispersion of the high aspect ratio nanoclay in the polymer matrix provides remarkable improvements on gas barrier (and other properties like mechanical, fire retardant, rheological, and optical properties), especially at low clay loading levels (as low as 1 wt. %) in comparison with more conventional microcomposites (30 wt. % of fillers).

The research is also oriented to the formulation of PLA matrix composites with antibacterial properties [29-33]. It has been shown that the use of active agents incorporated in the polymeric material for packaging enables significantly increasing the shelf-life of the packaged product (life duration of a foodstuff before its consumption), going to act on those mechanisms of degradation that cause the deterioration by reducing the speed of growth of microorganisms [34,35]. The antibacterial activity of a polymer is usually obtained by adding organic compounds or metal particles. Particles of metal, metal oxides (size sub-micrometric and / or nanometric) and carbon nanotubes are the most used particles to develop antimicrobial activity [4]. Silver particles are already found in many commercial products. In literature it is reported that Ag exerts antibacterial and fungicidal against about 150 different types of bacteria when the metal particles have nanoscale size [36,37]. Zinc oxide (ZnO), titanium dioxide (TiO_2),

magnesium oxide (MgO) and silicon dioxide (SiO_2) are known to act as antibacterial agents in addition to their ability to block UV radiation and to act as disinfectant agents [38]. Compared to silver, the particles of ZnO and MgO are presented as the best and safest solution for food packaging. As regards the zinc oxide has been observed that it shows an increase of antibacterial activity with the increase of its dimensions [39,40].

On the other hand, the study of degradation of polymer nanocomposites is an extremely important area from the scientific and industrial point of view. Chemical degradation of polymers is an irreversible change and it is a very important phenomenon, which affects the performance of all plastic materials in daily life and leads finally to the loss of functionality [41]. Therefore, the material usefulness depends on its durability in a particular environment in which materials are used or their interaction with environmental factors [42]. The study of durability/degradability of polymers-nanoparticulate systems under environmental conditions will give an insight to their applications as well as limitations.

Photo-oxidative degradation is the process of decomposition of the material by the action of light, which is considered as one of the primary sources of damage of polymeric substrates in ambient conditions [43]. Although a significant scientific activity has been carried out on the photo-oxidation of nanocomposites with classical polymer matrices such as polypropylene, polyethylene, and polycarbonate [44], however the literature is rather scarce with regard to nanobiocomposites. So far, the major part of the research work dealing with nanobiocomposite materials have been focused mainly on the preparation methods as well as the structure/properties relationships, especially the nanodispersion effect of the nanofiller on the functional properties. Other studies regarding the susceptibility of PLA nanocomposites for both hydrolytic and thermal degradation are reported in literature [26,45].

It is important to note that depending on the field of application, there are cases where the acceleration of degradation is desirable, while in other cases, it is required to extend the service life of PLA. As reported in the literature, the effective use of (bio)- degradable polymers relies on the ability to control the onset and time needed for degradation [46,47]. Thus, not only, the challenge is that PLA properties should be kept at the required level during the specific period of utilization but the material should degrade in a rapid and controlled manner afterward. On the other hand, it is generally assumed that PLA hydrolysis in presence of nanofillers is a complex phenomenon depending on their specific morphology, dispersion, relative hydrophilicity, or in some cases, hydrophobicity, catalytic activity, etc [48]. However, by considering the complex effect of nanofillers, it was reported that they can favour or delay the hydrolytic degradation of PLA [49]. The hydrolytic stability of PLA based materials can be tailored to obtain predetermined degradation profiles. As aforementioned, PLA is known to mostly degrade through hydrolytic chain cleavage occurring at the level of the aliphatic ester functions and yielding to low molecular weight residues, i.e. lactic acid and related oligomers, able to biodegrade and ultimately be bioassimilated [47].

Microbial and enzymatic degradation of PLA have recently been studied by many researchers because these types of degradations usually do not need the high temperatures to be accomplished. Williams (1981) [50] was the first to report the degradation for PLLA by proteinase K from *Tritirachium.album.*, afterward many studies were done for finding different enzymes corresponding PLA degradation. Reported enzymes that enable to degrade PLA in different scale include, alkaline protease [51], serine proteases such as subtilisin, trypsin, elastase, and α-chymotrypsin [52], Cutinase-like enzyme [53]. Lipase could hydrolyze low molecular weight PLLA and some copolymers such as PDLLA (poly D,L-lactic acid) and, poly(D-lactid-co-glycolide) but not PDLA (poly D-lactic acid) and

high molecular weight PLLA [54]. Pranamuda and others (2001) [55] found an enzyme from *Amycolatopsis*sp. cultures and named it PLLA depolymerase. The optimum pH and temperature for this enzyme were 6.0 and 37 to 45°C, respectively. PLLA depolymerase can also hydrolyze casein, silk fibroin, succinyl- *p*-nitroanilide, but not PHB and PCL. The enzymatic degradation of aliphatic polyesters by hydrolysis is a 2-step process. The 1st step is adsorption of the enzyme on the surface of the substrate through surface-binding and the 2nd step is hydrolysis of the ester bond [56].

Pranamuda and others (2001) [55] were the first to isolate a PLA-degrading microorganism of *Amycolatopsis*strain from soil environment, which was capable of degrading 60% of the PLA film after 14 d.   Suyama and others (1998) [57] reported that PLA-degrading microorganisms are not widely distributed in the natural environment and, thus, PLA is less susceptible to microbial attack in the natural environment than other synthetic aliphatic polyesters like PHB, PCL, and Poly(butylenes succinate) (PBS). Upon disposal in the environment, PLA is hydrolyzed into low molecular weight oligomers and then mineralized into CO_2 and H_2O by the microorganisms present in the environment.

Microbial degradation of PLA should be studied for packaging of foods containing microorganisms including lactic acid bacteria, and fungi for their probable abilities of PLA degradation. Torres and others (1996) [58] reported the ability of assimilation of lactic acid and racemic oligomer products of PLA for 2 strains of *Fusarium moniliforme* (widely distributed in soil) and on strain of *Penicillium roqueforti* (the main fungus in blue cheese, and can be isolated from soil) [57]. As it is shown, literature proposes many works on PLA enzymatic degradation, but PLA composite enzymatic degradation is not yet deeply studied.

The aim of this work is, therefore, to develop new film based on PLA for applications in the food packaging with improved properties such as barrier

properties, mechanical, UV properties, antibacterial activity using TiO_2 nanoparticles (modified by plasma treatment, and not modified), micro-particles of ZnO (obtained by a process of spray pyrolysis) and nanoparticles of MMT (modified by dimethyl dihydrogenated tallow ammonium). In a first step structural and morphological characterizations were performed, and then a particular study was made on the degradation of PLA composites. The incorporation of particles is an effective tool to control the degradation process in various media [58-59], so it was evaluated the UV, hydrolytic, enzymatic and thermal degradation of the PLA with the addition of different fillers (TiO_2, ZnO and MMT).

REFERENCES

[1] "Food Packaging Technology" Edited by Richard Coles, Derek McDowell and Mark J. Kirwan, Blackwell Publishing, CRC press (2003);

[2] Robinson, S. Breaking the Mould, Chemistry and Industry, SCI Press, London, UK, No. 12, pp. 377–378 . (2001) and http://europe.ilsi.org/publications/Report+Series/pkgfoodbeve3.htm.

[3] Forum Tecnologico sul Polipropilene, MACPLAS 215, 82 Gennaio/Febbraio (2000).

[4] "Food packaging based on polymer nanomaterials" C. Silvestre, D. Duraccio, S. Cimmino, Prog Polym Sci (2011), doi:10.1016/j.progpolymsci.2011.02.003.

[5] (Poly-Lactic Acid: Production, Applications, Nanocomposites, and Release Studies M. Jamshidian, E. A. Tehrany, M. Imran, M. Jacquot and S. Desobry.

[6] *"General characteristics, processability, industrial applications and market evolution of biodegradable polymers."* Bohlaman GM. 2005, *In:* BastioliC*, editor.* Handbook of biodegradable polymers. 1st ed. *Shropshire , U.K. : Rapra Technology Limited. p* 183–218.

[7] "Alternate‑day buprenorphine dosing is preferred to daily dosing by opioid‑dependent humans" L. Amass, W.K. Bickel, J.P. Crean, J. Blake, S.T. Higgins Psychopharmacology. 1998;136(3):217–225.

[8] "Biofibres, biodegradable polymers and biocomposites: an overview" AK. Mohanty, M. Misra, G. Hinric , Macromolecular Materials and Engineering, 1-24.

[9] "Biodegradable polymers for food packaging: a review" Siracusa V, Rocculi P, Romani S, Rosa MD. 2008. Trends Food Sci Technol19:634–43.

[10] " 'Green' polymers" , Scott G. 2000, Polym Degrad Stab 68:1–7.

[11] "Biodegradability of polymers–Mechanisms and evaluation methods" Zee MV. 2005. In: BastioliC, editor. Handbook of biodegradable polymer. 1st ed. Shropshire , U.K. : Rapra Technology Limited. p 1–22.

[12] "Biodegradable polymers " R. Chandra, R. Rustgi (1998) Prog Polym Sci 23:1273–335.

[13] "Classification and comparison of thermal and mechanical properties of commercialized polymers*" International Congress & Trade Show,* Clarinval AM. 2002. *The Industrial Applications of Bioplastics, 2002 February 3–5; York, UK.* Clarinval AM, Halleux J. 2005. Classification of biodegradable polymers. *In:* SmithR*, editor.* Biodegradable polymers for industrial applications. 1st ed. *Boca Raton , FL, USA : CRC Press. p* 3–31.

[14] " Mathematical modeling of the poly(lactic acid) ring-opening polymerization using stannous octoate as a catalyst" R. Mehta , V. Kumar , Upadhyay SN. 2007Polym Plast Technol Eng 46:933–7.

[15] "Thermal and rheological properties of commercial-grade poly(lactic acids)s" JR. Dorgan, H. Lehermeier, M. Mang (2000). J Polym Environ 8:1–9.

[16] "Safety assessment of polylactide (PLA) for use as a food-contact polymer" RE. Conn, JJ. Kolstad, JF. Borzelleca, DS. Dixler, LJ. Filer, BN. LaDu, MW. Pariza (1995). Food Chem Toxicol 33:273–83.

[17] FDA. 2001. *FDA/CFSAN/OPA: Agency response letter: GRAS Notice No. GRN 000065.* FDA. 2002. *Inventory of Effective Food Contact Substance (FCS) Notifications No. 178.*

[18] "Potential Application of Nanomaterials in Food Packaging and Intercaction of Nanomaterials with Food" Z. Ayhan, Ecosustainable Polymer Nanomaterials for Food Packaging, (2013) 10, pp. 253-279

[19] "Nanotechnology for the food and bioprocessing industries", S. Neethirajan and D.S. Jayas Food and Bioprocess Technology, 4 (2011) 39.

[20] "Functional materials in food nanotechnology" P. Weiss, Takhistov and J. McClements, Journal of Food Science, 71 (9) (2006) 107.

[21] "Poly-lactic acid: production, applications, nanocomposites, and release studies" M. Jamshidian, E.A. Tehrany, M. Imran, M. Jacquot and S. Desobry, Comprehensive Reviews in Food Science and Food Safety, 9 (2010) 552.

[22] "Potential applications of nanotechnology in the agro-food sector" M. Garcia, T. Forbe and E. Gonzalez, Ciencia e Technologia de Alimentos, 30(3) (2010) 573.

[23] "Potential applications of nanotechnology in food packaging" Z. Ayhan, 1st international congress on food technology. November 3-6, 2010. Antalya, Turkey.

[24] "Nanocomposites and food packaging" O. Esturk and Z. Ayhan, VI. International packaging congress and exhibition. September 16-18, 2010. Volume 1, s. 215-224. Istanbul, Turkey.

[25] "Photo-Degradation of Poly(Lactic Acid) (PLA)/Organo-Modified Clay Nanocomposites under Natural Weathering Exposure" M. Kaci, A. Benhamida, L. Zaidi, N. Touati and C. Remili Ecosustainable Polymer Nanomaterials for Food Packaging, (2013) 11, pp. 281-312.

[26] M. Alexandre and P. Dubois, Mater. Sci. Eng., 28 (2000) 1.

[27] S. Bourbigot, F. Samyn, T. Turf and S. Duquesne, Polym. Degrad. Stab., 95 (2010) 320.

[28] "Antimicrobial activity of nanocomposites: poly(amide) 6 and low density poly ethylene filled with zinc oxide" G. Droval, I. Arranberri, A. Bilbao, L. German, M. Verelst, J. Dexpert-Ghys e-polymers, no. 128 ISSN 1618-7229 (2008).

[29] "Modelling of Spray Pyrolysis-Why the Synthesized Y2O3 Microparticles hollow?" N. Reuge, B. Caussat, N. Joffin, J. Dexpert-Ghys, M. Verelst, H. Dxpert, AlChE journal 54, 2, 394-405 (2008).

[30] "Synthesis of undoped ZnO nanoparticles by Spray Pyrolysis", C. Rossignol, M. Verelst, J. Dexpert-Ghys, S. Rul Advances in Science and Thecnolgy, 45, 237-241 (2006).

[31] "Elaboration of Boehmite Nano-powders by spray-Pyrolisis", J.M.A. Caiut, J. Dexpert-Ghys, Y. Kihn, M. Veelst, H. Dexpert, S.J.L. Ribeiro, Y. Messaddeq Power Thecnology, 190, 95-98, (2009).

[32] "Large ScaleSynthesis of Zinc Oxide Nanorods by homogeneous Chemical Vapour Deposition and their Characterization", R. Bacsa, Y. Kihn, M. Verelst, J. Dexpert-Ghys, W. Bacsa, P. Serp, Surface & Coating Technology 201, 9200-204 (2007).

[33] Zhou, N.; Liu, Y.; LI,L.; Meng, N.; Huang, Y.; Zhang, J.; Wei, S.; Shen, J. Curr. Appl.Phys., 7, 58 (2007).

[34] Seyfriedsberger, G.; Rametsteine, K., Kern, W. Eur. Polym. J.; 2006, 42, 3383.

[35] "Ion release from antimicrobial polyamide/silver composites" R. Kumar, H. Münstedt Silver Biomaterials 2005;26:2081-8.

[36] "Interaction of silver nitrate with readily identifiable groups: relationship to the antibacterial action of silver ions". SY. Liau, DC. Read, Wj. JR. Pugh, Furr, AD. Russell Lett Appl Microbiol 1997;25:279-83.

[37] "Titanium dioxide photocatalysis" A. Fujishima, TN. Rao, DA. Tryk, J Photochem Photobiol C 2000;1:1-21.

[38] "Antibacterial activity of ZnO nanoparticle suspensions on a broad spectrum of microorganisms" N. Jones, B. Ray, KT. Ranjit, AC. Manna, FEMS Microbiol Lett 2008; 279:71-6.

[39] L. Zaidi, M. Kaci, S. Bruzaud, A. Bourmaud and Y. Grohens, Polym. Degrad. Stab., 95 (2010) 1751.

[40] J. K. Pandey, K. R. Reddy, A. P. Kumar and R. P. Singh, Polym. Degrad. Stab., 88 (2005) 234.

[41] B. Singh and N. Sharma, Polym. Degrad. Stab., 93 (2008) 561.

[42] N. Touati, M. Kaci, S. Bruzaud and Y. Grohens, Polym. Degrad. Stab., 96 (2011) 1064.

[43] H. Tsuji and T. Tsuruno, Polym. Degrad. Stab, 95 (2010) 477.

[44] "Key factors for tuning hydrolytic degradation of polylactide/zinc oxide nanocomposites" S. Benali, S. Aouadi, A.L. Dechief, M. Murariu and P. Dubois,_ W. S. Maney & Son Ltd 2015 DOI 10.1179/2055033214Y.0000000007.

[45] V. Arias, A. Höglund, K. Odelius and A.-C. Albertsson: Biomacromolecules,

2013, 15, (1), 391–402.

[46] S. Sinha Ray, K. Yamada, M. Okamoto, Y. Fujimoto, A. Ogami and K. Ueda: Polymer, 2003, 44, (21), 6633–6646.

[47] E. Kontou, P. Georgiopoulos and M. Niaounakis: Polym. Compos., 2012, 33, (2), 282–294.

[48] "Enzymatic hydrolysis of polylactic acid" DF. Williams, Eng Med (1981). 10:5.

[49] "Degradation of polylactide by commercial proteases" Y. Oda ,A. Yonetsu, T. Urakami, K. Tonomura, J Polym Environ(2000), 8:29–32.

[50] "Hydrolysis of polyesters by serine proteases" HA. Lim,T. Raku,Y. Tokiwa, Biotechnol Lett,(2005), 27:459–64.

[51] "Cutinase-like enzyme from the yeast Cryptococcus sp. strain S-2 hydrolyses polylactic acid and other biodegradable plastics" K. Masaki, NR. Kamini, H. Ikeda, H. Iefuji, Appl Environ Microbiol, (2005) 7:7548–50.

[52] "Synthesis of copoly(D,L-Lactic acid) with relatively low molecular weight and in vitro degradation" H. Fukuzaki, M. Yoshida , M. Asano, M. Kumakura Eur Polym J(1989) 25:1019–26.

[53] "Poly(L-lactide)-degrading enzyme produced by Amycolatopsis sp." H. Pranamuda, A. Tsuchii, Y. Tokiwa Macromol Biosci (2001)1:25–9.

[54] "Biodegradability and biodegradation of poly(lactide)" Y. Tokiwa, BP. Calabia Appl Microbiol Biotechnol (2006) 72:244–51.

[55] "Phylogenetic affiliation of soil bacteria that degrade aliphatic polyesters available commercially as biodegradable plastics" T. Suyama, Y. Tokiwa, P. Ouichanpagdee, T. Kanagawa, Y. Kamagata, Appl Environ Microbiol (1998) 64:5008–11.

[56] "Screening of microorganisms for biodegradation of poly(lactic acid) and lactic acid-containing polymers" A. Torres, SM. Li, S. Roussos, M. Vert, Appl Environ Microbiol(1996) 62:2393–7.

[57] "Progress in Nanocomposite of Biodegradable Polymer" K. Yang, X. Wang, and Y. Wang, J. Ind. Eng. Chem., Vol. 13, No. 4, (2007) 485-500.

[58] "Biodegradable poly(L-lactic acid)/TiO_2 nanocomposites: Thermal properties and degradation" A. Buzarovska and A. Grozdanov, Journal of Applied of Polymer Science, (2012)Vol. 123, 2187-2193.

CHAPTER 1

MATERIALS AND METHODS

1.1 MATERIALS

The materials used in this work are:

i) Polylactic acid (PLA) in pellets;

ii) Titanium dioxide (TiO_2) nanoparticles powder;

iii) Zinc oxide (ZnO) particles powder;

iv) Organically modified montmorillonite powder.

i) The PLA is a commercial product supplied by Nature Works®.

Its molecular characteristics are reported in Table 1.1.

The value of M_n and M_w were determined by the GPC analysis and the value of Tg and Tm were determined by DSC at IPCB-CNR as discussed later.

Table 1.1. *Molecular characteristics of PLA*

Material	PLA 4032D
Producer	NATURE WORKS®
M_n(g/mol)	1.3×10^5
M_w(g/mol)	2.1×10^5
M_w / M_n	1.6
T_m(°C)	160
T_g(°C) (by DSC)	58
Density(g/cm^3)	1.24

ii) Hydrophilic TiO_2 nanoparticles were supplied by Degussa Inc.
The characteristics of the material are reported in Table 1.2.

Table 1.2.*Characteristic of TiO₂ nanoparticles*

Material	TiO₂ P25
Producer	Degussa
Purity	99.5%
Average particle size	25nm
Mineral form	80% anatase and 20% rutile

The Degussa P-25 standard TiO_2 nanoparticles were modified by plasma treatment at University of Texas in Arlington.
A custom built $360^{°}$ rotating plasma reactor, operable under vacuum conditions, was employed to functionalize the surface of pure TiO_2 nanoparticles. A schematic diagram of the apparatus employed is shown in Figure 1.1.1 The reactor details are similar to that described [1]. The plasma was generated using Radio-Frequency (13.56 MHz frequency) power input.

TiO_2 nanoparticles were dried in oven at 120°C under vacuum prior to use. The perfluorohexane monomer employed in the plasma depositions was obtained from Alpha Aesar Chemical Company and had a stated purity of

+98%. Repeated freeze-thaw cycles, accompanied by vacuum pumping were employed to remove dissolved gases in the C6F14 prior to use.

Important steps in the successful surface functionalization of the TiO_2 involved an initial treatment of the particles to a brief, high power O_2 plasma discharge to remove any adsorbed carboneous materials and, simultaneously, activate the surfaces of these crystals. Subsequently, and immediately following the oxygen treatment, the perfluorocarbon monomer was introduced and a high power continuous wave plasma discharge was employed briefly (1 minute) to graft a thin, strongly adherent, amorphous carbon-like layer to the TiO_2 particles. The function of this layer is to overcome the inherent chemical incompatibility between the inorganic particles and the plasma deposited organic films. Subsequently, the RF power input was converted to a pulse operational mode and the plasma duty cycle, i.e. ratio of plasma on to plasma off times, was slowly decreased, thus creating a gradient layered structure in which the fluorine content of the plasma polymer film is slowly increased as the pulsed plasma duty cycle is decreased. The process was terminated at a plasma duty of 10 ms on and 100 ms off and peak power input of 200W. FT-IR and XPS spectra of films separately deposited on flat silicon substrates clearly revealed the increasing F/C ratio of the polymer films as the plasma duty cycle employed was reduced.

The successful surface modification of the TiO_2 nanoparticles is highlight in Figure 1.1.2 In this picture, the spontaneous dispersion of the nanoparticles, before and after plasma treatment, are shown with respect to a two layer liquid mixture consisting of water (bottom layer) and hexane (top layer). The initial addition of untreated TiO_2 particles, which are hydrophilic, clearly disperse selectively in the water layer [vial (A)], to surface energy considerations. In contrast, after the plasma treatment involving deposition of the perfluorocarbon films on the TiO_2 substrates, the nanoparticles exhibit preference for the nonpolar hexane layer [vial (C)

in fig. 1.1.2]. The figure 1.1.2 shows as by this plasma approach it is possible to have an excellent controllability of surface energy modifications. TiO_2 nanoparticles, treated for short time by perfluorocarbon plasma, exhibit an equal preference for the water and hexane layers; as show in vial (B).

360º Rotating Pulsed RF Plasma Reactor
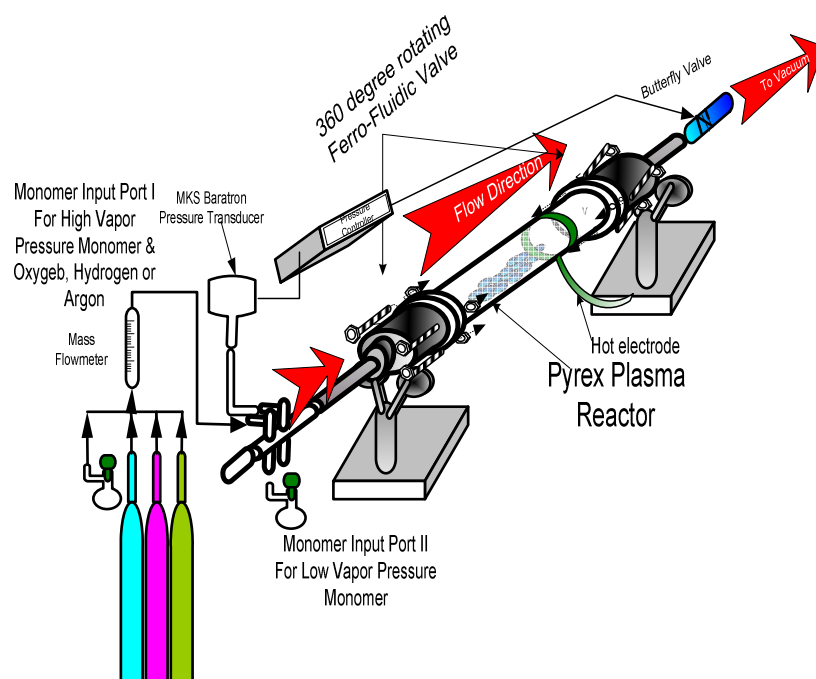
Figure 1.1.1 *A schematic diagram of the rotating plasma reactor system employed to coat the TiO_2 nanoparticles with a fluorocarbon film*

Figure 1.1.2 *The selective dispersion of untreated [vial (A)] and plasma modified [vial (C)] TiO₂ nanoparticles in a two-layer liquid mixture of water (bottom layer) and hexane (top layer). TiO₂ particles treated only for a brief period, and thus only partially fluorinated, are shown in vial (B)*

iii) ZnO particles were synthesized using a preindustrial spray scale pyrolysis platform at the Pylote in Toulouse-France, Figure 1.1.3. This technique provides many advantages compared to other techniques of preparation: the simplicity of the process, high purity of the powders obtained, more uniform chemical composition, narrow size distribution, better regularity in shape and the ability to synthesize multicomponent materials [2-5].The spray is generated by ultrasonic vibrations produced by a piezoelectric material (2.4 MHz) immersed in a solution of zinc acetate and water of appropriate composition [6]. The droplets are collected by a flow of air and transported in a first drying zone (100-120°C) and then in a zone of decomposition-densification in which the temperature can be adjusted up to 1200°C. The gas stream containing solvent vapours, decomposition products and solid particles, arrives in an electrostatic collector from which it is possible to collect the dried particles.

The powders of ZnO are prepared from a solution of zinc acetate ZnO $(CH_3CO_2) \bullet 2H_2O$ in a mixture of deionized water and isopropyl alcohol (in a ratio 2: 3). Few drops of acetic acid are added to the solution to prevent the precipitation of zinc hydroxide. Using the zinc acetate as a precursor of the layers are obtained without contamination of chlorine, the added value of the acetate of zinc is its vapour pressure. The stock solution was vaporized inside of glass substrates, using heated compressed air as a

carrier gas. The glass substrates were placed on a tin bath welded. The bath temperature was kept constant between 252 and 312°C [7] . The production rate was ~100g/h of powders. Their characteristics are reported in Table 1.3.
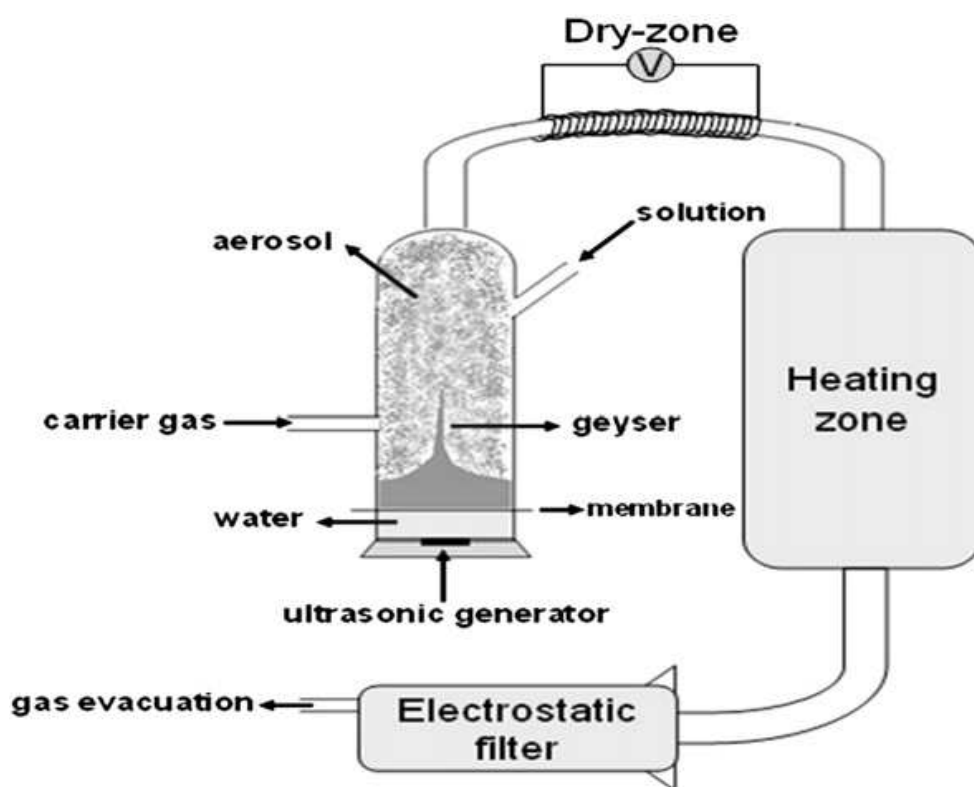
Figure 1.1.3 *Pilot scale Spray Pyrolysis apparatus [8]*

Table 1.3.*Characteristic of ZnO particles*

Material	ZnO
Producer	PYLOTE
Particle size (dry) (nm)	100-500
Purity	100%

iiii) The montmorillonite is a commercial product supplied by Laviosa® (Dellite 67G) modified with a high content of quaternary ammonium salt. The characteristics of the material are reported in Table 1.4.

Table 1.4.*Characteristic of Montmorillonite Dellite 67G nanoparticles*

Material	Montmorillonite (Dellite 67G)
Producer	LAVIOSA®
Particle size (dry) (µm)	7-9 (medium)
Modifier	dimethyl dihydrogenated tallow ammonium

1.2 PREPARATION OF PLA NANOCOMPOSITES AND PLA COMPOSITES.

1.2.1 Preparation of PLA/TiO$_2$ nanocomposites

Before mixing, TiO$_2$ and PLA were dried in an oven for 24h at 65°C under vacuum. PLA was mixed with the powder of TiO$_2$ using a Barbender Plastograph EC mixer. The screw speed was 50 rpm. Components were mixed at 180°C for 15 minutes.

Two formulations were prepared by using both modified and unmodified TiO$_2$ nanoparticles: 2% in wt and 5% in wt. The composition is reported in table 1.5, where mTiO$_2$ stands for the modified TiO$_2$ nanoparticles.

1.2.2 Preparation of PLA/ZnO composites and PLA/MMT nanocomposites

Before mixing, the PLA pellets, ZnO and MMT powders were dried in an oven for 24h at 65°C under vacuum. The composites were prepared by mixing of the components from the melt using a twin-screw extruder.

Masterbatch with fillers (ZnO and MMT) content 20 wt% and PLA content 80 wt% was prepared to improve the dispersion of the fillers within the polymer matrix. Subsequently, the masterbatch was diluted in PLA in

such quantities as to obtain the desired composition (1, 3 and 5% by weight of ZnO and MMT, see table 1.6 and 1.7).

Tables 1.5, 1.6 and 1.7 show the compositions of the mixtures as percentage.

Table 1.5 *PLA/TiO$_2$ compositions*

CODE Sample	PLA (wt%)	TiO$_2$ (wt%)	mTiO$_2$ (wt%)
PLA	100	-	-
PLA/2% TiO$_2$	98	2	-
PLA/2% mTiO$_2$	98	-	2
PLA/5% TiO$_2$	95	5	-
PLA/5% mTiO$_2$	95	-	5

Table 1.6 *PLA/ZnO compositions*

CODE Sample	PLA (wt%)	ZnO (wt %)
PLA	100	-
PLA/1% ZnO	99	1
PLA/3% ZnO	97	3
PLA/5% ZnO	95	5

Table 1.7 *PLA/MMT compositions*

CODE Sample	PLA (wt%)	Montmorillonite (Dellite67G) (wt%)
PLA	100	-
PLA/1% D67G	99	1
PLA/3% D67G	97	3
PLA/5% D67G	95	5

For comparison also the PLA was extruded so that all samples have the same thermal history. The extruder used was a tool Collin ZK 25 (D = 25 mm and L / D = 56). All extruded materials in the form of spaghetti were

cooled in water (figure 1.2.1 A) and then cut into pellets (figure 1.2.1 B). The extruder was substantially constituted by a cylinder resistant to external pressure and by two helical screws that rotate within the cylinder. The first part of the vine is the feed zone - Zone 1 -. The beginning of the screw is located under the loading hopper where the material can be introduced (fig. 1.2.1 C). The screw then pushes the material in the solid state, first, compressing and heating it. A transition zone follows - Zone 2-3 - in which the material melts or softens and is heated to the processing temperature. Finally, there is the exit area - Zone 4-5 - of the screw of in which the pressure reached to the maximum value. Thermocouples are present along the extruder to control the temperature of five different zones.

A

	B
	C
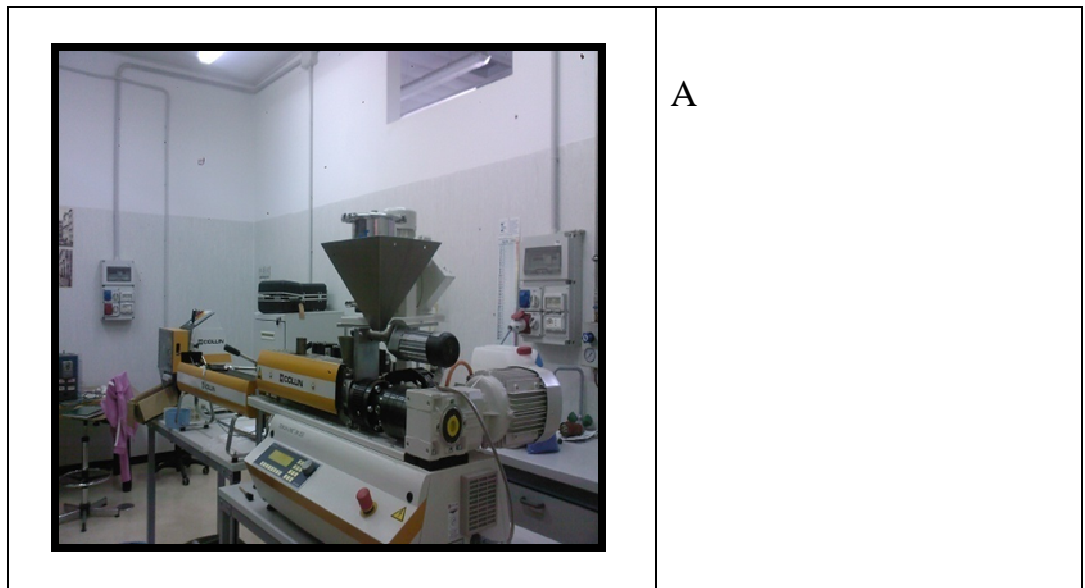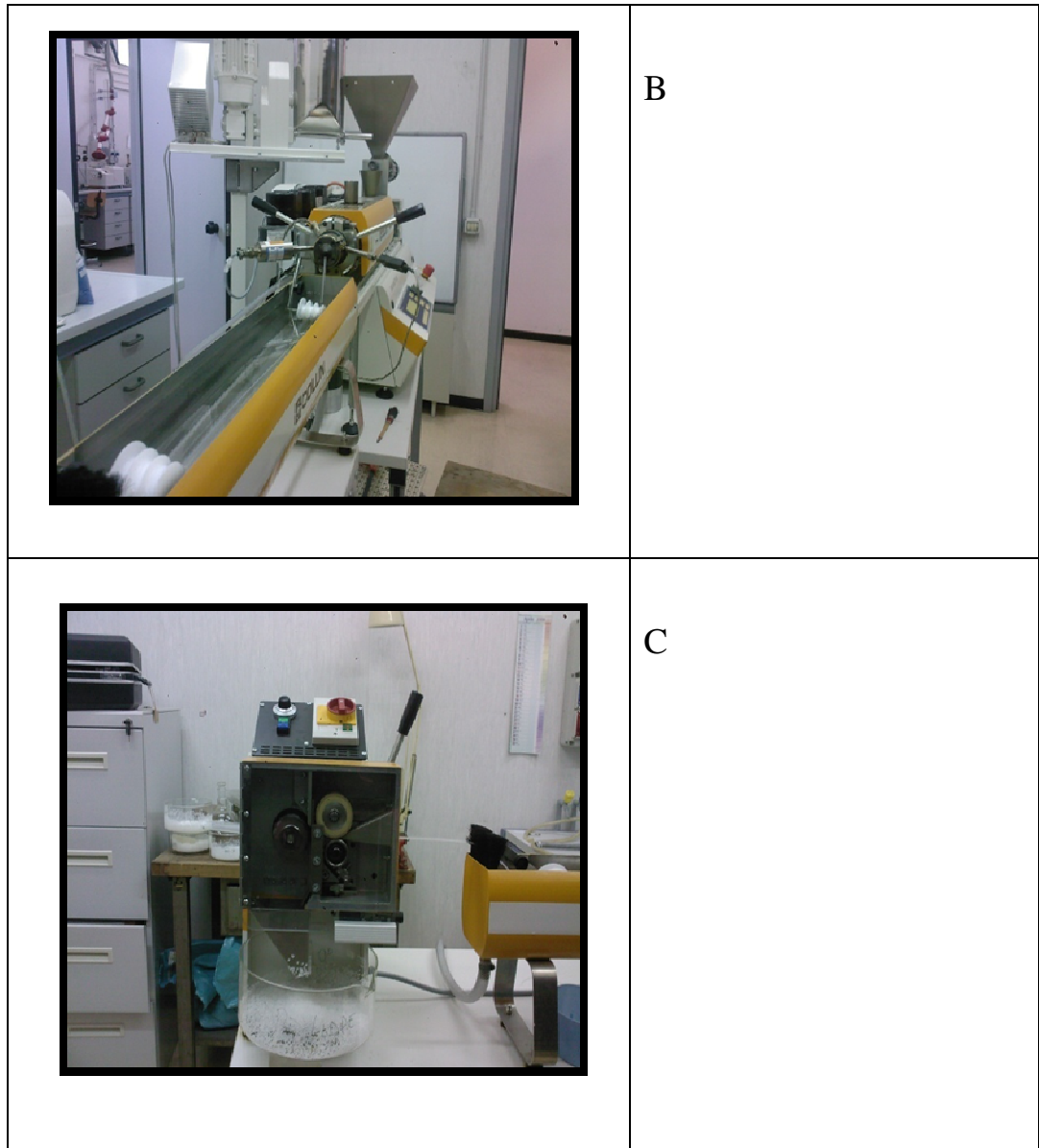
Figura 1.2.1 Extruder: Collin ZK 25 twin screw co-rotating extruder (D = 25 mm, L/D = 56). A = loading hopper; B = Cooling system; C = Pelletisation

The extrusion was conducted using the following temperatures:

Zone 1: T=150°C   Zone 2: T=170°C   Zone 3: T=170°C

Zone 4: T=170°C   Zone 5: T=160°C

The screw speed of the dispenser is 20 rpm while the speed of the extruder screws is 25 rpm.

1.3 PREPARATION OF PLA/TiO$_2$ NANOCOMPOSITE, PLA/ZnO COMPOSITE AND PLA/MMT NANOCOMPOSITE FILMS

1.3.1 Preparation of PLA/TiO$_2$ nanocomposite films

Films of PLA/TiO$_2$ were produced by compression moulding in a press at a temperature of 180°C for about 6minutes,without any additional pressure, to allow the melt of the material. Subsequently the pressure was increased up to 100 bar and kept constant for about 3 minutes. The press is equipped with a cooling system water to bring the system to room temperature in about 5 minutes.

Neat PLA and nanocomposite films had thickness of about 130 μm.

1.3.2 Preparation of PLA/ZnO composite and PLA/MMT nanocomposite films

The films were prepared using a single screw extruder (Figure 1.3.1), whose operation principle is similar to that used for the twin screw extruder. Before the extrusion the pellets of PLA/MMT and PLA/ZnO were again dried in an oven for 24 h at 80°C under vacuum. The single screw extruder has, as terminal, a calender characterized by two counter rotating cylinder that allow the film passing through them still in the plastic state and the third useful to direct the output material until the collecting cylinder. The extruder and the chill roll unit are Collin E 20T and Collin CR 72T, respectively.

The thickness of the film obtained depends on the light between the two counter-rotating cylinders and the speed of rotation of the collecting cylinder, in this case it is 60 μm.

Figura 1.3.1 *Calender: Collin E 20T single screw extruder and the chill roll unit Collin CR 72T*

For test samples, the extrusion was conducted using the following temperatures:

Zone 1: T=160°C   Zone 2: T=170°C   Zone 3: T=180°C

Zone 4: T=170°C   Zone 5: T=180°C

The screw speed of the dispenser was 20 rpm while the speed of the extruder screw was 40 rpm.

1.3.3 Slab preparation for PLA/TiO$_2$ nanocomposites

Slabs were prepared by using a particular procedure to avoid PLA degradation and bubble air in the final product. 20 g of material were put in the oven, under vacuum, at 180°C till the material is melt and cooled at room temperature. The material thus obtained from the oven, was placed in a mould with frame 6x7x0.3 cm, between sheets of Teflon, to allow easier removal of the film from the support. The sheets of Teflon are in turn placed between copper plates and finally between plates of brass. Such a system of plates, is inserted between the plates of a hydraulic press at a temperature of 180°C for about 6 minutes, without any additional pressure,

to allow the fusion of the material. Subsequently the pressure was increased up to 100 bar and kept constant for about 3 minutes. Then the heating power of the press was switched off and the water cooling system was open. The temperature of the mould reached the room temperature in 5 min and finally the slab was removed from the mould.

1.4 TECHNICAL ANALYSIS

The films were characterized using the following techniques:

- Wide angle X-ray diffraction (WAXD)
- Transmission electron microscopy (TEM)
- Attenuated total reflection (ATR) Spectroscopy ATR
- Scanning electron microscopy (SEM)
- Differential scanning calorimetry (DSC)
- Thermogravimetric Analysis (TGA)
- UV-visible spectroscopy

  Moreover the following analysis were carried out:
- mechanical properties
- barrier properties
- antibacterial properties
- degradation properties

1.4.1 X-ray diffraction high-angle (WAXD)

The use of the technique of X-ray diffraction at high angle (WAXD) allows the analysis of the structure of the macromolecules, their spatial arrangement and any polymorphic forms.

Wide-angle X-ray diffraction (WAXD) measurements were conducted by Philips XPW diffractometer (Philips Analytical, Almelo, The Netherlands) with Cu Ka radiation (1.542 Å) filtered by nickel. The scanning rate was

0.02 deg/s, and the scanning angle was from 5 to 50° for all films and from 2 to 10° for pellets.

The analysis was carried out on the films of all samples and, only for the samples PLA/MMT, also on pellets, to verify if the extrusion had induced intercalation or exfoliation of MMT.

Crystallinity degree, Xc, is defined as the ratio between the mass of crystalline material and the total amount of sample. Assuming that the diffracted intensity is proportional to the amount of material that diffracts, and that the scattering of the crystalline phase and the amorphous phase is equal, Xc is equal to the ratio between the intensity of diffraction of crystalline phase and the intensity of diffraction of the whole sample. Therefore the percentage of crystallinity was calculated with the following procedure: a base line was traced between two points selected in such a way that all spectra have a minimum at these points, the amorphous peak was traced arbitrarily conducting a line that joins the two minimum points of the base line with the minimum of the peaks of the crystal. The ratio between the areas under the crystalline peaks and the total area, multiplied by one hundred, represents the crystalline fraction percentage.

1.4.2 Transmission Electron Microscopy (TEM)

The structure of the TiO_2 and MMT powders and the microstructure and dispersion of the particles of MMT within the polymer matrix was determined using a transmission electron microscope (TEM). The transmission electron microscopy is a powerful technique for the characterization of materials at the nanoscale. With the TEM analysis electron beam is passed through a sample of very thin thickness. The use of TEM microstructural analysis allows very high spatial resolution. The observations were carried out by TEM FEI Tecnai Spirit Twin G12 with LaB6 emission source using spot size 1. The images were acquired by Fei Eagle 4000x4000 CCD camera, mounted on the same axis.

PLA/MMT films were embedded in epoxy resin and kept in the hood for 24 hours at a temperature of 60°C. Subsequently they were subjected to ultrasectioning by ultramicrotome LEICA UC6, at room temperature.

The cutting of ultrathin sections was performed by the use of a diamond blade. For the realization of the sections following experimental conditions were used:

Cutting speed: 1.0-1.2 mm/s - nominal thickness between 70 and 90 nm.

Ultra thin sections were then picked up with a perfect loop and placed on copper TEM grids from 400 mesh.

1.4.3 Attenuated total reflection (ATR) Spectroscopy

The attenuated total reflection (ATR) is a sampling technique of infrared spectroscopy. The analysis in internal reflection is based on internal reflection at a glass with high refractive index (usually diamond, ZnSe or GeSe) placed in direct contact with the sample. The radiation passes through the glass and is refracted; then it strikes the sample several times and penetrates for about 2 μm and is reflected, recrossing the crystal and reach the detector.

Film samples were analyzed by using a Perkin Elmer Spectrum 100 with resolution of 4 cm^{-1}, in a range of wave number from 4000 to 400 cm^{-1} and with a scan number of 8.

1.4.4 Scanning Electron Microscope (SEM)

The structure of ZnO powder and the morphology of the fractured surfaces of the PLA/TiO$_2$ and PLA/ZnO films were determined by the scanning electron microscope (SEM). The model used is a Fei Quanta 200 SEM Feg. The scanning electron microscope is an instrument characterized by a high resolving power, of the order of 200-300 Å, and provides three-dimensional images of the surfaces observed. The samples were then fixed on a support and metallized with a gold-palladium alloy, to ensure better

conductivity and prevent the formation of electrostatic charges. This survey was carried out on the samples before and after irradiation with electron beam for both doses, to see what may have led to changes in the surface treatment.

1.4.5 Analysis calorimetry (DSC)

The DSC allows to measure the amount of heat involved during phase transitions. occurring with absorption or emission of energy.

The analysis was performed using a calorimeter Mettler DSC-822.

The thermoanalytical technique measure the difference of the heat required to increase the temperature of a sample pan compared to a reference pan, as a function of temperature, when the sample and the reference pans are submitted to the same heating or cooling rate. The sample pan and reference pan are maintained as possible at the same temperature throughout the experiment.

The experiments were carried out on PLA/TiO$_2$, PLA/ZnO and PLA/MMT films.

Each sample (approximately 4 mg) was subjected to the following temperature program:

• From -30 °C to 200 °C at 10 °C/min

• At 200 ° C for 5 minutes

• From 200 °C to -30 °C to 30 °C/min

• At -30 ° C for 2 minutes

• From -30 °C to 200 °C at 10 °C/min

From DSC thermograms, besides the enthalpies involved during melting and/or crystallization processes, it is possible to obtain also other thermal parameters, such as the glass transition temperature (Tg), the melting temperature Tm and cold crystallization (Tcc) temperature. Tg is generally determined at the inflection point observable on the DSC curve. The change on the curve is due to the different values the heat capacity of the amorphous phase of the polymer before (glassy state) and after (rubbery state) the second order transition. An easy mathematical method to read the Tg value is to make the first derivative of the DSC curve so that the inflection point corresponds to the maximum of the peak of the curve of the first derivative. Tm is determined at the maximum of the endothermic peak of the thermogram during the heating run and Tcc is read in correspondence of the maximum of the exothermic peak of the thermogram during the cooling rate.

1.4.6 Thermogravimetric Analysis (TGA)

The thermal stability of the samples was studied by TGA.

The instrument used was a Perkin Elmer Diamond.

Thermogravimetry consists in recording the variation of mass of a sample as a function of time and / or temperature in a controlled atmosphere.

The measurements were conducted at a heating rate of 20°C/min from 30 to 800°C, using about 1.5/2.0 mg of the sample in alumina pan. The experiments were done oxygen atmosphere at flow rate of 200 ml/min. From thermograms it is determined the temperature at which the degradation rate is maximum (Tmax) which corresponds to abscissa of the inflection point of the thermogram.

1.4.7 UV-visible spectroscopy

UV-visible spectra were monitored with Jasco V-570 spectrophotometer.

The spectra were recorded by using films in transmission mode.

1.4.8 Mechanical Properties

1.4.8.1Tensile properties

The analysis of tensile properties was carried out by using a dynamometer Instron 4505 with appropriate software for data processing.

The software, interfaced with the machine, processes the data stored to give a curve in which the force applied to produce the deformation of the specimen is expressed in function of the elongation percentage of the sample as a result of traction.

From the length of the sample at zero elongation, Lo, its thickness and its width, it's possible to calculate the elongation at break (ε_b) and the elongation at yield (ε_y) as well as the stress at break (σ_b) and the stress at yield (σ_y).

The Young's modulus of elasticity in tension (E) is calculated by the following equation:

$$E = \sigma / \varepsilon$$

where ε is the strain of the sample and σ the stress.

The modulus and the stress have the same unit: MPa. The tests were carried out at ambient temperature and at a speed of the moving crosshead of 2 mm / min. For PLA/ZnO composites and PLA/MMT nanocomposites the tests were performed in both the machine direction and in transverse direction.

1.4.8.2 Charpy impact test

The impact test allows to determine the degree of toughness of a polymer.

For the impact test analysis rectangular samples, with width of 3 mm, thickness of about 4 mm and length of 5 cm were used. The samples were cut from the slabs obtained by using the same conditions adopted for the preparation of films.

The instrument used is a Charpy pendulum. It consists of a pendulum heavy-based stainless, on which a clamp jaws to keep balance of the test sample and a metal column are mounted. At the top of the column an impact hammer is mounted on ball bearings. A circular protractor, fixed to the column and divided into degrees, indicates the inclination of the pendulum. At the lower end of the pendulum a metal hammer is fixed, while a clip stops the oscillations of the pendulum. Set the standard of the material between the parallel jaws of the clamp, the pendulum is dropped from a height (h) to break with one shot the sample.

The tool records the force (N) lost by the tool needed to break the sample, the energy (J) required to fracture the material and the toughness (KJ/m^2). Charpy impact tests were performed by using a pendulum CEAST with appropriate software for processing the data. The tests were carried out, for PLA/TiO$_2$ nanocomposites, at room temperature.

1.4.9 Barrier properties

The barrier properties are of primary importance in food packaging and pharmaceutical because are responsible of the ability to preserve the contents of the package from gases. The UNI (UNI 10534 12/94) defines the limits of permeability values associated with low and high barrier properties (Table 1.8).

Table 1.8 *Quantitative value of the permeability defined by UNI 10534 12/94*

Barrier	Permeability $[cm^3/(m^2 x24h)]x(cm/bar)$
very high	<0.5
high	0.5-3.0
medium	3.1-30
low	31-150
very low	>150

The specific barrier requirement of the package system is related to the product characteristics and the intended end-use application. Generally plastics are relatively permeable to small molecules such as gases, water vapour, organic vapours and liquids and they provide a broad range of mass transfer characteristics, ranging from excellent to low barrier value, which is important in the case of food products. Water vapour and oxygen are two of the main permeants studied in packaging applications, because they may transfer from the internal or external environment through the polymer package wall, resulting in a continuous change in product quality and shelf-life [9]. Carbon dioxide is also important for the packaging in modified atmosphere (MAP technology) because it can potentially reduce the problems associated with processed fresh product, leading a significantly longer shelf-life.

1.4.9.1 Oxygen transmission rate (OTR)

The apparatus used is PermeO$_2$ Extra Solution, Figure 1.4.1. The test consists in determining the amount of oxygen that passes through the surface (50 cm^2) of the film of a given thickness, in a certain time (24h), with precise relative humidity conditions H = 0% and temperature (23°C).
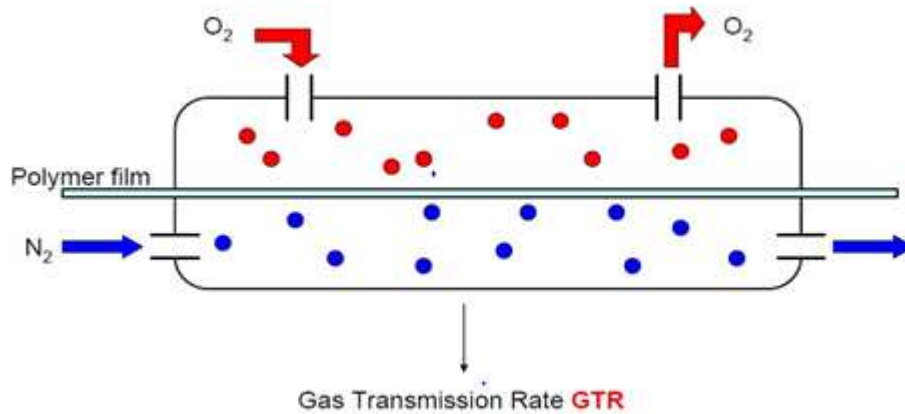
Figure 1.4.1 *PermO₂ Extra Solution*

The instrumental apparatus is constituted by a double diffusion chamber and the film is inserted between the two rooms. A mixture of nitrogen and oxygen enters into the upper chamber, while anhydrous nitrogen enters at the bottom. The rooms are conditioned at 23°C. The diffusion of oxygen through the film is measured by a sensor of zirconium oxide, which measures the mass of gas in the upper chamber.

This new instrument uses coulometric sensor for oxygen, in accordance with the new ASTM. This systems employ two chambers with a specimen mounted as a sealed semi-barrier between them. One chamber contains oxygen while the other is slowly purged with a stream of a carrier gas such as nitrogen.

As the oxygen gas permeates through the specimen into the carrier gas, it is transported to the coulometric detector where it creates an electric current

with a magnitude that is proportional to the number of oxygen atoms flowing into the detector.

The oxygen transmission rate (OTR) is defined as the amount of oxygen gas passing through a unit area in units of time:

$$OTR = cm^3/(m^2 \text{ x } 24h)$$

The permeability is obtained, multiplying the OTR for the film thickness and dividing by the difference of partial pressure present in the two chambers, Eq.1:

$$PERMEABILITY = [cm^3/(m^2 \text{ x } 24h)] \text{ x } (cm/bar)$$
$$= OTR \text{ x } (THICKNESS/\Delta P) \qquad\qquad Eq.1$$

1.4.9.2 Water vapour (WVTR) and Carbon dioxide transmission rate (CO_2TR)

With the same principle of operation, but using Multiperm Extra Solution instrument, the CO_2 and H_2O permeability were measured.

The water vapour barrier properties for the packaged product whose physical or chemical deterioration is related to its equilibrium moisture content, are of great importance for maintaining or extending its shelf-life. For fresh food products it is important to avoid dehydration while for bakery or delicatessen is important to avoid water permeation.

The permeability is obtained, multiplying the WVTR for the film thickness and dividing by the difference of partial pressure present in the two chambers, Eq.2:

$$PERMEABILITY = [cm^3/(m^2 \text{ x } 24h)] \text{ x } (cm/bar)$$
$$= WVTR \text{ x } (THICKNESS/\Delta P) \qquad\qquad Eq.2$$

Like the oxygen and water vapour barrier properties, also the carbon dioxide barrier property is of particular importance on food packaging application.

For CO_2 permeability the following parameters and conditions were used: surface of the film about 50 cm^2 (fixed by the dimension the sample place in the equipment) thickness of the film as homogenous as possible, a time of 24h for the experiment, precise relative humidity condition H = 0% and temperature at 23°C; for H_2O permeability the same parameters and conditions were used except for the relative humidity conditions, H =90%.

1.4.10 Antibacterial properties

The antimicrobial activity of the composites was evaluated using *E. Coli* DSM 498T (DSMZ, Braunschweig, Germany) as test microorganisms. The evaluation was performed using the ASTM Standard Test Method E 2149-10 preparation of the bacterial inoculum required to grow a fresh 18-h shake culture of *E. Coli* DSM 498 in a sterile nutrient broth (LB composition for 1 l: 10 g of triptone, 5 g of yeast extract and 10 g of sodium chloride) The colonies were maintained according to good microbiological practice and examined for purity by creating a streak plate. The bacterial inoculum was diluted using a sterile buffer solution (composition for one liter: 0.150 g of potassium chloride, 2.25 g of sodium chloride, 0.05 g of sodium bicarbonate, 0.12 g of calcium chloride hexahydrate and a pH of 7) until the solution reached an absorbance of 0.3±0.01 at 600 nm, as measured spectrophotometrically. This solution, which had a concentration of 1.5–3·10^8 colony forming units (CFUs) ml^{-1}, was diluted with the buffer solution to obtain a final concentration of 1.5–3·10^6 CFUs ml^{-1}. This solution was the working bacterial dilution. The experiments were performed in 50 ml sterilized flasks. One gram of the

film was maintained in contact with 10ml of the working bacterial dilution. After 2 min, 100 ml of the working bacterial dilution was transferred to a test tube, which was followed by serial dilution and plating out on Petri dishes (10mmX90mm) in which the culture media was previously poured. The Petri dishes were incubated at 35 °C for 24 h. These dishes represented the T_0 contact time. The flasks were then placed on a wrist-action shaker for 1 h (T_1), 24 h (T_2), 48h (T_3), 5days (T_4). The bacterial concentration in the solutions at these time points was evaluated by again performing serial dilutions and standard plate counting techniques. Three experiments were performed for each composition. The number of colonies in the Petri dish after incubation was converted into the number of colonies that form a unit per millilitre (CFUs ml^{-1}). The percentage reduction was calculated using the following formula Eq.3:

Reduction % (CFU ml^{-1}) = [(B-A)/B] x100   Eq.3

where A=CFUs ml^{-1} for the flask containing the sample after the specific contact time and B=CFUs ml^{-1} at T_0.

1.4.11 Degradation properties

1.4.11.1 UV degradation

The PLA and composite films were exposed to UV-accelerated weathering tester (Sunrise, Angelantoni Industrie ACS, Perugia, Italy UVA 360 nm) characterized by light intensity of 20 Wm^{-2}. The films were subjected to the UV irradiation at 40°C and at 25% of humidity and removed at given time to be weighed.

For PLA film the test was done once a day for 17 days, whereas for the PLA/TiO$_2$ nanocomposites the test was done once a day up to the 17th day, then once a week up to the 73rd day of the experiment. For PLA and PLA/ZnO composites the test was done once a day up to the 4th day, then

once a week up to the 21st day of the experiment. For PLA and PLA/MMT nanocomposites the test was done once a day up to the 3rd day , then once a week up to the 15th day of the experiment.

The weight loss W_{loss}% was calculated using the following formula Eq.4:

$$W_{loss}\% = [(W_0 - W_t)/ W_0] x100 \qquad Eq.4$$

where W_0 is the initial weight of sample and W_t is the weight at t time of UV light exposure.

1.4.11.2 Hydrolytic degradation

Hydrolytic degradation was carried out on the films (10mm x10 mm) at 37°C in a flasks containing a solutions 1M of NaOH.

Samples were kept or maintained in stirring for a given time and periodically removed, washed with distilled water and dried in vacuum at 36 °C for 48h before the weighing. The mass loss was calculated by the (Eq.4) where W_0 is the initial weight of samples and W_t is the weight at t time of NaOH solution contact, after dried. For PLA and PLA/TiO$_2$ nanocomposites the incubation time was: 30, 60, 120, 180, 240, 300, 360, 420, 480 and 540 minutes; for PLA and PLA/ZnO composites the incubation time was: 10, 20, 30 and 40 minutes and for PLA and PLA/MMT nanocomposites the incubation time was: 10, 20, 30 and 40 minutes.

1.4.11.3 Enzymatic degradation (Proteinase K)

Sample films (2.5cm x 1.0cm) were placed in vials containing 5mL of Tris-HCl buffer (pH 8.6), 1mg of proteinase K (Sigma, lyophilized powder 80% protein) and 1mg of sodium azide (Sigma-Aldrich, purified 99.5%) in distilled water. For each experiment, three replicate films in separate vials

were used to determine the weight loss at specified incubation time (2-4-8-10-12h). The film/enzyme was kept at 37 °C in the rotary shaker (150 rpm). The buffer/enzyme solution was replaced every incubation time to ensure that enzyme activity remained at a desired level throughout the experiment duration and that the solution pH did not drop below pH 8.00.

At specified incubation time (2-4-8-10-12h) the film was removed from the vial, washed with distilled water and dried under vacuum at 36°C for 48h before the weighing.

The weight loss was calculated with Eq.4, where W_0 is the initial weight of sample and W_t is the weight of the sample after being removed from the Proteinase K solution at the end of each specified incubation time (2-4-8-10-12h) and dried as described above.

1.4.11.4 Isothermal degradation

Isothermal tests were recorded by Perkin Elmer Diamond instrument, using alumina pans and an oxygen atmosphere at flow rate of 200 ml/min. The following procedure has been used: heating ramp at 20° C / min from room temperature up to the desired temperature (200-220-240°C) followed by an isotherm for 30 min. The experiments were carried out on 3 mg of PLA/TiO$_2$, PLA/ZnO and PLA/MMT films.

REFERENCES

[1]"Plasma processing approach to molecular surface tailoring of nanoparticles: Improved photocatalytic activity of TiO_2 "J. Cho, F.S. Denes, R.B. Timmons, Chemistry of Materials, 18: 2989-2996 (2006).

[2] "Aerosol processing of materials" A. Gurav, T. Kodas, t. Pluym, Y. Xiong, Aerosol Science and technology 19 (1993) 411-452.

[3] "Particle formation in gases, Powder technology" S.E. Pratsinis, S. Vemury,88 (1996) 267-273.

[4] "Ceramic powder synthesis by spray pyrolysis" G.L. Messing, S.C. Zhang, G.V. Jayanthi, Journal American Ceramic Society 76 (11) (1993) 2707-2726.

[5] "Spray pyrolysis synthesis of submicronic particles. Possibilities and limits" S. Alavi, B. Caussat, J.P. Couderc, J. Dexpert-Ghys, N. Joffin, D. Neumeyer, M. Verelst Advances in Science and technology A 30 (2003) 417-424.

[6] "Aluminium oxide, activated" in: A. Person (Ed.), Kirk-Othmer Encyclopedia of Chemical Technology, vol. 2, J. Wiley, New York, 1994, pp. 291.

[7] "Zinc oxide thin films by the spray pirolysis method", M. Krunks, E. Mellikov, Thin Solid Films 270 (1995), pp. 33-36.

[8] "Elaboration of Boehmite Nano-powders by spray-Pyrolisis" J.M.A. Caiut, J. Dexpert-Ghys, Y. Kihn, M. Veelst, H. Dexpert, S.J.L. Ribeiro, Y. Messaddeq, Power Thecnology, (2009), 190, pp. 95-98.

[9] "Conception de films polymer à permeabilité contrôlée pour l'embalage alimentaire" Y. Germain, Industriée Alimentaire et Agricules (1997), pp. 137–140.

CHAPTER 2

MORPHOLOGY AND STRUCTURE

2.1 MORPHOLOGY AND STRUCTURE OF TiO$_2$ (MODIEFIED AND UNMODIFIED)

The morphology and structure of TiO$_2$ (modified and unmodified) nanoparticles are highlighted using the transmission electron microscopy (TEM) and X-ray diffraction (WAXD). In Figure 2.1.1 the TEM micrographs of unmodified (A) and modified (B) TiO$_2$ are reported.
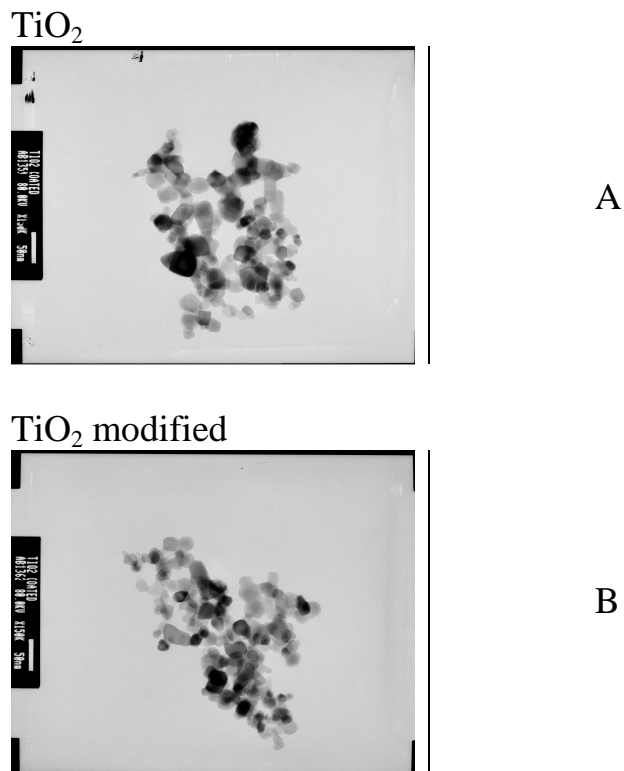
TiO$_2$

A

TiO$_2$ modified

B

Figure 2.1.1 *TEM micrograph 15000x for unmodified (A) and modified TiO$_2$ nanoparticles (B)*

From the images, it is evident that TiO_2 powder is constituted by spherical particles, with a diameter of about $25 \pm 5nm$ for modified and unmodified nanoparticles. This result confirms that the layer of perfluorocarbons on the surface is very thin and it does not affect significantly the particle dimension.
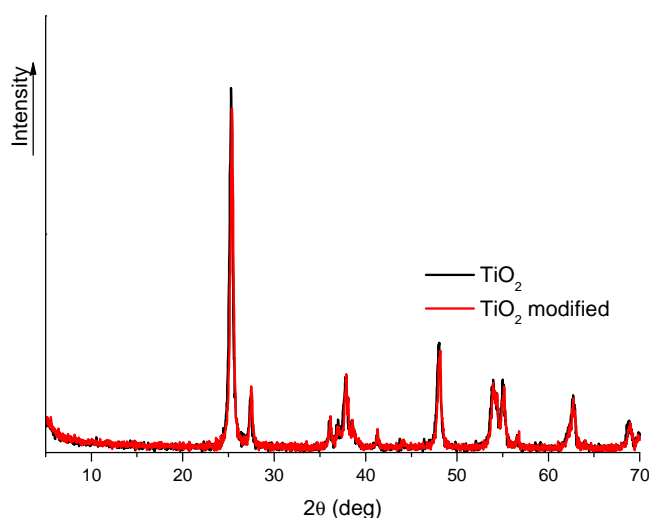

Figure 2.1.2 X-ray diffraction spectrum of the nanoparticles modified by plasma treatment and unmodified

The TiO_2 nanoparticles WAXD spectra are reported in figure 2.1.2. The diffraction peaks observed at $2\theta=25.3°$, $37.8°$, $48.1°$, $53.9°$, $55.1°$ and $62.7°$ correspond to (101), (004), (220), (105), (211) and (204) reflections of anatase phase of TiO_2. The other diffraction peaks are observed at $2\theta= 27.5°$, $36.2°$, $41.3°$, $43.7°$ and $56.5°$ can be assigned to (110), (101), (200), (111) and (220) reflections of rutile phase of TiO_2.

The ATR spectra of modified and unmodified TiO_2 powder are showed in the figure 2.1.3 Before measuring, the powders are dried at 65°C for 24h. The spectra appear identical except for the presence of a

peak at 1226 cm^{-1} for modified TiO_2. This peak is due to the stretch of the C-O bond of the ether group (-C-O-C).
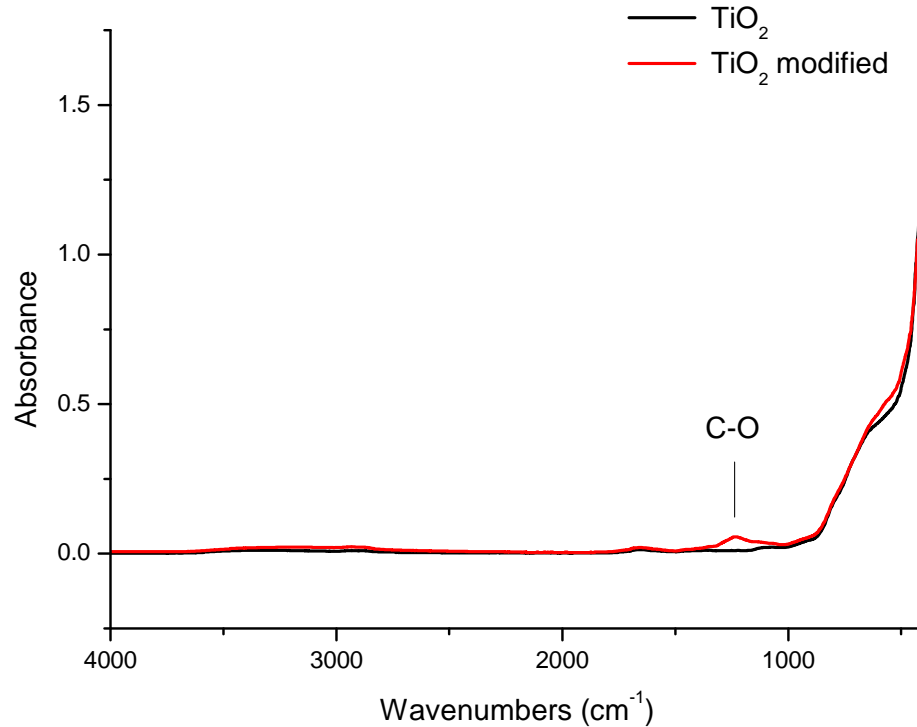

Figure 2.1.3 *ATR spectra of the TiO_2 nanoparticles (modified and unmodified)*

This result confirms that the perfluorocarbon layer is covalently linked to the nanoparticles surface.

2.2 ANGLE (WAXD) X-RAY ON PLA/TiO_2 NANOCOMPOSITES

WAXD measurements are performed with the aim to study the influence of nanofiller on the polymer matrix structure to the vary composition and on the crystallinity degree of the polymer matrix.

The WAXD spectra of PLA/TiO_2 nanocomposite films are shown in figure 2.2.1. All the spectra display the classical halo of amorphous materials. TiO_2 modified and unmodified nanoparticles do not induce

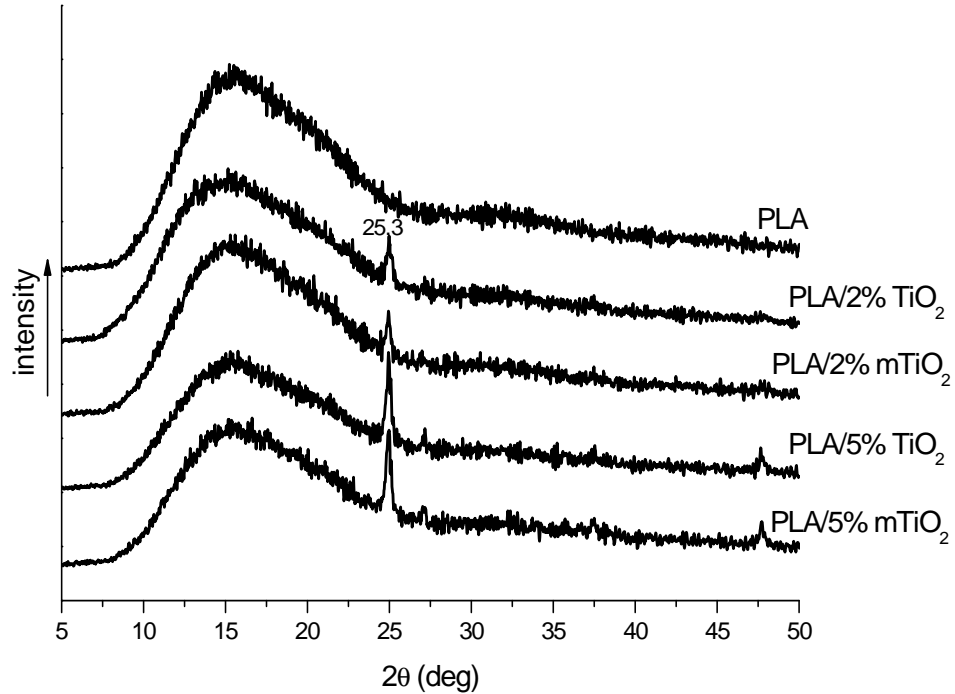crystallization. In the spectra of nanocomposites appears at $2\theta=25.3°$ the peak of anatase phase of TiO_2.

25.3

PLA

PLA/2% TiO_2

PLA/2% $mTiO_2$

PLA/5% TiO_2

PLA/5% $mTiO_2$

intensity

2θ (deg)

Figure 2.2.1 *WAXD spectra of PLA, PLA /2-5% TiO_2 modified and unmodified*

2.3 MORPHOLOGY OF PLA/TiO_2 NANOCOMPOSITES

TiO_2 (modified and unmodified) dispersion and distribution in PLA matrix was evaluated by scanning electron microscopy analysis performed on surfaces obtained by fracturing the films in liquid nitrogen.

PLA shows a homogeneous fracture surface as expected for a pure polymer (Figure 2.3.1).
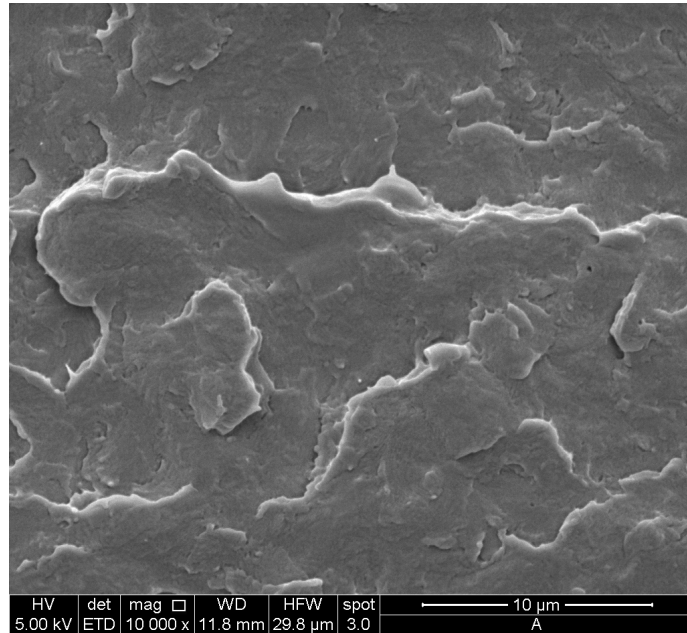
Figure 2.3.1 SEM image of PLA film fractured in liquid nitrogen (magnification 10000X)

Figures 2.3.2, 2.3.3, 2.3.4 and 2.3.5 show the micrographs for the fractured film surfaces of PLA, PLA / 2%TiO$_2$, PLA/2% mTiO$_2$, PLA/ 5% TiO$_2$ and PLA/ 5% mTiO$_2$ respectively. For each composition, two different magnification are reported: A 10.000X and B 20.000X.

For all the compositions, it can be observed that the nanoparticles dispersion and distribution is homogeneous. Moreover, the nanoparticles are perfectly embedded in the matrix both if they are modified or not.
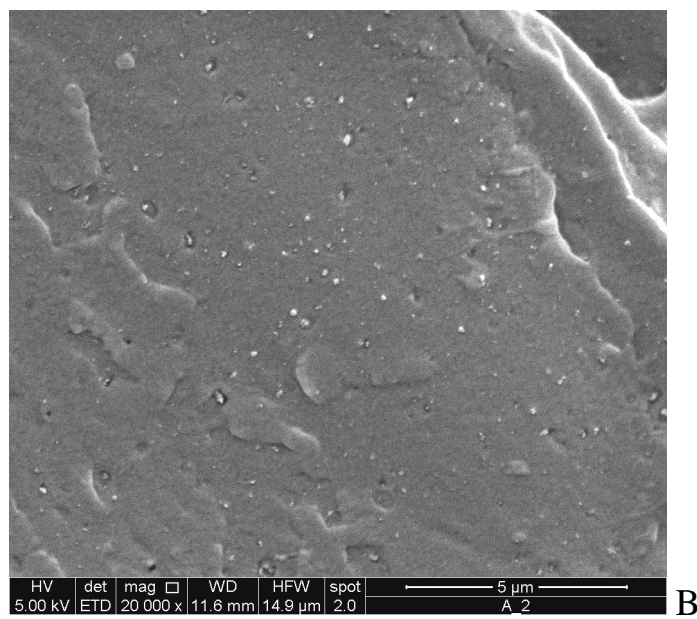
Figure 2.3.2. *Scanning electron micrographs of PLA/2%TiO$_2$ film fractured in liquid nitrogen (A: magnification 10000X, B: 20000X)*

Figure 2.3.3. *Scanning electron micrographs of PLA/2% mTiO$_2$ film fractured in liquid nitrogen (A: magnification 10000X, B: 20000X)*
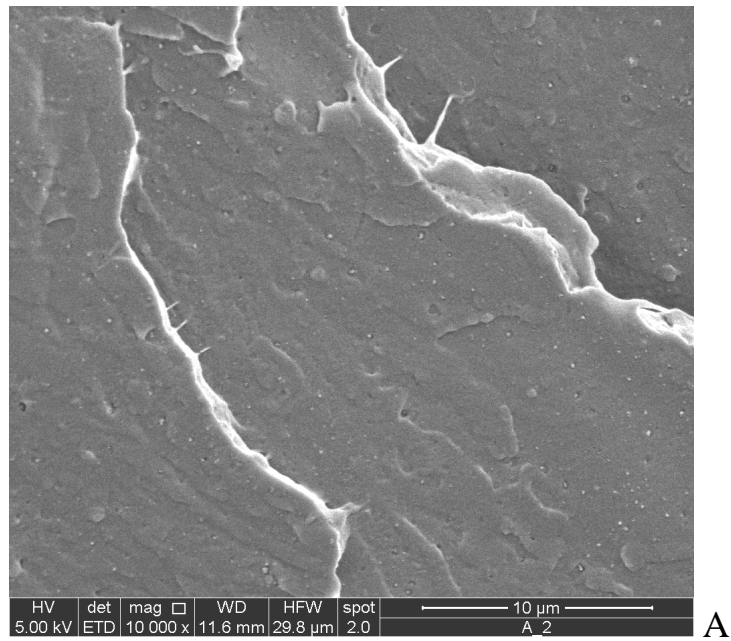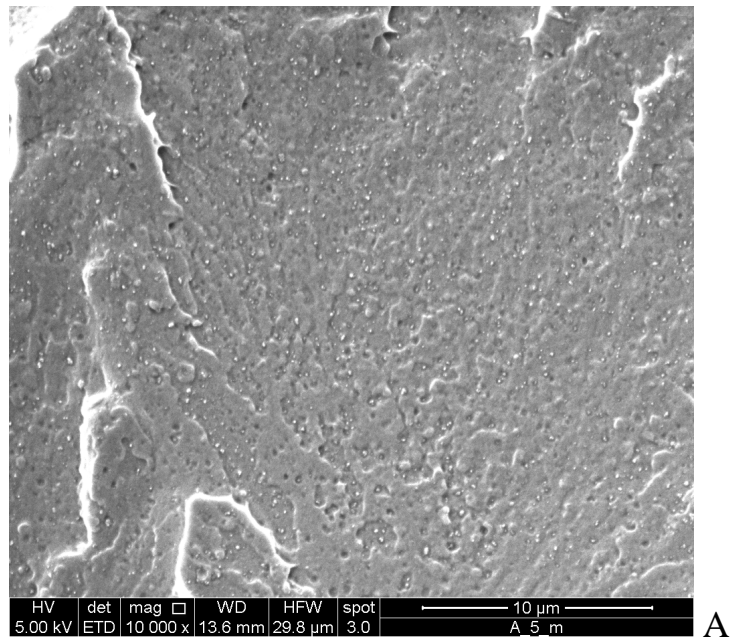
Figure 2.3.4. *Scanning electron micrographs of PLA/5% TiO$_2$ film fractured in liquid nitrogen (A: magnification 10000X, B: 20000X)*
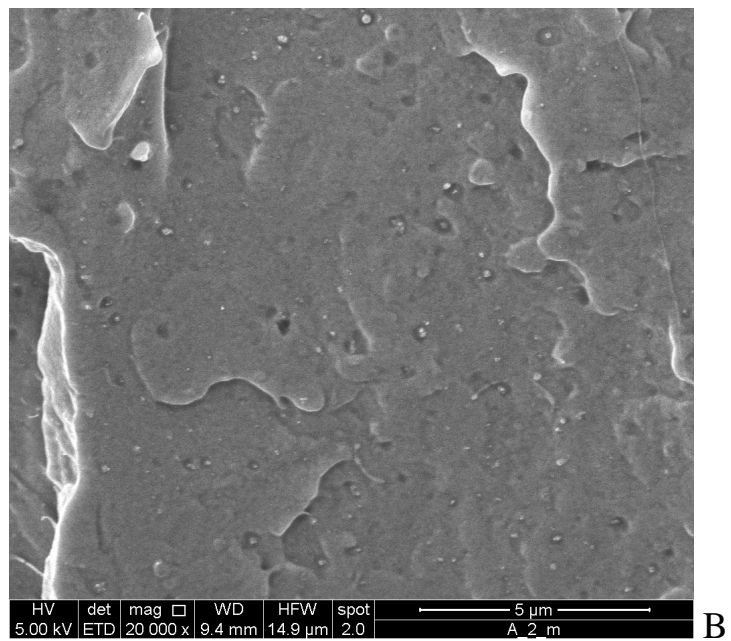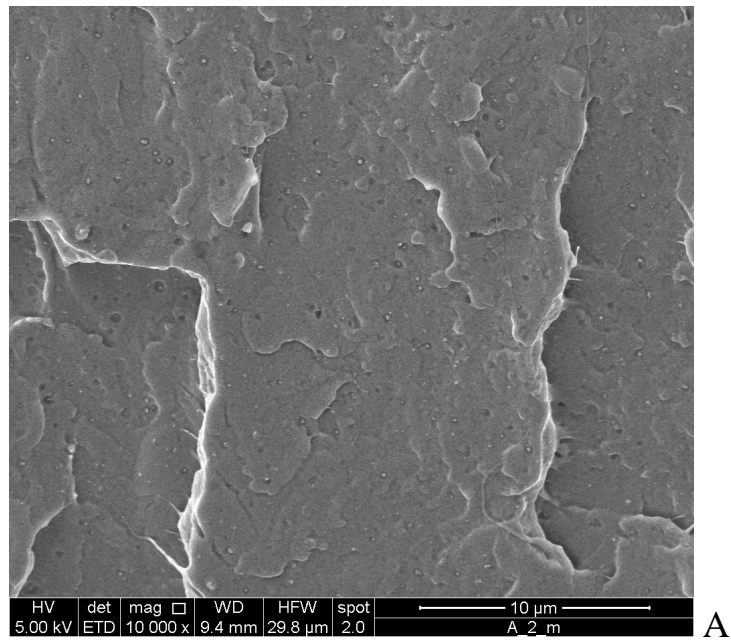
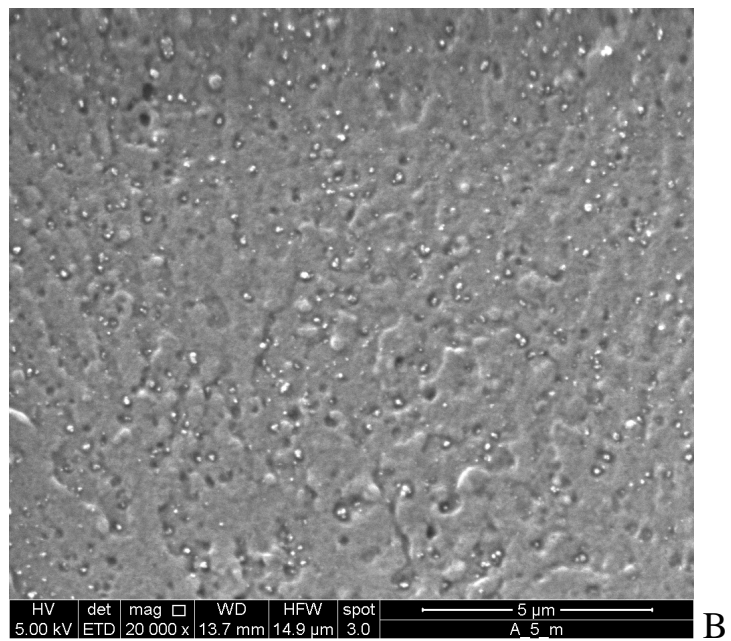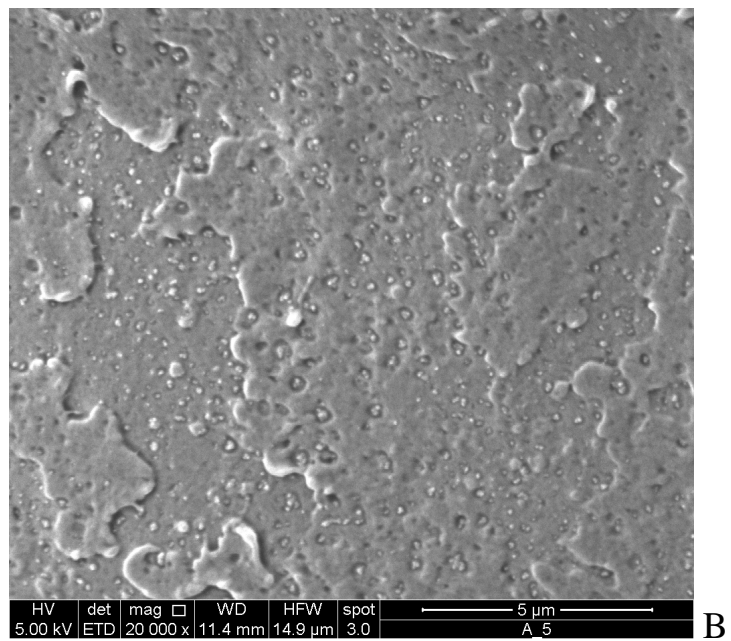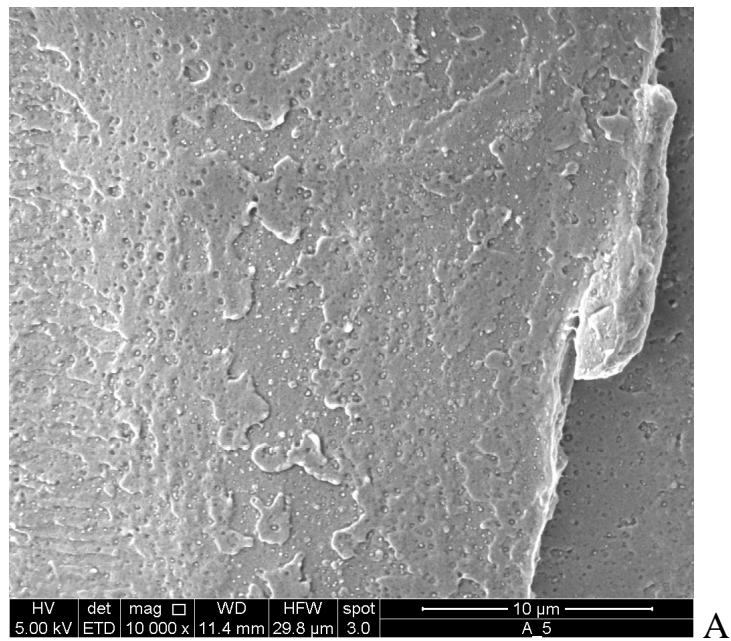***Figure 2.3.5.*** *Scanning electron micrographs of PLA/5% mTiO$_2$ films fractured in liquid nitrogen (A: magnification 10000X, B: 20000X)*

2.4 MORPHOLOGY AND STRUCTURE OF ZnO

The morphology and structure of ZnO powders obtained by spray pyrolysis are shown respectively in figure 2.4.1, 2.4.2 and 2.4.3.

The SEM micrograph shows that the ZnO powder is constituted by spherical particles. Some have a diameter of 1 μm, while the majority has a diameter much smaller (estimated between 500 and 100 nm). The spectrum of X-ray diffraction shows the presence in the powder exclusively of ZnO crystals (planes hkl) [1,2].
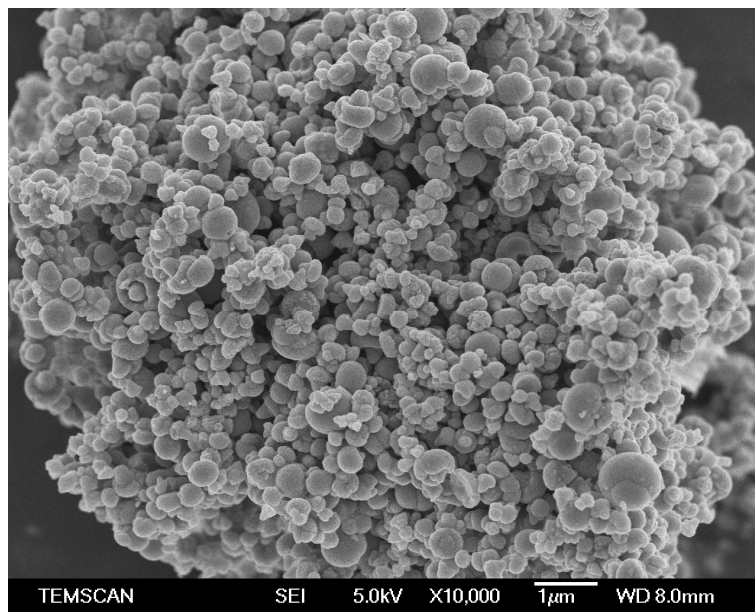
Figure 2.4.1 *SEM micrograph 10000x of the particles obtained by spray-pyrolysis*
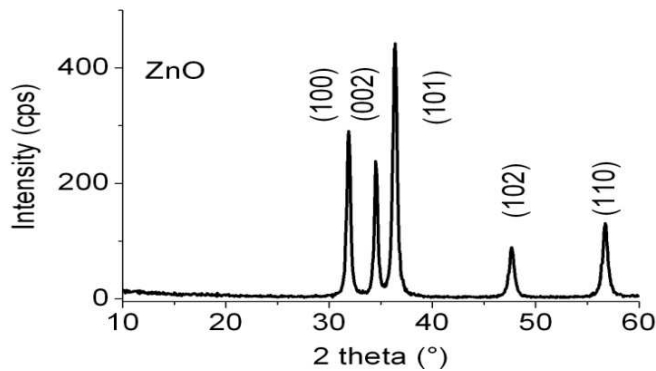
Figure 2.4.2. *X-ray diffraction spectrum of the particles obtained by spray-pyrolysis*

Figure 2.4.3 shows the ATR spectrum of ZnO particles from 40.000 to 400cm^{-1}.

Depending on the morphology of the particles they have characteristic absorptions in the region of low frequencies (400-500 cm^{-1}), a shoulder is found at 500 cm^{-1} that corresponds to the stretching of Zn–O bond [3,4].

Using the theory of dielectric media it can obtain information on the shape and morphology of the particles [5]. In particular the single band for ZnO indicates a spherical structure of the particles.
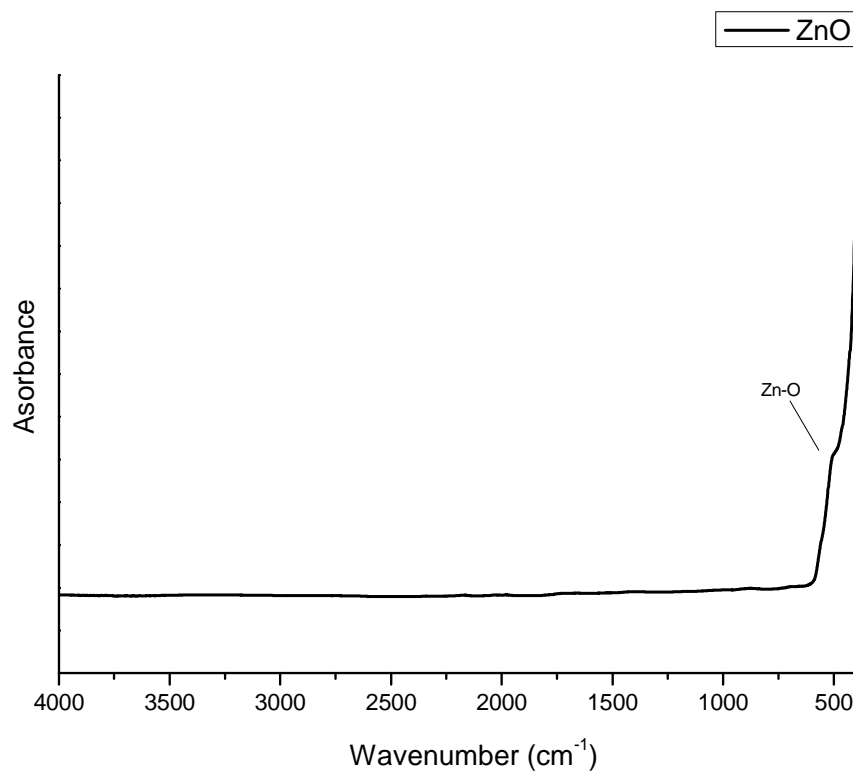
Figure 2.4.3 *ATR spectrum of ZnO particles*

2.5 X-RAY ANALYSIS OF THE PLA/ZnO COMPOSITES

The WAXD spectra of the PLA/ZnO films are shown in figure 2.5.1 From this analysis it is evident that the PLA and composites are completely amorphous. Furthermore the specific peak evidenced at

2θ=31.6° and 2θ=36.2° can be ascribed respectively to the diffraction planes (100) and (101) of ZnO crystals Their intensity is clearly increasing with filler loading [6,7].
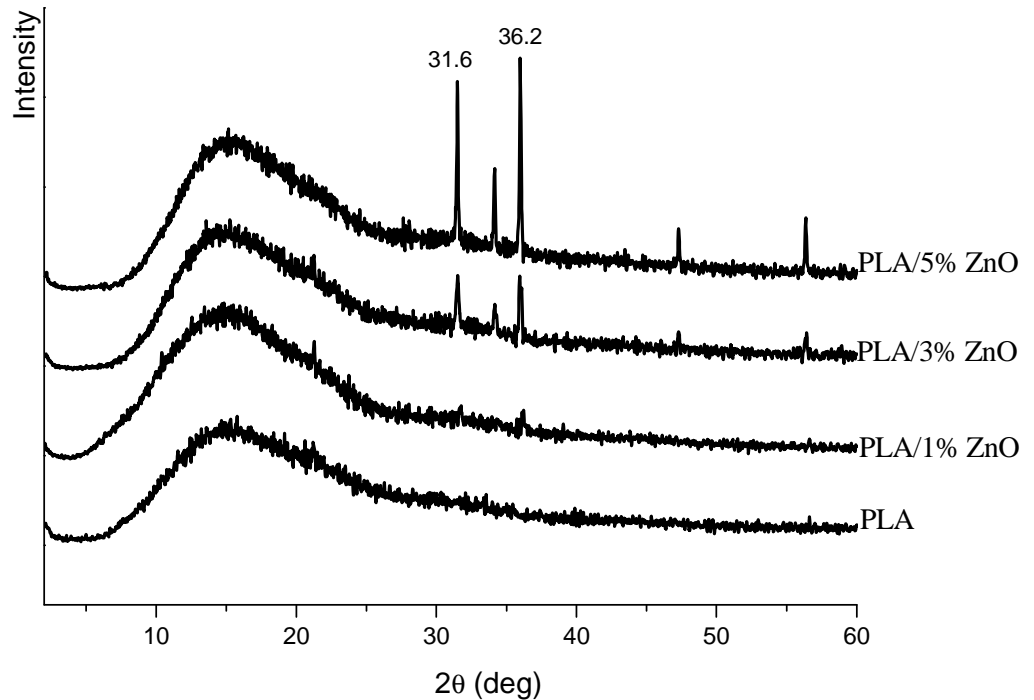
Figure 2.5.1 *X-ray spectra of PLA, PLA /1% ZnO, PLA/3% ZnO and PLA/5% ZnO*

2.6 MORPHOLOGY OF PLA/ZnO COMPOSITES

The dispersion of the particles in the matrix of PLA was evaluated by scanning electron microscopy on surface film fractured in liquid nitrogen. Again, The SEM image of PLA shows a homogeneous surface as expected for a pure polymer (Figure 2.6.1)
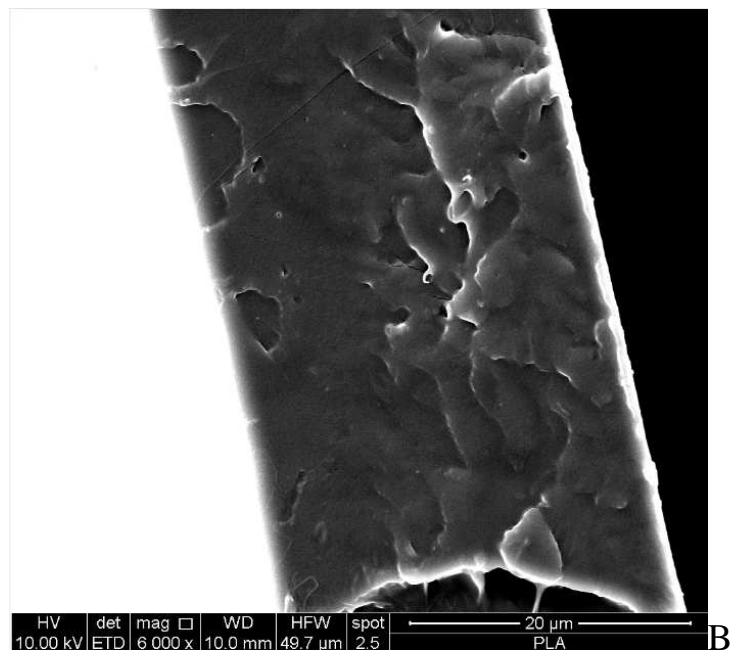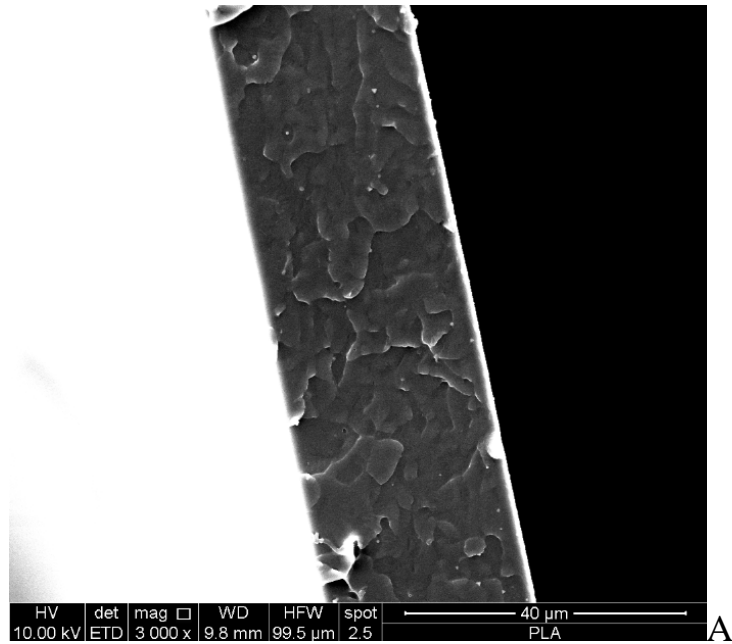
Figure 2.6.1. *Scanning electron micrographs of PLA films fractured in liquid nitrogen (A: magnification 3000X, B: 6000X)*

Figures 2.6.2, 2.6.3 and 2.6.4 show, respectively, the micrographs for the fracture surfaces of the samples PLA/1% ZnO, PLA/3% ZnO and PLA/5% ZnO. In all the samples the particles are fairly distributed in

the polymer matrix with an average size about of 1.2 μm. This result is to be expected just by the nature inherently incompatible between the organic and the inorganic phase and the natural tendency of particles of sub-micrometer and nanometer size to agglomerate by virtue of their high surface energy.

The number and the size of the clusters in the sample with 1% of ZnO are few and small and they increase in the samples with 3 and 5% of ZnO.
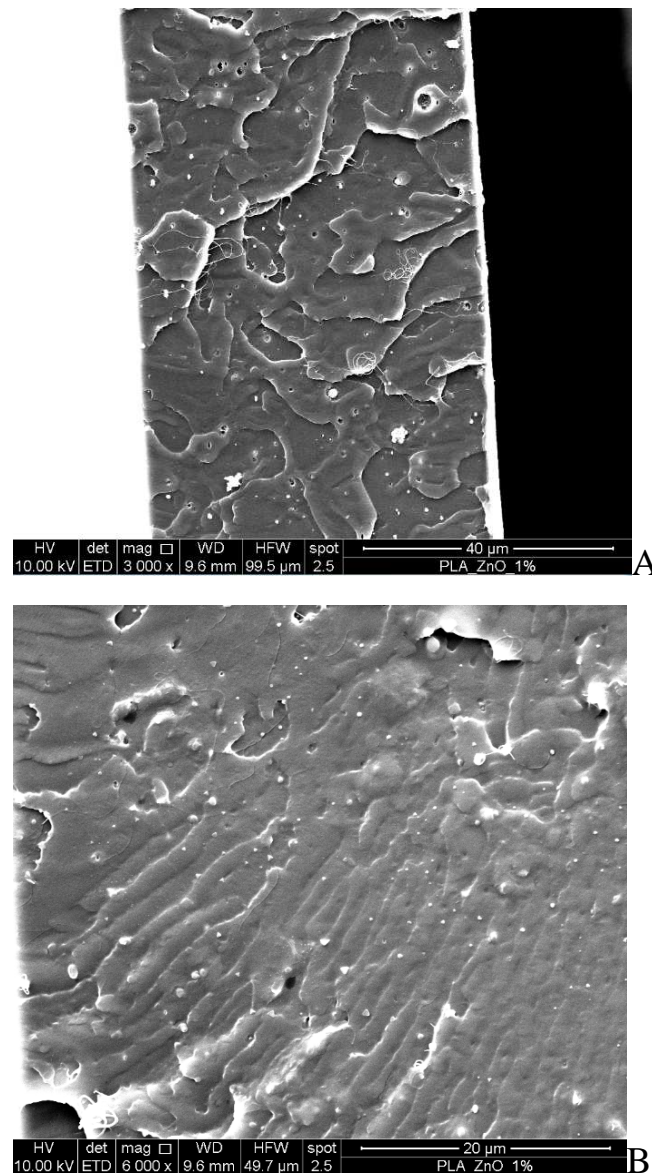
Figure 2.6.2 *Scanning electron micrographs of PLA/ 1% ZnO film fractured in liquid nitrogen (A: magnification 3000X, B: 6000X)*
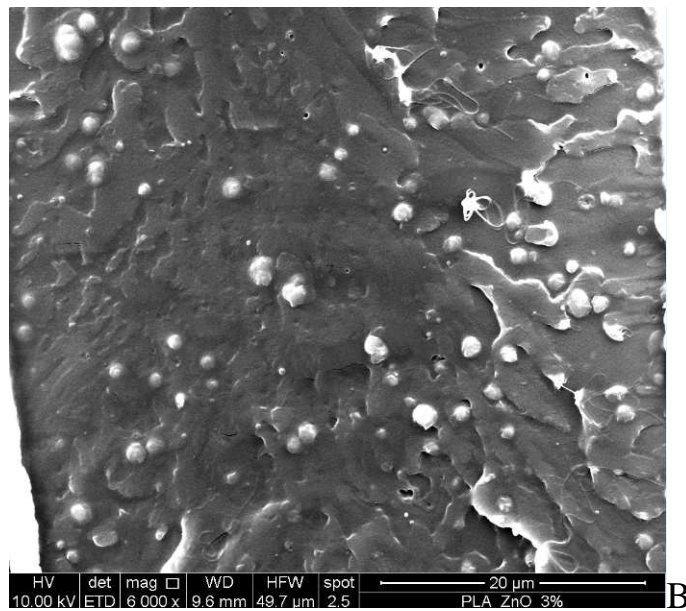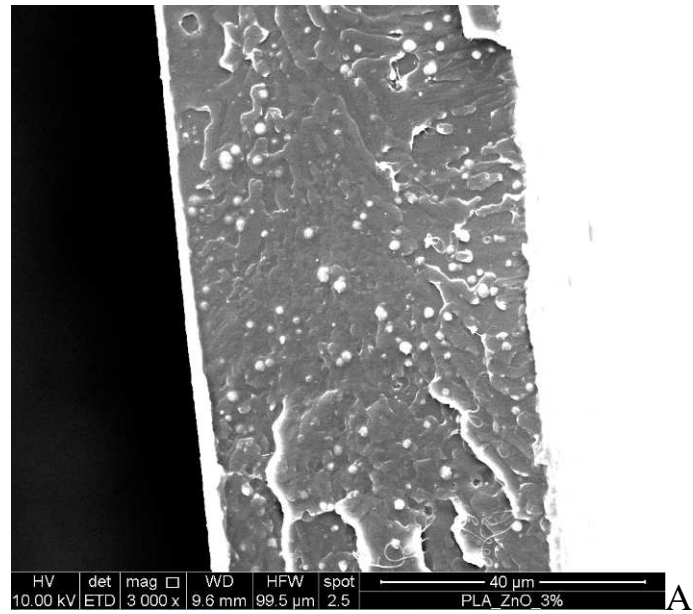
Figure 2.6.3 *Scanning electron micrographs of PLA/3% ZnO film fractured in liquid nitrogen (A: magnification 3000X, B: 6000X)*
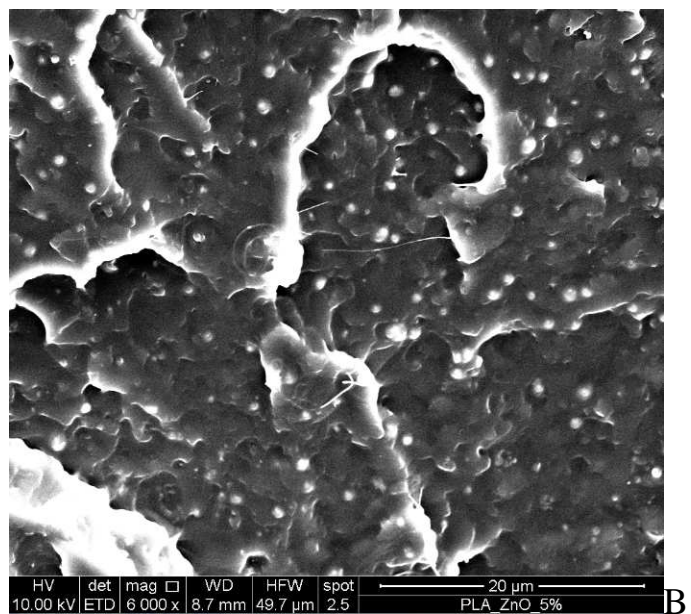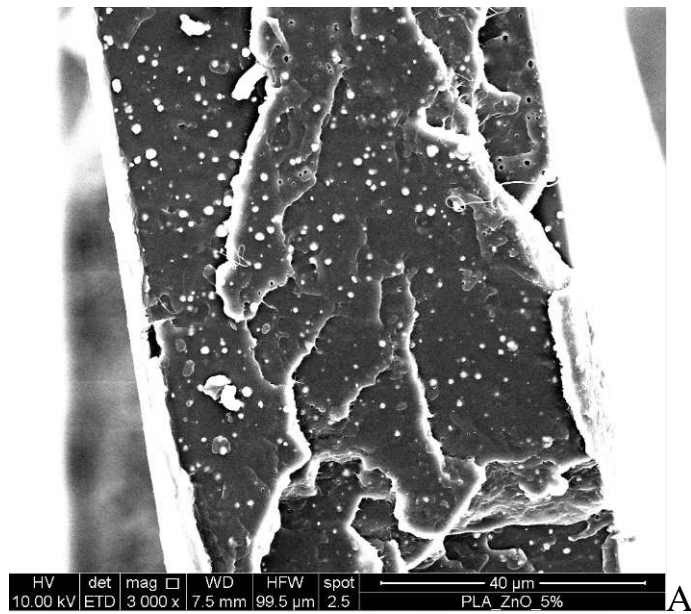
Figure 2.6.4 *Scanning electron micrographs of PLA/ 5% ZnO film fractured in liquid nitrogen (A: magnification 3000X, B: 6000X)*

2.7 MORPHOLOGY AND STRUCTURE OF MMT (DELLITE 67G)

The morphology and structure of MMT powder were observed using the transmission electron microscopy (TEM), X-ray diffraction (WAXD) and attenuated total reflection (ATR). The TEM image, WAXD and ATR spectra are shown respectively in figure 2.7.1, 2.7.2 and 2.7.3.
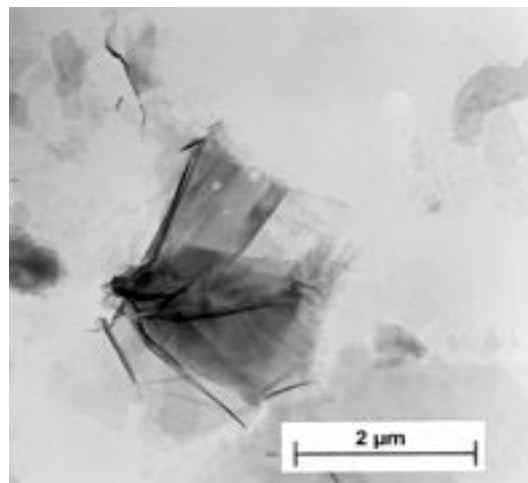
Figure 2.7.1 TEM Micrograph of MMT nanoparticles [8]
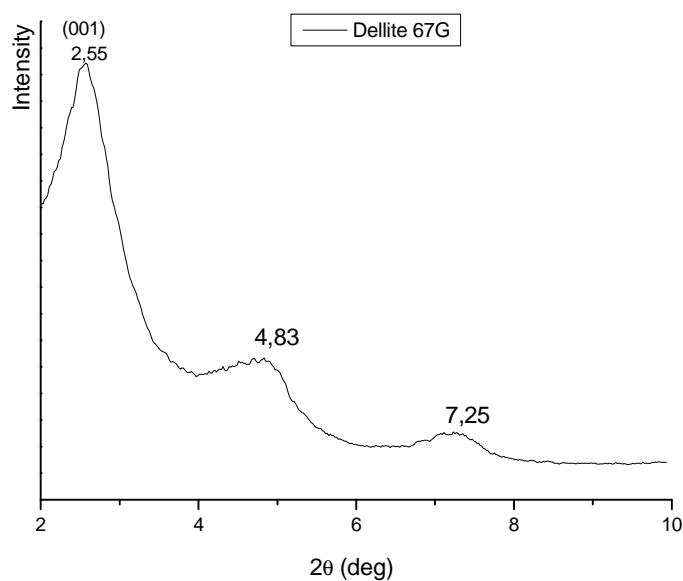
Figure 2.7.2 WAXD spectrum of MMT nanoparticles
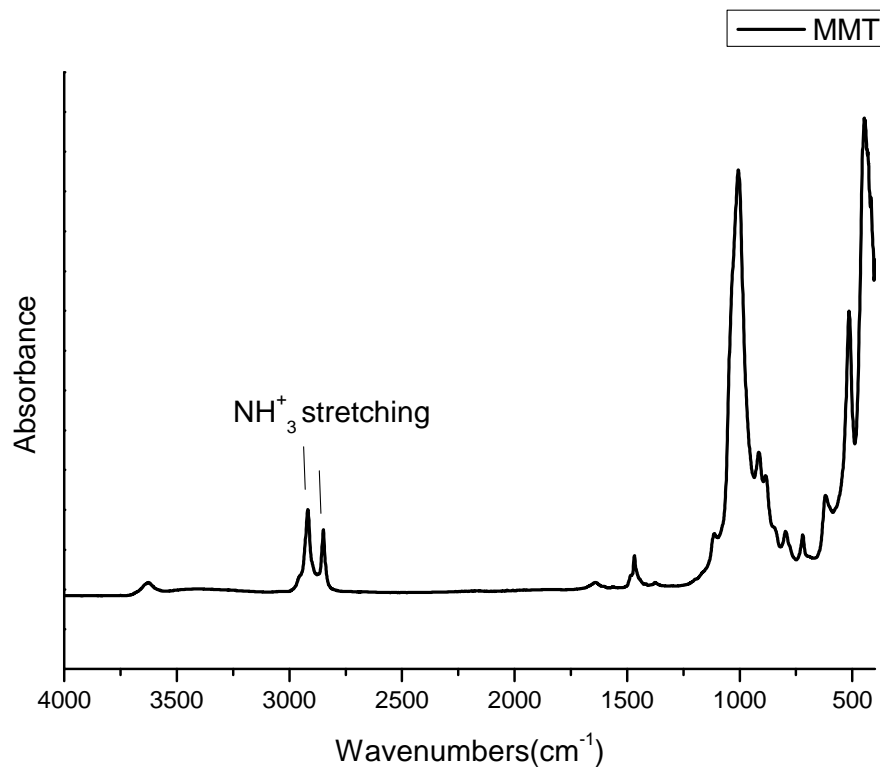
Figure 2.7.3 *ATR spectrum of MMT nanoparticles*

The TEM micrograph (Figure 2.7.1) shows that the powder of MMT consists in lamellae of rectangular shape; each lamella has several layers.

The WAXD spectrum of MMT, Figure 2.7.2, is reported in the range 2° - 10°.

The peak at $2\theta = 2.55°$ corresponds to the crystallographic planes with Miller indices 001.The basal spacing of the silicate layer $d_{001} = 3.51$ nm is calculated using the Bragg's law, $\lambda = 2d \sin\theta$, where λ is the wavelength of the X-ray radiation used (0.1546 nm), d is the spacing between diffractional lattice planes and θ is the measured diffraction angle. This distance also represents the interlamellar distance between two successive states of clay and from its analysis (position and

intensity) can be determined in some cases intercalated and/or exfoliated structures in the nanocomposites [9].

Figure 2.7.3 shows ATR spectrum of powder of MMT nanoparticles. The characteristic peaks of MMT are present in the range from 1500 to 500 cm^{-1} . The two peaks at 2919-2848 cm^{-1} are due to the asymmetric and symmetric NH$_3^+$ stretching because the nanoparticles are modified with quaternary ammonium salt.

2.8 X-RAY ANALYSIS OF PLA/MMT(Dellite 67G) PELLETS

The spectra of X-ray diffraction of the composite, in the form of pellets, are shown in Figure 2.8.1. The characteristic peaks of Dellite 67G are slightly shifted towards lower values of 2θ systems PLA /MMT. This result indicates that the extrusion led to a first weak intercalation of Dellite particles within the polymer matrix.
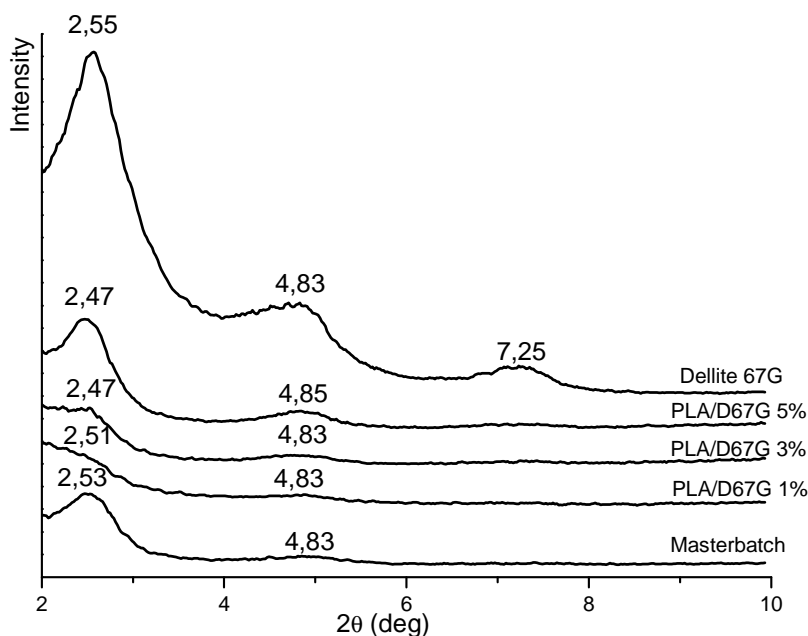
Figure 2.8.1 *Spectrum of X-ray diffraction of Dellite 67G powder, PLA/1% D67G, PLA/3% D67G, PLA/5% D67G and masterbatch pellets*

2.9 X-RAY ANALYSIS OF PLA/MMT(Dellite 67G) NANOCOMPOSITES

The WAXD spectra of PLA and PLA/D67G films are shown in figure 2.8.1. From the spectra it is evident that the PLA and PLA / D67G 1% nanocomposite are completely amorphous, while at composition of 3 and 5% of D67G a small amount of crystallinity (X_c) is detectable, 4 and 8%, respectively as reported in Table 2.6. This result is in agreement with literature data that reports the nucleating action of the clay [10,11].

In the nanocomposites PLA/D67G 3 and 5%, the PLA matrix crystallizes in the α form with rhomboid crystals [12] as evidenced by the presence of peaks at $2\theta = 17°$ and $19°$ corresponding to the lattice planes with Miller indices (200) or 110) and (203), respectively.
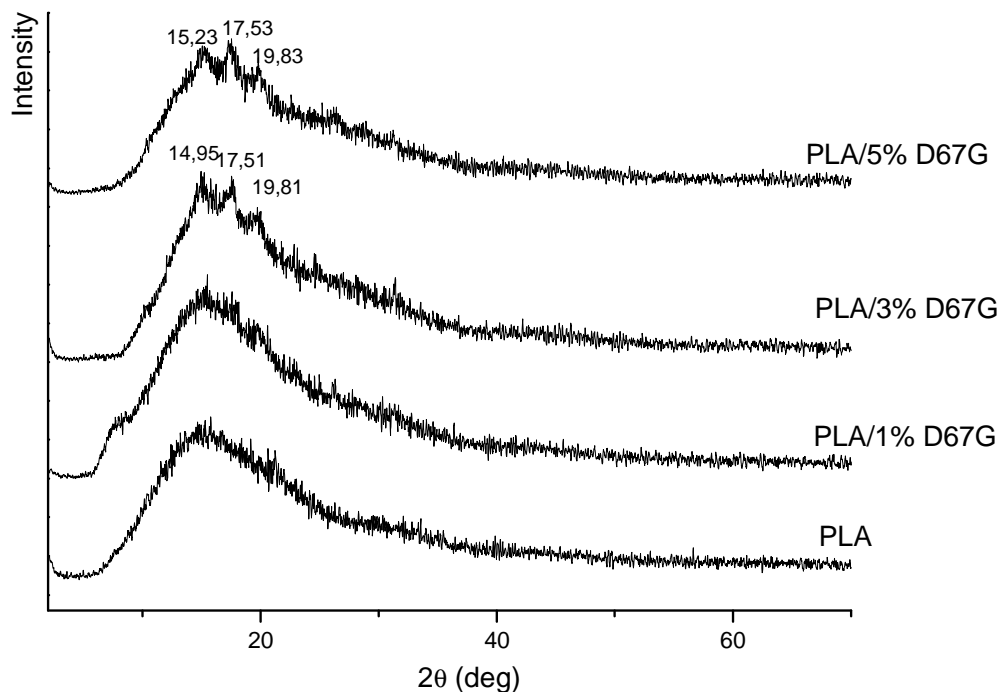
Figure 2.9.1 *X-ray diffraction spectrum of pure PLA and systems PLA /1% D67G, PLA /3% D67G and PLA /5% D67G nanocomposites*

Table 2.6 *Crystallinity percentage of PLA and PLA/D67G nanocomposites*

Sample	Xc(%)
PLA	-
PLA/1% D67G	-
PLA/3% D67G	4
PLA/5% D67G	8

2.10   MORPHOLOGY   OF   PLA/MMT   (Dellite   67G) NANOCOMPOSITES

The dispersion of the particles in the matrix of the PLA, the adhesion between the phases, the eventual exfoliation and / or intercalation of nano-charging systems PLA / D67G was evaluated by transmission electron microscopy (TEM) of the calendered films.

First the film was incorporated in an epoxy resin; after the solidification of the epoxy resin, the film was cut along the direction TD so that the surface for the TEM observation is that corresponding to the plane TD-ND (Figure 2.9.1).
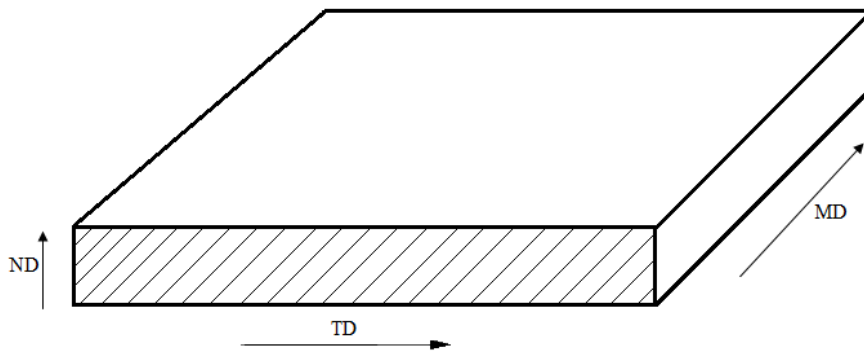
Figure 2.9.1 *Diagram of the three directions of the film*

Figure 2.9.2 A, B and C shows the micrographs for PLA/1% D67G, PLA/3% D67G and PLA/5% D67G nanocomposites.

For all compositions, it can be observed a good distribution and dispersion of the clay in the polymer matrix. The clay is also oriented (in machine direction that is the direction of exit from the extruder) as indicated by the arrow in the figures. From the images lamellar stacks of different dimensions are present. The thickness of the laminated stacks depends on the composition. In particular, it is of about 100-150 nm for the system PLA/1% D67G, of about 250 nm for the system PLA/3% D67G and of about 180-200 nm for the system PLA/5% D67G. It can be observed smaller lamellar stacks, respect the average values reported above (corresponding to 1-2 layers of lamellae), but also bigger lamellar stacks, these increase their size increasing the concentration of clay in the nanocomposites (the biggest reach even size of 500 nm.
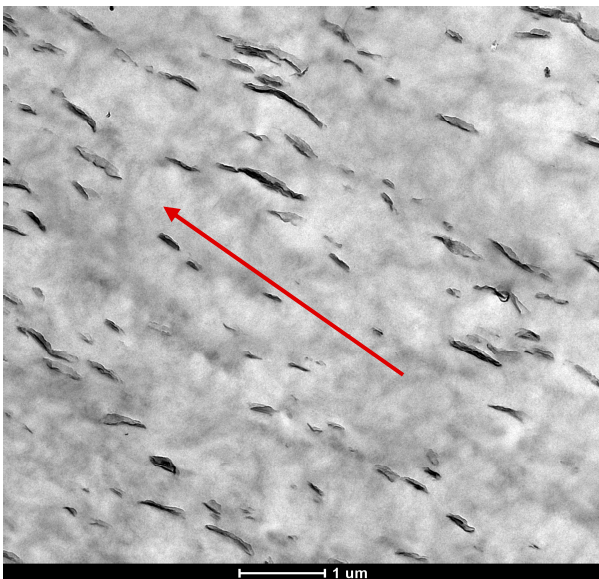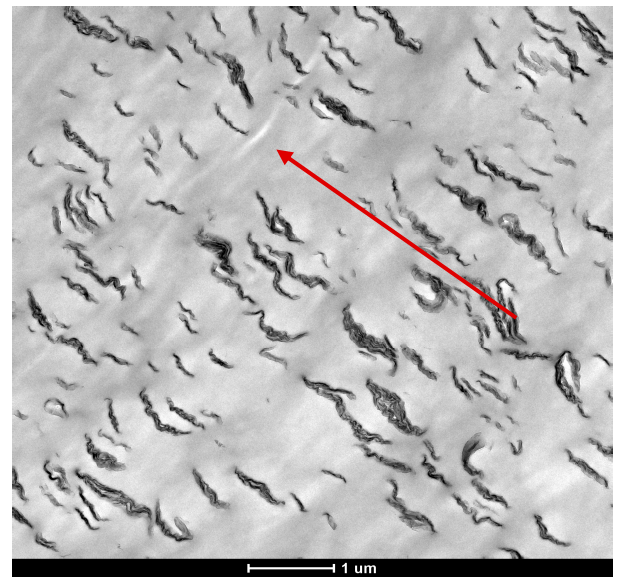
A   **B**
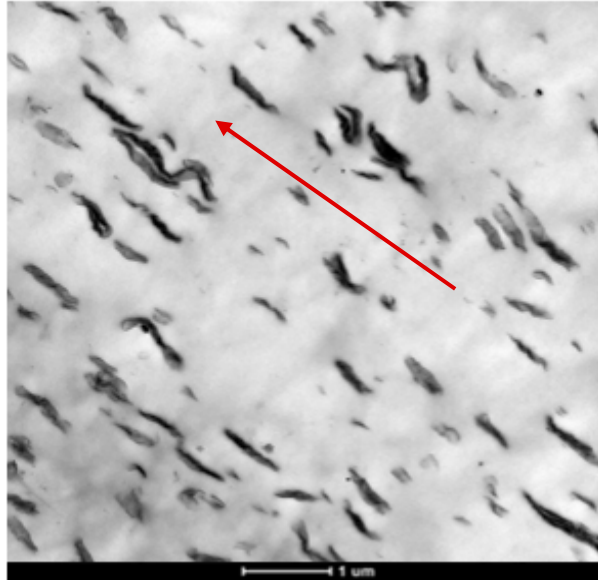
C

Figure 2.9.2 *Transmission electron micrographs of PLA/D67G films: A PLA/1% D67G, B PLA/3% D67G, C PLA/5% D67G*

Figure 2.9.3 A, B and C show micrographs at high magnification for PLA/1% D67G, PLA/3% D67G and PLA/5% D67G, respectively. From these images it is possible to calculate the distance between the clay layers. In particular, for all systems, there is an increase in the interlayer distance respect to that calculated for the clay powder (d = 3.5 nm): d ~ 7.80 nm for PLA/1% D67G, d ~ 9.20 nm for PLA/3% D67G and ~ 8.10 nm for PLA/5% D67G.

It is possible to conclude that PLA/MMT nanocomposites have mainly an intercalated morphology as observed by WAXD analysis. The intercalation is more pronounced for the PLA/3% D67G.
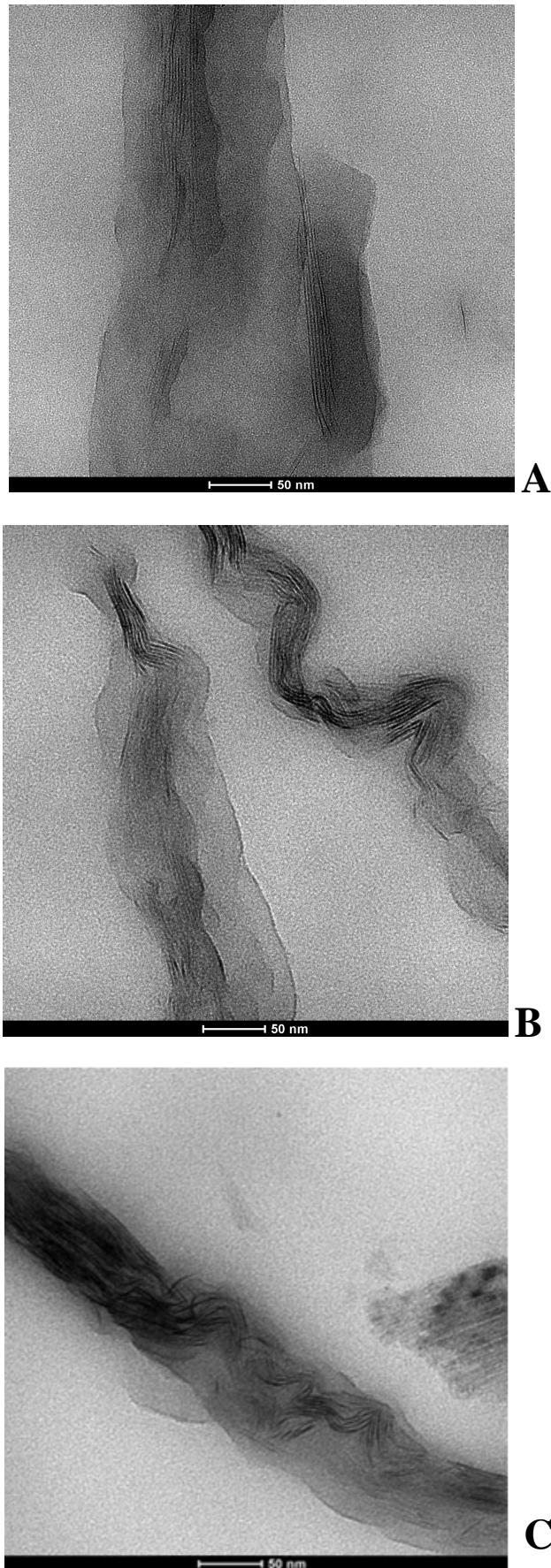
***Figure 2.9.3** Transmission electron micrographs at high magnification of film PLA/D67G (A PLA/1% D67G,   B PLA/3% D67G, C PLA/5% D67G)*

The structural and morphological analysis reported here highlights some important results: i) the process of extrusion and subsequent calendering was able to create, for PLA/Dellite 67G nanocomposites a good distribution, dispersion and orientation (in machine direction) of the clay in the PLA matrix; ii) this preparation process has allowed to obtain a morphology (as often found in the literature), partially intercalated [10,13,14] .

2.11 ATR SPECTROSCOPIC ANALYSIS OF PLA/TiO$_2$ NANOCOMPOSITES, PLA/ZnO COMPOSITES AND PLA/MMT(Dellite 67G) NANOCOMPOSITES

All samples were subjected to spectroscopic analysis ATR to detect the presence of new chemical bonds due to the inclusion of the filler within the polymer matrix to vary the composition (PLA/2-5%TiO$_2$, PLA/2-5% mTiO$_2$, PLA/1-3-5% ZnO and PLA/1-3-5% D67G). All the curves shown below are offset along the y-axis for an easy comparison.

The ATR spectra of PLA and all the nanocomposites films are shown in figure 2.10.1(A) , figure 2.10.2(A) and 2.10.3(A) in the range from 4000 to 1500 cm^{-1} and   in figure 2.10.1(B) , figure 2.10.2(B) and 2.10.3(B) in the range from 1500 to 400 cm^{-1}. The PLA is shown for comparison in all the figures. In all the figures A, the PLA spectrum shows CH$_3$ stretching at 3000–2940 cm^{-1}, the C=O stretching at 1761 cm^{-1} , characteristic of ester bonds. In all the figures B, the PLA spectrum shows: in the range from 1452 to 1381 cm^{-1} CH$_3$ bending and the O–C=O stretching at 1190–1090 cm^{-1}, characteristic of ester bonds[15]. From the graphs, for all composites and nanocomposites, are not observed differences between the various curves shown, respect PLA. The typical peaks of TiO$_2$, and MMT nanoparticles and

ZnO particles (see Figure 2.1.3, 2.4.3 and 2.7.3, Chapter 2) in these spectra are not visible, because their peaks are overlapped by those of PLA. Furthermore it is not present the appearance of new peaks for any of the binary mixtures under examination, indicating that there is no formation of new chemical bonds between the matrix and the fillers.
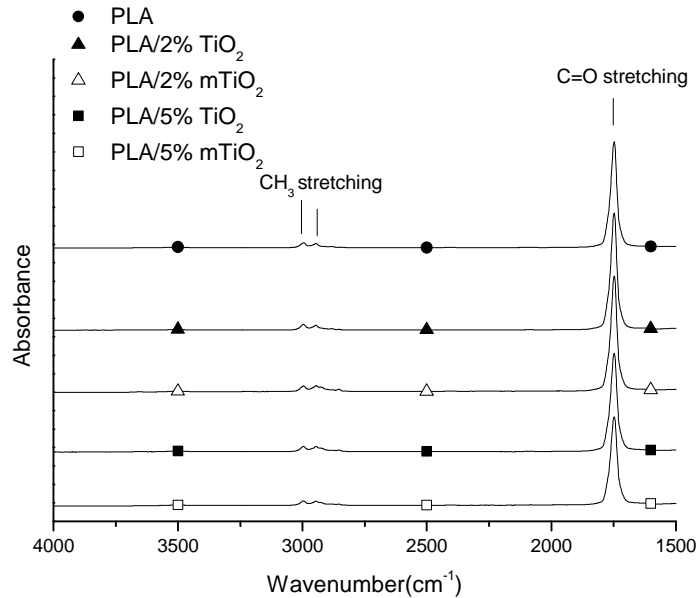
A
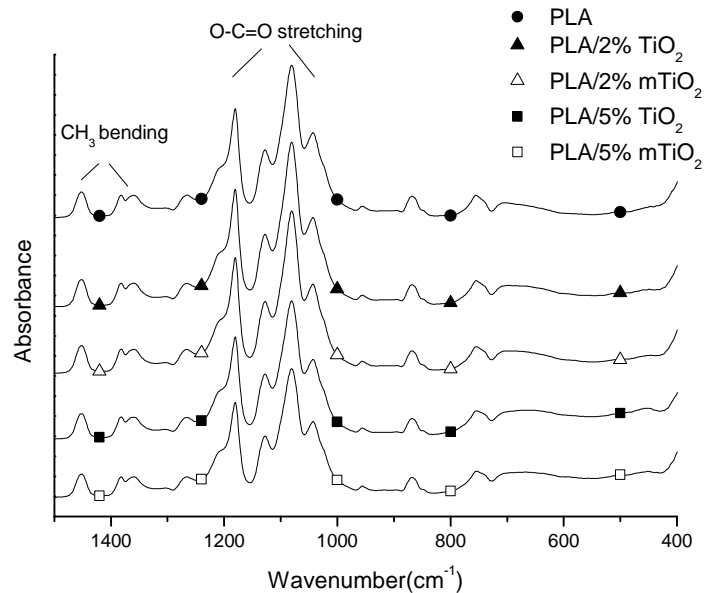
B

Figure 2.10.1 *FTIR-ATR of PLA, PLA/2% TiO$_2$; PLA/2% mTiO$_2$, PLA/5% TiO$_2$, PLA/5% m TiO$_2$ films in the range of wave number from 4000 to 1500 (A) and from 1500 to 400 (B)*
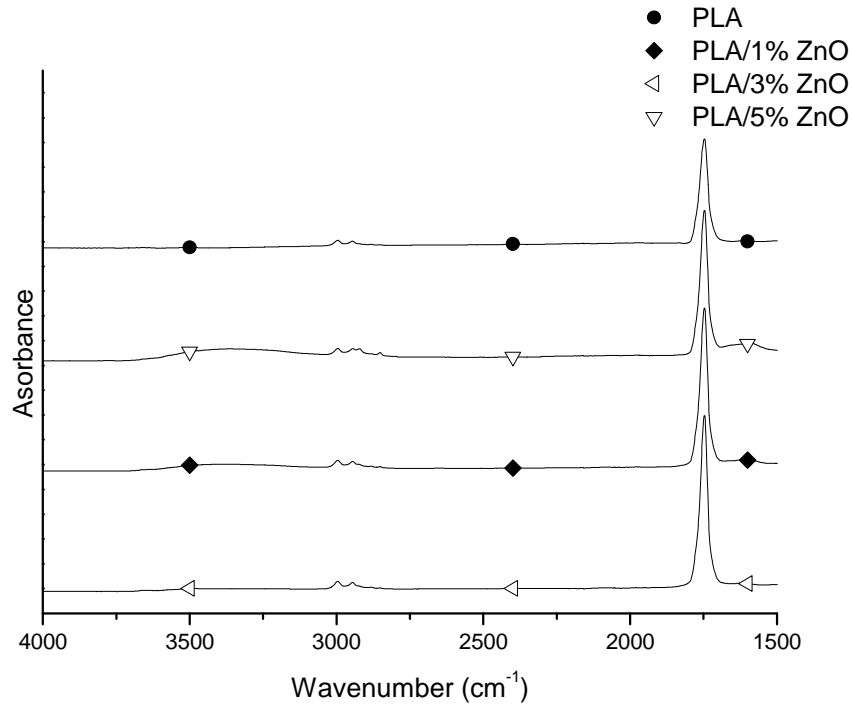
A
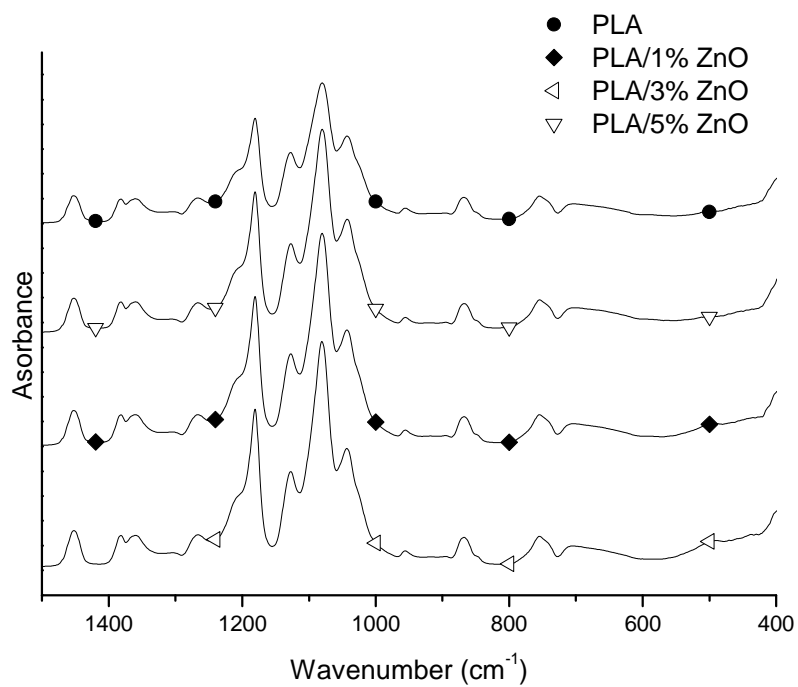
B

Figure 2.10.2. *FTIR-ATR of PLA, PLA/1% ZnO, PLA/3% ZnO, PLA/5% ZnO films, in the range of wave number from 4000 to 1500 (A)and from 1500 to 500 (B)*
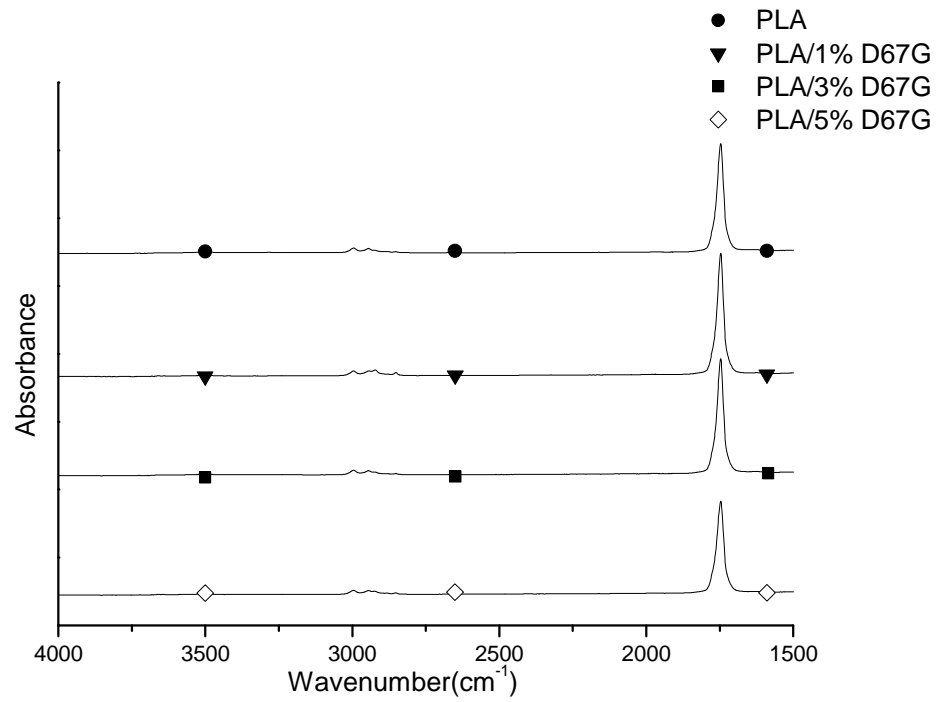
A
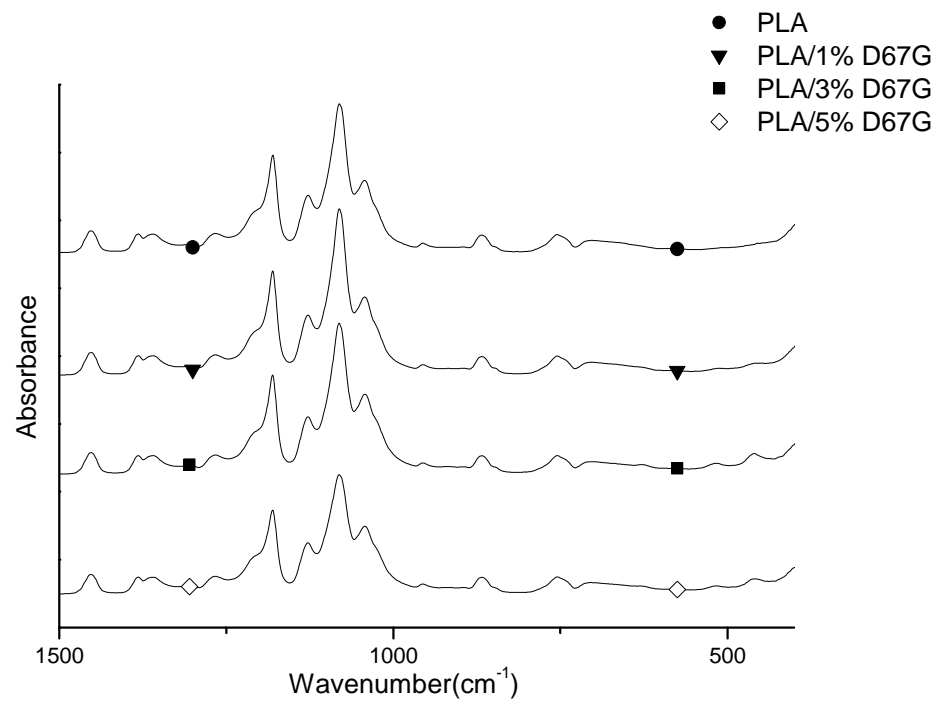
B

Figure 2.10.3. *ATR of PLA/D67G, PLA/1% D67G, PLA/3% D67G, PLA/5% D67G films in the range of wave number from 4000 to 1500 (A), from 1500 to 400 (B)*

REFERENCES

[1] "Metodi spettroscopici nella chimica organica organica" M. Hesse, H. Meier, B. Zeeh 1996 Edises ISBN 8879590812.

[2] "Synthesis of Undoped ZnO nanoparticles by spray pyrolysis" C. Rossignol, M. Verelst, J. Dexpert-Ghys and S. Rul Advances in Science and Technology vol. 45 2006 pp 237-241.

[3] "Poly(3-hydroxybutyrate)/ZnO Bionanocomposites with Improved Mechanical, Barrier and Antibacterial Properties" Ana M. Díez-Pascual and Angel L. Díez-Vicente, International Journal of Molecular Sciences 15: 10950- 10973 (2014) .

[4] "Effect of silane-modified ZnO on morphology and properties of bionanocomposites based on poly(ester-amide) containing tyrosine linkages" A. Abdolmaleki, S. Mallakpour, S. Borandeh, Polym. Bull. 2012, 69, pp. 15–28.

[5]"Formation of rod-like zinc oxide microcrystals in homogeneous solution" M. Andrés Vergés, A. Mifsud, C. J. Serna, , J. Chem. Soc. Farday Trans, 1990, 86(6), pp. 959-963.

[6] "PLA-ZnO nanocomposite films: Water vapor barrier properties and specific end-use characteristics" R.Pantani, G. Gorrasi, G. Vigliotta, M. Murariu, P. Dubois. European Polymer Journal(2013), 49/11, pp. 3471-3482.

[7] "The application of complex multiple forklike ZnO nanostructures to rapid and ultrahigh sensitive hydrogen peroxide biosensors" Z. Yang, X.L. Zong, Z.Z. Ye, B.H. Zhao, Q.L. Wang, P. Wang Biomaterials, 31 (2010), pp. 7534–7541.

[8] "Structure analysis of montmorillonite crystallites by convergent-beam electron diffraction" T Beermann, O Brockamp - Clay Minerals, 2005.

[9] "Rubber clay Nanocomposites industrial applications" ; Maurizio Galimberti, Padova, 10 November 2005.

[10] "Influence of Crystallization on Intercalation, Morphology, and Mechanical Properties of Polypropylene/Clay Nanocomposites" Pralay Maiti, Pham Hoai Nam, and Masami Okamoto, Advanced Polymeric Materials Engineering, Graduate School of Engineering, Toyota Technological Institute, Hisakata 2-12-1, Tempaku, Nagoya 468-8511, Japan Naoki Hasegawa and Arimitsu Usuki Toyota Central R&D Labs., Inc., Nagakute, Aichi 480-1192, Japan Received May 15, 2001; Revised Manuscript Received December 27, 2001.

[11]"Poly(ethylene terephthalate) ionomer based clay nanocomposites produced via melt extrusion" Grant D. Barber, Bret H. Calhoun, Robert B. Moore, School of Polymers and High Performance Materials, The University of Southern Mississippi, 118 College Drive #10076, Hattiesburg, MS 39406-0001, USA Available online 13 June 2005.

[12] "Structure and process relationship of electrospun bioabsorbable nanofiber membranes" Xinhua Zong, Kwangsok Kim, Dufei Fang, Shaofeng Ran, Benjamin S. Hsiao, Benjamin Chu. Research Inc., P.O. Box 1336, Stony Brook, NY 11790, USA.

[13] "Polymer-layered silicate nanocomposites: an overview" Peter C. LeBaron, Zhen Wang, Thomas J. Pinnavaia Department of Chemistry, Center for Fundamental Materials Research and Composite Materials and Structure Center, Michigan State Uniĺersity, East Lansing, MI 48824, USA.

[14] "Polylactic acid nanocomposites: comparison of their properties with montmorillonite and synthetic mica (II)" Jin-Hae Changa, Yeong Uk Ana, Donghwan Choa, Emmanuel P. Giannelisb, 2003.

[15] "Preparation and Characterization of Poly(Lactic Acid)- g-Maleic Anhydride+Starch Blends" Victor H. Orozco, Witold Brostow,Wunpen Chonkaew, Betty L. Lo´pez, Mocromulecular Symposia, (2009), 277, pp. 69-80.

CHAPTER 3
THERMAL AND THERMOGRAVIMETRIC ANALYSIS

3.1 THERMAL ANALYSIS

Calorimetric analysis was performed to determine, in addition to the thermal properties of the pure component, the influence of fillers and composition on the glass transition (T_g), the melting (T_m) and the cold crystallization (T_{cc}) temperature of PLA.

3.1.1 Thermal analysis of PLA/TiO$_2$ nanocomposites

Figure 3.1.1 shows the thermograms of PLA/TiO$_2$ nanocomposites, films obtained by compression moulding, in the temperature range from 40 to 200°C. The curves are shifted along the y axis to illustrate the trends. The heating rate used is 10°C/min under N$_2$ atmosphere.

The plain PLA presents the glass transition temperature at 62°C followed by an exothermic peak extending from about 85 to 136°C. Its maximum, taken as cold crytallization temperature (T_{cc}) is 119 ° C. Then there is an endothermic peak which extends from about 150 to 190°C. The peak maximum, taken as the melting temperature (T_m), is 173° C.

The thermoanalytical curves of PLA/TiO$_2$ nanocomposites present the same thermal behaviour as that of PLA.

The T_g and T_m values, reported in Table 3.1, indicate that TiO$_2$ nanoparticles have not effect on the thermal parameters of PLA. The T_{cc} values, reported in table 3.1 too, are slightly influenced by the presence of TiO$_2$ nanoparticles. In particular T_{cc} for PLA/2% TiO$_2$ nanocomposite is 119°C as neat PLA; T_{cc} for PLA/2% mTiO$_2$ and PLA/5% TiO$_2$ nanocomposites is 116°C; T_{cc} for PLA/5% mTiO$_2$ nanocomposite is 117°C.

The crystallization peaks of nanocomposites are not sharp as that of neat PLA and are characterized by the presence of a shoulder. These shoulders are present before the main crystallization peak and are centered at about 100°C (101°C for PLA/2% TiO_2 and PLA/2% $mTiO_2$ nanocomposites and 99°C for the PLA/5% TiO_2 and PLA/5% $mTiO_2$ nanocomposites). These shoulders are probably due to the formation of less perfect crystals that have time to melt and reorganize into crystals with higher structural perfection in correspondence of the main crystallization peak (see **NOTE**).
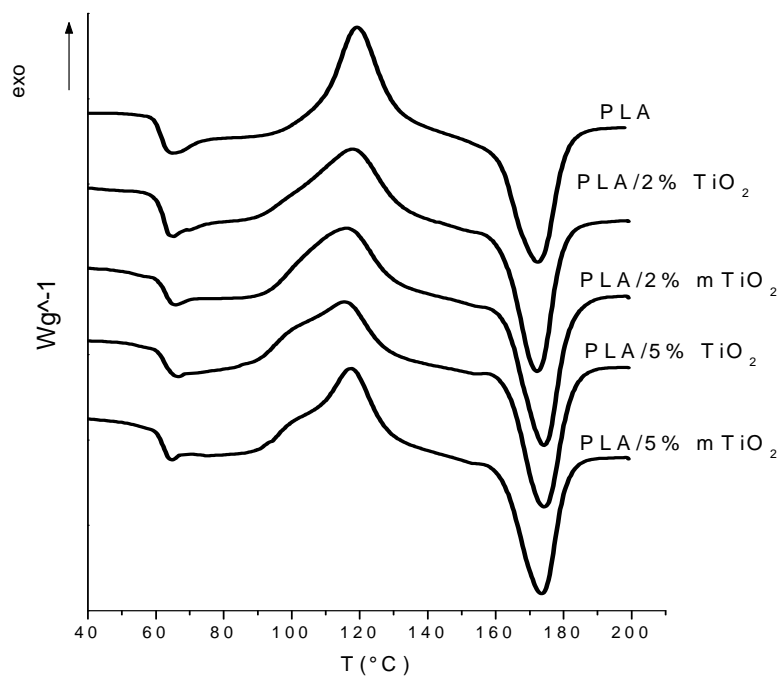
Figure 3.1.1 *DSC heating scans of PLA, PLA/2%TiO₂ , PLA/2% mTiO₂ , PLA/5%TiO₂ and PLA/5% mTiO₂*

Table 3.1. *Thermal properties of PLA, PLA/2%TiO₂ , PLA/2% mTiO₂ , PLA/5%TiO₂ and PLA/5% mTiO₂*

Sample	T_g (°C)	T_{cc} (°C)	T_m (°C)
PLA	62±1	119±1	173±1
PLA/2% TiO₂	62±1	119±1	172±1
PLA/2% mTiO₂	63±1	116±1	174±1
PLA/5% TiO₂	62±1	116±1	174±1
PLA/5% mTiO₂	62±1	117±1	174±1

3.1.2 Thermal analysis of PLA/ZnO composites and PLA/MMT(Dellite 67G) nanocomposites

Figures 3.1.2 and 3.1.3 show the thermograms of PLA/ZnO and PLA/MMT films, obtained by calender, in the temperature range from 40 to 200°C, respectively. The curves are shifted along the y axis to illustrate the trends. The heating rate used is 10 ° C / min under an inert atmosphere (N₂). The calorimetric parameters for PLA/ZnO and PLA/MMT systems are summarized in Table 3.2 and 3.3, respectively.

The PLA presents: i) the glass transition temperature at 61 ° C; ii) an exothermic peak that extends from about 85°C to 115°C. The maximum, taken as the temperature of cold crytallization temperature (Tcc), is at 100° C, iii) an endothermic peak which extends from about 155°C to 175°C. The peak maximum, taken as the melting temperature (Tm), is 169°C.

The thermoanalytical curves of PLA/ZnO composites and PLA/MMT nanocomposites do not show significant differences compared to pure PLA. The extension of the endothermic and exothermic peaks, respectively crystallization and melting peaks, remain fairly unchanged as well as the corresponding maxima and the glass transition temperature of the PLA amorphous phase.

Comparing PLA/ZnO composites and PLA/MMT nanocomposites it is possible to observe that these systems are similar in the calorimetric

parameters. In particular the systems have the same Tm value and the PLA/ZnO composites show Tg and Tcc values of 1-2 °C higher than those of PLA/MMT nanocomposites. These results, for PLA/ZnO and PLA/MMT, are in agreement with those reported in the literature [1-4].
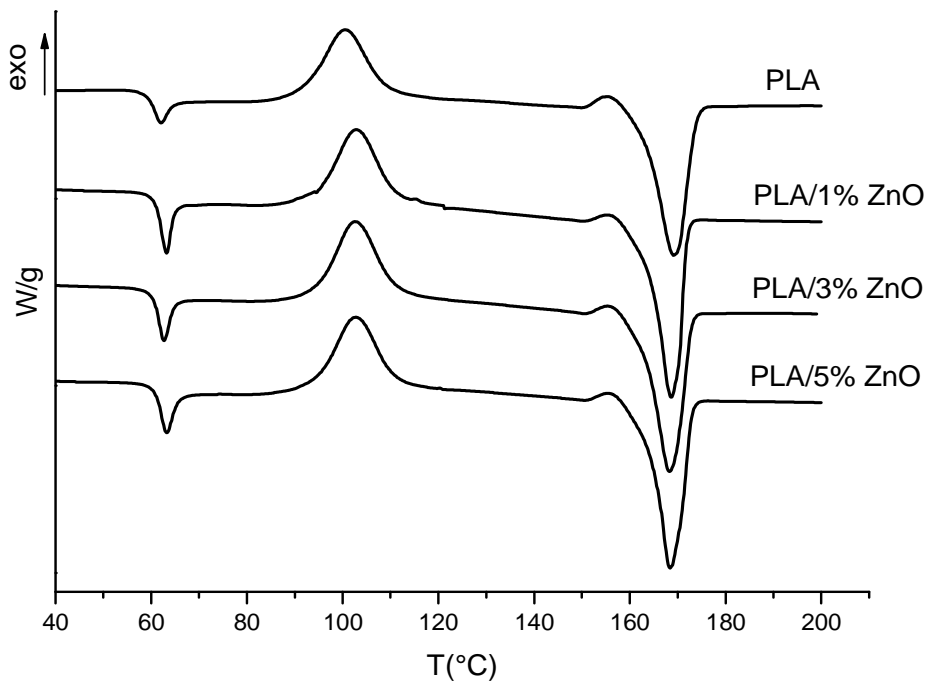
Figure 3.1.2 *DSC heating scans of PLA, PLA/1% ZnO, PLA/3% ZnO and PLA/5%ZnO composites*

Table 3.2. *Thermal properties of PLA, PLA/1% ZnO, PLA/3% ZnO and PLA/5% ZnOcomposites*

Sample	T_g (°C)	T_{cc} (°C)	T_m (°C)
PLA	61±1	100±1	169±1
PLA/1% ZnO	62±1	103±1	169±1
PLA/3% ZnO	62±1	103±1	169±1
PLA/5% ZnO	62±1	103±1	169±1
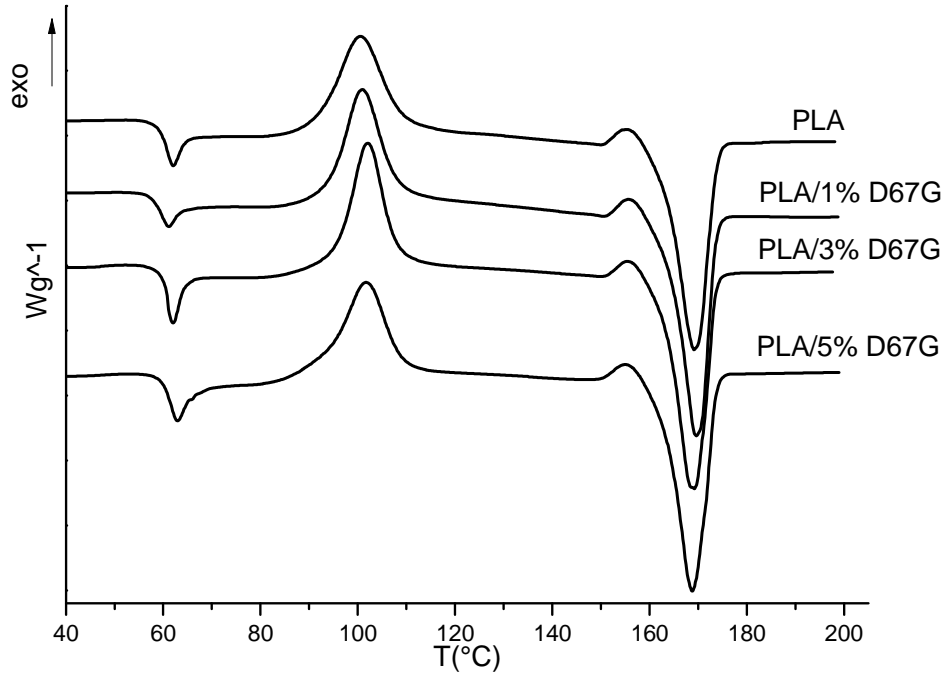
Figure 3.1.3 *DSC heating scans of PLA, PLA/1% D67G, PLA/3% D67G and PLA/5% D67G nanocomposites*

Table 3.3. *Thermal properties of PLA, PLA/1% D67G, PLA/3% D67G and PLA/5% D67G nanocomposites*

Sample	T_g (°C)	T_{cc} (°C)	T_m (°C)
PLA	61±1	100±1	169±1
PLA/1% D67G	60±1	101±1	169±1
PLA/3% D67G	61±1	102±1	169±1
PLA/5% D67G	61±1	102±1	169±1

The different temperature values (Tm, Tcc and Tg) of PLA/TiO$_2$ respect to those of PLA/ZnO and PLA/MMT systems can be ascribed to the different films preparation methods.

It can be also concluded that the different fillers do not influence the cold crystallization process or the melting behaviour of PLA and do not alter the glass transition temperature of the polymer amorphous phase.

3.2 THERMOGRAVIMETRIC ANALYSIS

All thermogravimetric curves were recorded between 30 and 800°C by heating the samples at 20 ° C/minute under a reactive atmosphere (air).

From thermogravimetric analysis it is possible to extrapolate the onset (Tonset) and endset (Tendset) thermal degradation temperature and the temperature at which the degradation rate is maximum (Tmax). The Tonset is the temperature at which the weight loss is 5%, the Tendset is temperature in correspondence of the final plateau (no more weight variation), the Tmax is the temperature in correspondence of the peak of the first derivative of the thermogravimetric curve.

3.2.1 Thermogravimetric Analysis of PLA/TiO$_2$ nanocomposites

Figure 3.2.1 shows TGA curves of neat PLA, PLA/2% TiO$_2$, PLA/2% mTiO$_2$, PLA/5% TiO$_2$ and PLA/5% mTiO$_2$ nanocomposites in the range from 280 to 360°C.
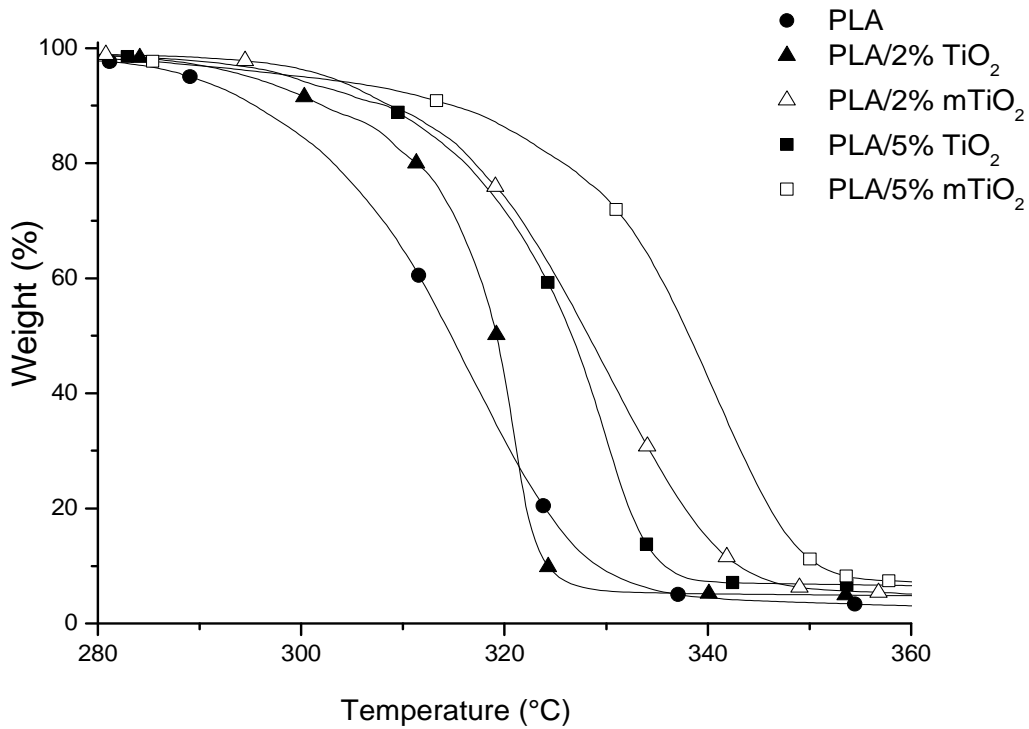
Figure 3.2.1 *Weight (%) of PLA, PLA/2% TiO$_2$, PLA/2% mTiO$_2$, PLA/5% TiO$_2$ and PLA/5% mTiO$_2$ nanocomposites*

Table 3.4. *Thermal degradation temperature when the weight loss is 5% (Tonset), the degradation rate is maximum (Tmax) and in correspondence of the final plateau (Tendset)*

SAMPLE	Tonset(°C)	Tmax(°C)	Tendset(°C)
PLA	289±1	317±1	340±1
PLA/2% TiO$_2$	295±1	319±1	329±1
PLA/2% mTiO$_2$	303±1	331±1	350±1
PLA/5% TiO$_2$	299±1	328±1	340±1
PLA/5% mTiO$_2$	300±1	344±1	355±1

Table 3.4 shows the values of thermogravimetric analysis when the weight loss is 5% (Tonset), the degradation rate is maximum (Tmax) and in correspondence of the final plateau (Tendset).

Neat PLA degrades in the range from Tonset 289 °C and Tendset 340 °C. The nanocomposites degradation range shifts to higher temperatures by increasing the TiO_2 content and with the modified TiO_2 nanoparticles. The PLA/2% TiO_2 nanocomposite presents a different behavior: the degradation process is faster than PLA and modified systems and it ends before the other samples. The process of degradation is faster in the nanocomposites with unmodified TiO_2 nanoparticles than the nanocomposites with modified TiO_2 nanoparticles.

In particular: PLA/2% TiO_2 nanocomposite has Tonset 295 °C and Tendset 329 °C; PLA/2% $mTiO_2$ nanocomposite has Tonset 303 °C and Tendset 350 °C ; PLA/5% TiO_2 nanocomposite has Tonset 299 °C and Tendset 340 °C and PLA/5% $mTiO_2$ nanocomposite has Tonset 300 °C and Tendset 355 °C.

Moreover Tmax of nanocomposites increases with the amount of TiO_2 nanoparticles, respect to PLA, and in particular in the systems containing the modified TiO_2 nanoparticles (Table 3.4).

The char of pure PLA at 500 °C is 0.4% ± 0.2%, whilst those of nanocomposites correspond to the amount of added nanoparticles in the different systems. The PLA/$mTiO_2$ systems have lower char respect to that of the PLA/TiO_2 systems due to the degradation of the perfluorocarbon thin layer covering the nanoparticles.

3.2.2 Thermogravimetric Analysis of PLA/ZnO composites

Figure 3.2.2 shows TGA curves of PLA and PLA/1% ZnO, PLA/3% ZnO and PLA/5% ZnO composites in the range from 230 to 40
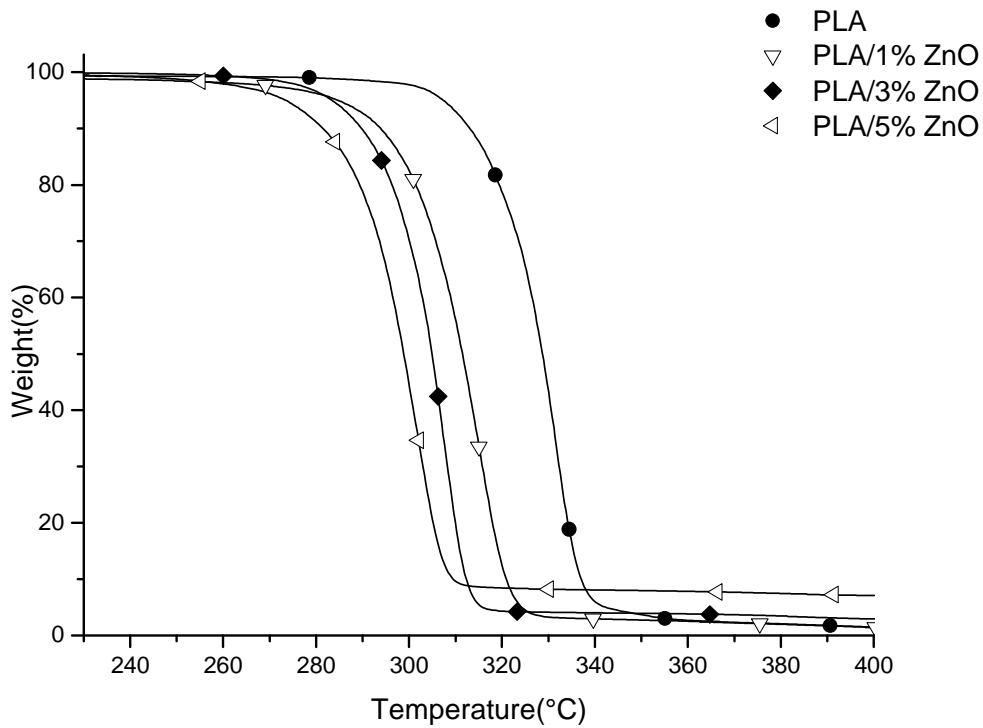
Figure 3.2.2 Weight (%) of PLA, PLA /1% ZnO, PLA / 3% ZnO and PLA /5% ZnO composites

Table 3.5. *Thermal degradation temperature when the weight loss is 5% (Tonset), the degradation rate is maximum (Tmax) and in correspondence of the final plateau (Tendset)*

SAMPLE	Tonset($°C$)	Tmax($°C$)	Tendset($°C$)
PLA	307±1	332±1	355±1
PLA/1% ZnO	285±1	317±1	330±1
PLA/3% ZnO	283±1	308±1	318±1
PLA/5% ZnO	273±1	303±1	315±1

Table 3.5 shows the values of thermogravimetric analysis when the weight loss is 5% (Tonset), the degradation rate is maximum (Tmax) and in correspondence of the final plateau (Tendset).

PLA degrades in the range from Tonset 307 °C and Tendset 355°C. The degradation range shifts to lower temperatures by increasing the ZnO content.

In details: PLA/1% ZnO has Tonset 285°C and Tendset 330°C; PLA/3% ZnO has Tonset 283°C and Tendset 318°C ; PLA/5% ZnO composite has Tonset 273°C and the Tendset 315°C.

Moreover for each composites, as expected, the value of Tmax decreases, respect to neat PLA, with the amount of ZnO particles (Table 3.5).

These results are in agreement with those found in literature and are explained considering that probably ZnO nanoparticles catalyze the depolymerization of PLA [5]. The char of pure PLA at 500°C is 0.4% ± 0.2%, for all the PLA/ZnO composites it corresponds with the percentage of fillers present in the samples (1, 3 and 5%).

3.2.3 Thermogravimetric Analysis of PLA/MMT nanocomposites

Figure 3.2.3 shows TGA curves of neat PLA and PLA/1% D67G, PLA/3% D67G and PLA/5% D67G nanocomposites in the range from 280 to 500°C.
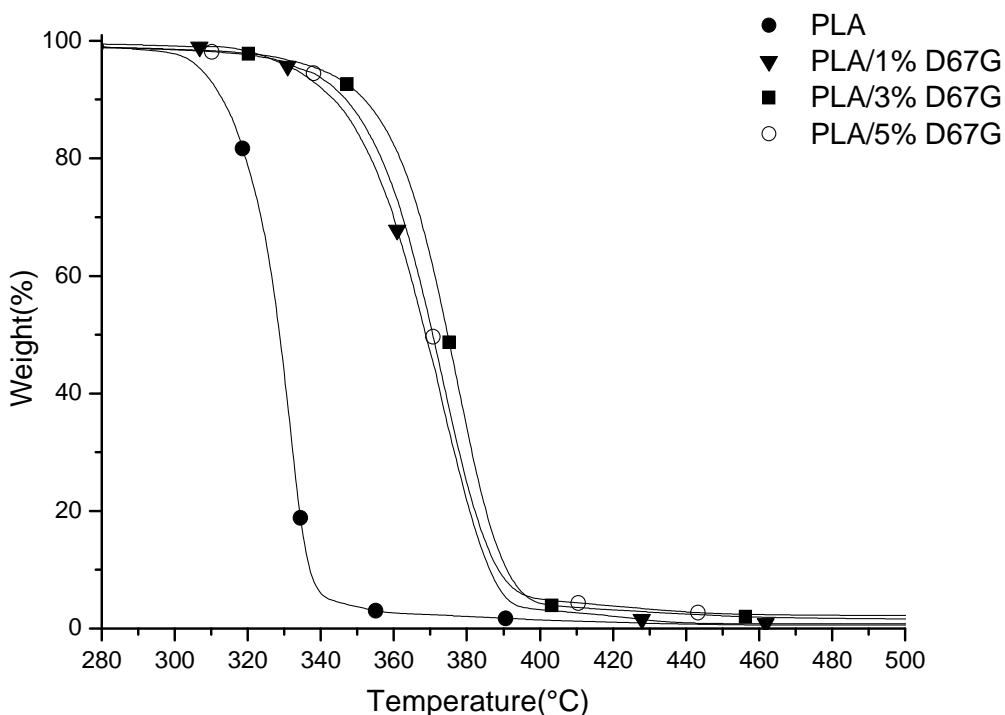
Figure 3.2.3 *Weight (%) of PLA, PLA /1% D67G, PLA /3% D67G and PLA /5% D67G nanocomposites*

Table 3.6. *Thermal degradation temperature when the weight loss is 5% (Tonset), the degradation rate is maximum (Tmax) and in correspondence of the final plateau Tendset*

SAMPLE	Tonset($^\circ$C)	Tmax($^\circ$C)	Tendset($^\circ$C)
PLA	307±1	332±1	355±1
PLA/1% D67G	320±1	372±1	397±1
PLA/3% D67G	328±1	377±1	402±1
PLA/5% D67G	324±1	373±1	399±1

Table 3.6 shows the values of thermogravimetric analysis when the weight loss is 5% (Tonset), the degradation rate is maximum (Tmax) and in correspondence of the final plateau (Tendset).

Neat PLA degrades in the range between Tonset 307°C and Tendset 355°C. In the case of PLA/MMT nanocomposite films, onset and end set thermal degradation temperatures (i.e. the degradation process) are shifted to higher temperatures when increasing MMT nanoparticles content.

The addition of MMT in the polymer matrix influences deeply the thermal stability of PLA for all PLA/MMT nanocomposites. In particular for the PLA /3% D67G system is found the best increase in stability respect to PLA/1% D67G and PLA/5% D67G nanocomposites. In details : PLA/1% D67G nanocomposite has Tonset 320°C and Tendset 397°C; PLA/3% D67G nanocomposite has Tonset 328 °C and Tendset 402°C ; for PLA/5% D67G nanocomposite has Tonset 324°C and Tendset 399°C. This can probably be attributed to the better intercalation found for PLA /3% D67G (see TEM analysis, Chapter 2) respect to the other two systems.

The Tmax of the PLA/3% D67G is 4-5 degrees higher than the other two composites and about 45 degrees than the PLA (Table 3.6).

The char of pure PLA at 500°C is 0.4% ± 0.2%, for all the PLA/MMT nanocomposites, the char at 500°C does not correspond with the percentage of fillers present in the samples (1, 3 and 5%) because the MMT is organically modified with quaternary ammonium salt, the organic part degrades during the heat treatment.

The TGA analysis has shown that TiO_2 and MMT nanoparticles increase the PLA thermal stability, whereas ZnO particles have an opposite effect.

NOTE

In order to investigate the nature of the shoulder present in the cold crystallization peaks of PLA/TiO_2 nanocomposites, all the films were subjected to the following DSC program:

The samples were heated from 25°C a 110°C at 20°C/min and then rapidly cooled from 110°C to 25°C at 50°C/min. The temperature 110°C has been

chosen because it is the temperature between the first (shoulder) and the second crystallization peak. After these two runs the samples were taken from DSC and their structure was investigate by WAXD. In figure 3.1.4 the X ray diffraction patterns for all the PLA/TiO$_2$ films are reported. At 110°C, all the nanocomposites display the same structure of neat PLA. In particular are present peaks at 2θ=16.6°, 18.9° and 22.3° which respectively correspond to the (110/200), (203) and (015) plane of PLA α-form orthorhombic crystal lattice[6-8]. This result means that the shoulder in the cold crystallization peak of nanocomposites can not be ascribed to the crystallization of a different PLA form. Consequently, we believe that that these shoulders are due to the formation of less perfect crystals that have time to melt and reorganize into crystals with higher structural perfection. The phenomenon of crystallization-melting crystallization can be ascribed to the presence of TiO$_2$ nanoparticles that influence the crystallization process of PLA.
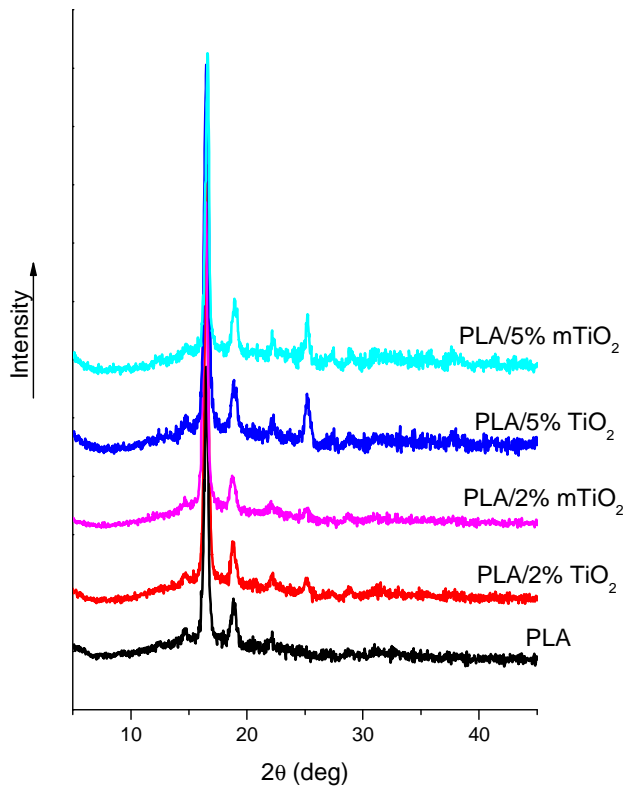
Figure 3.1.4 *X-ray diffraction spectra of PLA/TiO$_2$ nanocomposites after DSC heating at 110°C*

REFERENCES

[1] "PLA-ZnO nanocomposite films: Water vapor barrier properties and specific end-use characteristics" R.Pantani, G. Gorrasi, G. Vigliotta, M. Murariu, P. Dubois. European Polymer Journal (2013), 49/11, pp. 3471-3482.

[2] "Antibacterial activity of ZnO nanorods prepared by a hydrothermal method" K.H. Tam, A.B. Djuri, C.M.N. Chan, Y.Y. Xi, C.W. Tse, Y.H. Leung, *et al.* Thin Solid Films, 516 (2008), pp. 6167–6174.

[3] "A Literature Review of Poly(Lactic Acid)" D. Garlotta, Journal of Polymers and the Environment, Vol. 9, No. 2, (2002).

[4] "Preparation and properties of nanocomposites based on poly(lactic acid) and functionalized TiO_2" Yan-Bing Luo, Wen-Da Li, Xiu-Li Wang, Da-Yun Xu, Yu-Zhong Wang, Acta Materialia Volume 57, Issue 11, June 2009, Pages 3182–3191.

[5] "High-performance polylactide/ZnO nanocomposites designed for films and fibers with special end-use properties" M. Murariu ,A. Doumbia , L. Bonnaud, AL. Dechief , Y. Paint , M. Ferreira, C. Campagne, E. Devaux ,P. Dubois, Biomacromolecules. 2011 May 9;12(5):1762-71. doi: 10.1021/bm2001445. Epub 2011 Apr 19.

[6] Mechanical properties and *in vitro* degradation of electrospun bio-nanocomposite mats from PLA and cellulose nanocrystals Q. Shi, C. Zhou, Y. Yue, W. Guo, Y. Wu, Q.Wu, Carbohydrate Polymers (2012), 90(1) pp. 301–308.

[7] "Influence of the calender temperature on the crystallization behaviors of polylactide spun-bonded non-woven fabrics" M.Puchalski, I. Krucinska , K. Sulak, M. Chrzanowski, H. Wrzosek. Textile Research Journal 2015, Vol. 85(5) 535–547.

[8] "Poly(lactic acid): Synthesis, Structures, Properties, Processing, and application" edited by Rafael A. Auras, Loong-Tak Lim, Susan E. M. Selke, Hideto Tsuji, Wiley (2011).

CHAPTER 4

MECHANICAL AND BARRIER PROPERTIES

4.1 TENSILE PROPERTIES OF PLA/TiO$_2$ NANOCOMPOSITE, PLA/ZnO COMPOSITE AND PLA/MMT(Dellite 67G) FILMS

The analysis of the stress-strain curves provides information on the behaviour of the samples under tensile deformation and determination of tensile parameters such as at yield and break points

 and the elastic modulus.

The tensile tests were carried out on films obtained by compression moulding (for PLA/TiO$_2$ samples) and by calender (for PLA/ZnO and PLA/MMT samples) as described in Chapter 1. The tensile properties of PLA/ZnO and PLA/MMT films have been studied in two directions, the machine direction (MD) and the transverse direction (TD).

Figure 4.1.1 shows stress-strain curves PLA/TiO$_2$ nanocomposites, compared with PLA; the figures 4.1.2 and 4.1.4 show the curves, respectively, for PLA/ZnO and PLA/MMT obtained in machine direction; and the figures 4.1.3 and 4.1.5 show the curves, respectively, for PLA/ZnO and PLA/MMT obtained in the transverse direction. Table 4.1 shows the mechanical parameters for PLA/TiO$_2$ nanocomposites; the tables 4.2 and 4.4 show the same mechanical values, respectively, for PLA/ZnO and PLA/MMT in machine direction and the tables 4.3 and 4.5 for PLA/ZnO and PLA/MMT in transverse direction, respectively.

From the figures it is clear that the PLA shows a poor plastic behaviour, differently from petroleum-based plastics, however it is possible to observe yielding, drawing and final rupture. The value of the elastic modulus, reported in the Table 4.1, is typical of the polylactic acid [1,2]. The samples show similar behaviour to that of pure PLA. The addition of TiO$_2$ nanoparticles causes an improvement in the values of deformation at break

(ε_b) and a slight reduction of σ_b, σ_y and of the modulus (E); to be noted that the elongation at yield parameters (ε_y) is not strongly influenced by the presence of TiO_2 nanoparticles.

The PLA/ZnO composites show a similar trend to that of pure PLA. PLA/ZnO composites have an increase of stress at yield and break parameters and of Young's modulus; these parameters increase with the increasing of ZnO content. The elongation at yield values does not change; the elongation at break values have an increase for the PLA/1% ZnO and PLA/3% ZnO composites, whereas the PLA/5% ZnO composites shows a decrease. Comparing the results obtained for the two directions is possible to say that there is anisotropy of the tensile properties of the samples and the mechanical properties are better in the machine direction respect to the transverse direction, as the tables 4.2 and 4.3 show.

The PLA/MMT nanocomposites show a similar trend to that of pure PLA. The binary nanocomposites exhibit an improvement in elongation at break. This improvement increases with the proportion of MMT for composite PLA/1% D67G and PLA/3% D67G and decreases for the composite PLA/5% D67G.

The tables 4.4 and 4.5 show that the parameters at yield (σ_y, ε_y) are not strongly influenced by the presence of MMT, there is only a slight influence in the curves obtained in the machine direction.

The Young's modulus increases quite significantly with the addition of MMT for all composites and analyzed for both directions, and the results agrees with the finding reported in other studies [3]. The addition of MMT causes, also, an improvement in the values of the deformation at break (ε_b) and a reduction of σ_b. To be noted that the yield strength parameters, (ε_y, σ_y) are not strongly influenced by the presence of MMT.

Also in this case the comparison of the values of the mechanical parameters for the two directions indicate that in the machine direction the samples

behave better than in transverse direction confirming the structural anisotropy.
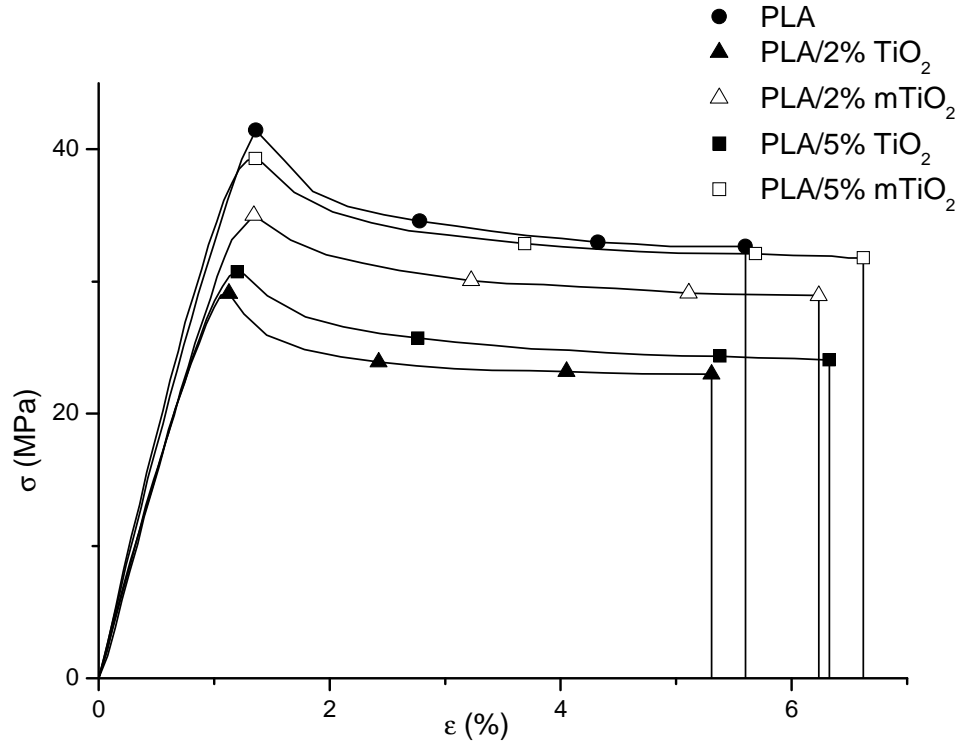
Figure 4.1.1* Stress-strain curves of *PLA, PLA/2% TiO₂, PLA/2% mTiO₂ , PLA/5% TiO₂, PLA/5% mTiO₂* *films*

Table 4.1. *Stress–strain parameters of PLA, PLA/2% TiO₂, PLA/2% mTiO₂,PLA/5% TiO₂, PLA/5% mTiO₂ films*

Sample	E (MPa)	σ_y (MPa)	ε_y (%)	σ_b (MPa)	ε_b (%)
PLA	3599 ± 228	41 ± 5	1.4 ± 0.1	33 ± 5	6 ± 3
PLA/2% TiO₂	3466 ± 276	29 ± 6	1.1 ± 0.1	23 ± 4	5 ± 3
PLA/2% mTiO₂	3225 ± 182	35 ± 5	1.3 ± 0.1	29 ± 4	6 ± 3
PLA/5% TiO₂	3396 ± 202	31 ± 4	1.2 ± 0.1	24 ± 3	6 ± 2
PLA/5% mTiO₂	3416 ± 308	39 ± 4	1.4 ± 0.1	32 ± 2	7 ± 8
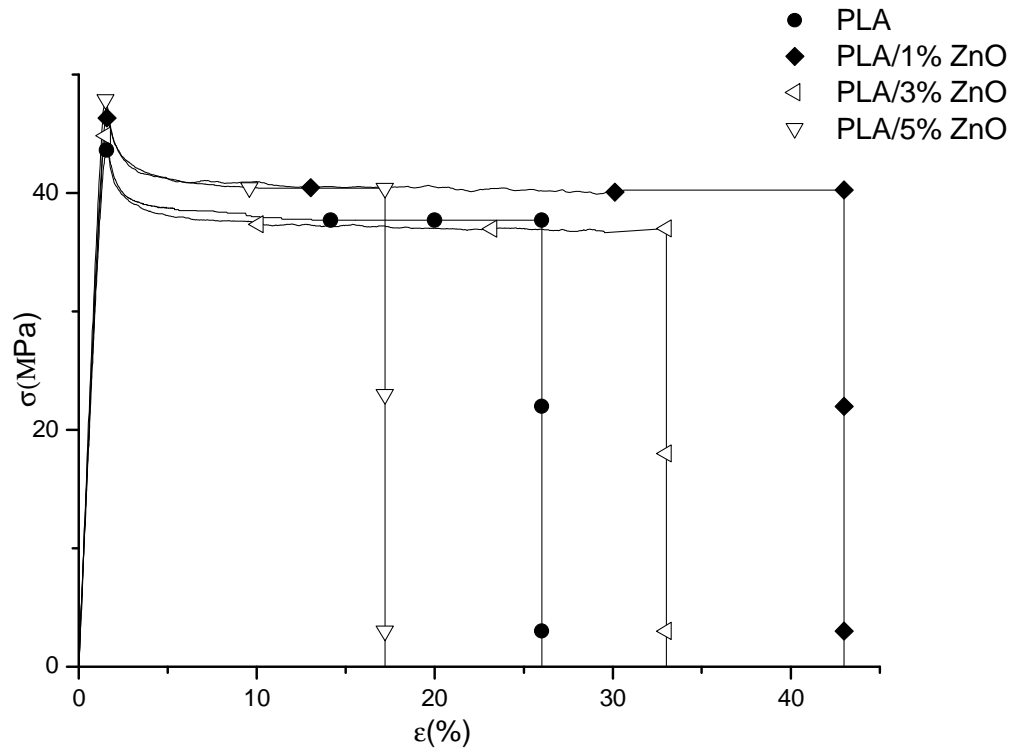
Figure 4.1.2 Stress-strain curves in machine direction of *PLA, PLA/1% ZnO, PLA/3% ZnO e PLA/5% ZnO films*
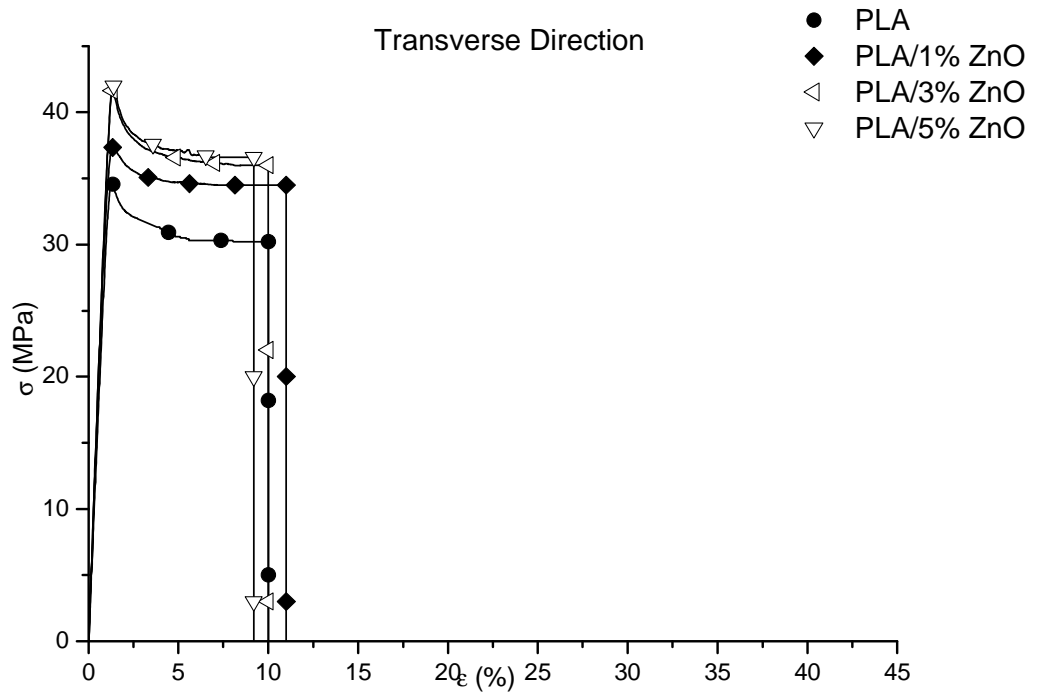
Figure 4.1.3 Stress-strain curves in transverse direction of *PLA, PLA/1% ZnO, PLA/3% ZnO e PLA/5% ZnO films*

Table 4.2. Stress–strain parameters in machine direction of *PLA, PLA/1% ZnO, PLA/3% ZnO e PLA/5% ZnO films*

Sample	E (MPa)	σ_y (MPa)	ε_y (%)	σ_b (MPa)	ε_b (%)
PLA	3470 ± 189	1.6 ± 0.1	44 ± 2	26 ± 5	38 ± 2
PLA/1% ZnO	3637 ± 131	1.6 ± 0.2	46 ± 2	43 ± 6	40 ± 3
PLA/3% ZnO	3575 ± 140	1.5 ± 0.1	45 ± 2	37 ± 3	33 ± 2
PLA/5% ZnO	3853 ± 107	1.5 ± 0.1	48 ± 3	17 ± 6	40 ± 3

Table 4.3. Stress–strain parameters in transverse direction of *PLA, PLA/1% ZnO, PLA/3% ZnO e PLA/5% ZnO films*

Sample	E (MPa)	σ_y (MPa)	ε_y (%)	σ_b (MPa)	ε_b (%)
PLA	3376 ± 393	35 ± 2	1.3 ± 0.1	30 ± 2	10 ± 4
PLA/1% ZnO	3671 ± 194	37 ± 4	1.3 ± 0.2	35 ± 4	11 ± 3
PLA/3% ZnO	3781 ± 115	42 ± 1	1.4 ± 0.1	36 ± 2	10 ± 5
PLA/5% ZnO	3854 ± 134	42 ± 2	1.4 ± 0.1	37 ± 2	9 ± 2
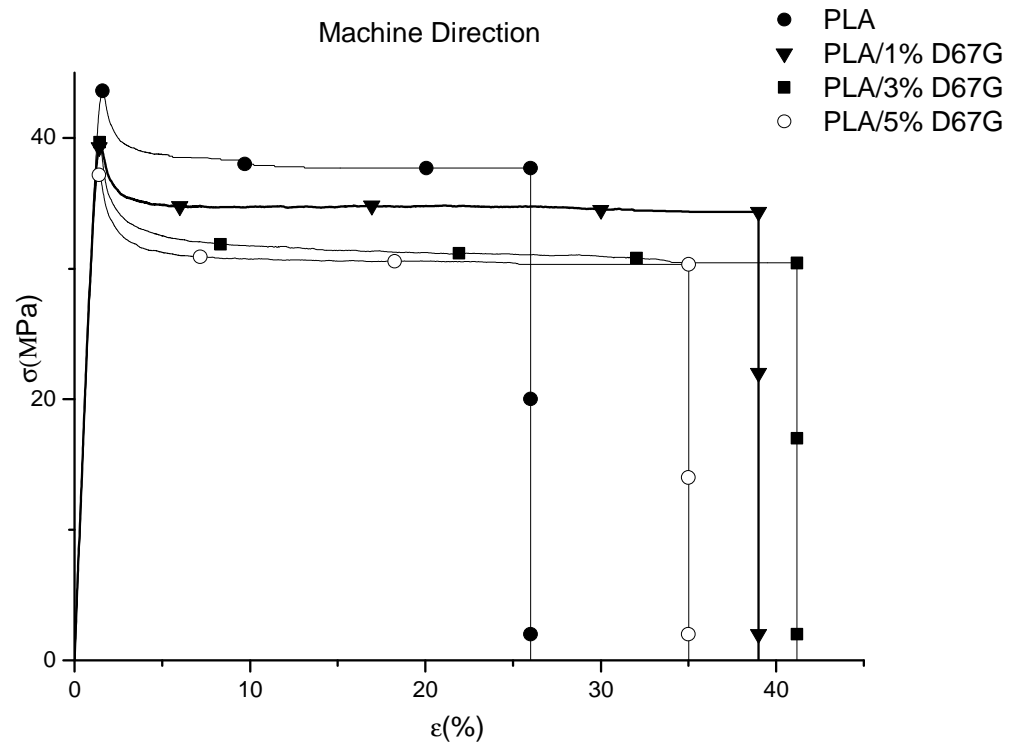
Figure 4.1.4 Stress-strain curves in machine direction of *PLA, PLA/1% D67G, PLA/3% D67G and PLA/5% D67G films*
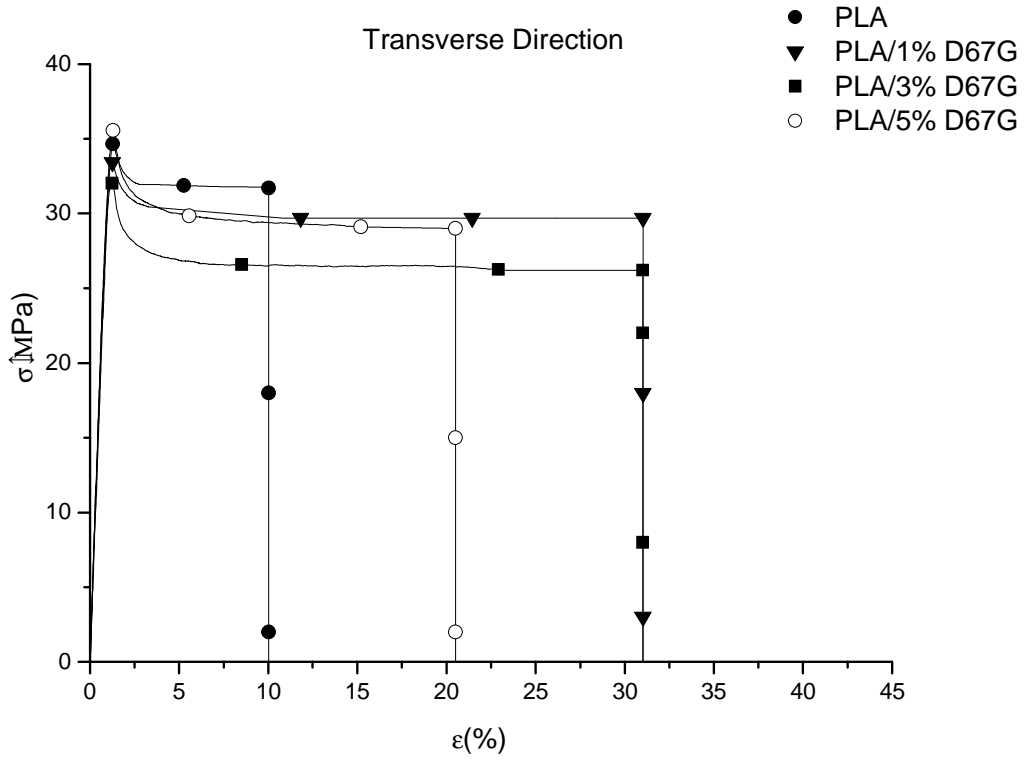
Figure 4.1.5 Stress-strain curves in transverse direction of *PLA, PLA/1% D67G, PLA/3% D67G and PLA/5% D67G films*

Table 4.4. Stress–strain parameters in machine direction of PLA, PLA/1% D67G, PLA/3% D67G and PLA/5% D67G films

Sample	E (MPa)	σ_y (MPa)	ε_y (%)	σ_b (MPa)	ε_b (%)
PLA	3470 ± 189	44 ± 2	1.6 ± 0.1	38 ± 2	26 ± 5
PLA/1% D67G	3622 ± 372	39 ± 5	1.4 ± 0.2	34 ± 4	39 ± 6
PLA/3% D67G	3530 ± 264	40 ± 3	1.4 ± 0.1	30 ± 2	41 ± 6
PLA/5% D67G	3550 ± 152	37 ± 4	1.4 ± 0.2	30 ± 3	35 ± 10

Table 4.5. Stress–strain parameters in transverse direction of *PLA, PLA/1% D67G, PLA/3% D67G e PLA/5% D67G films*

Sample	E (MPa)	σ_y (MPa)	ε_y (%)	σ_b (MPa)	ε_b (%)
PLA	3377 ± 393	35 ± 3	1.3 ± 0.1	32 ± 2	10 ± 4
PLA/1% D67G	3699 ± 207	33 ± 4	1.3 ± 0.1	31 ± 3	30 ± 5
PLA/3% D67G	3578 ± 256	32 ± 4	1.2 ± 0.1	26 ± 4	31 ± 6
PLA/5% D67G	3648 ± 228	36 ± 3	1.3 ± 0.1	29 ± 3	21 ± 6

From the results it can be stated that only for the composites with TiO_2 there is a decrease of the stress at break and yield values and a decrease of the Young's modulus. On the contrary, the presence of ZnO and MMT in the PLA matrix results in an improvement of the tensile properties of the material up to a certain composition. For higher compositions the properties undergo a decay. The best results for PLA/ZnO composites is obtained when the amount of ZnO is 1%. This is probably due to the good distribution and dispersion of particles, without aggregates in the sample PLA/1% ZnO as SEM analysis confirms. In the PLA/MMT nanocomposites the improvement of mechanical properties is not influenced by the amount of MMT.

4.1.2 Impact test of PLA/TiO_2 nanocomposite films

Impact test measure the energy necessary to break a notched sample subjected to high-rate loading with a pendulum hammer swinging through a fixed distance. The impact tests were conducted by subjecting the specimens (strips of 4mm thick) to crash through the Charpy pendulum. Knowing the pendulum energy (300 J) is obtained the energy absorbed by the sample. This energy is equivalent to the difference between the energy released when the pendulum is dropped and the energy associated to it in correspondence of the maximum path, after the sample breaking.

Table 4.6 shows the values of the force that the pendulum lost on impact with the specimen (F), the energy (U) absorbed by the samples at the break and the toughness (T), described as material's resistance to fracture; it is often expressed in terms of the amount of energy that a material can absorb before fracture. The results show an increase of the toughness of PLA/TiO_2 nanocomposites respect to PLA. In particular toughness doubles for the samples with 5% of TiO_2 (modified and unmodified) and it triples for the samples with 2% of TiO_2 (modified and unmodified). In other words, there is an increase of the toughness for all the composites but with better results for the samples with 2% of TiO_2 (modified and unmodified).

Table 4.6 *Impact tests for PLA, PLA/2-5% TiO$_2$ (modified and unmodified)*

Sample	F (N)	U (J)	T (KJ/m^2)
PLA	68 ± 12	0.02 ± 0.01	1 ± 0
PLA/2% TiO$_2$	116 ± 9	0.04 ± 0.01	3 ± 1
PLA/2% mTiO$_2$	116 ± 10	0.05 ± 0.00	3 ± 1
PLA/5% TiO$_2$	86 ± 12	0.02 ± 0.00	2 ± 1
PLA/5% mTiO$_2$	94 ± 10	0.03 ± 0.00	2 ± 1

4.2 O_2, CO_2 AND H_2O PERMEABILITY OF PLA/ TiO_2 NANOCOMPOSITE, PLA/ZnO COMPOSITE AND PLA/MMT(Dellite 67G) NANOCOMPOSITE FILMS

The measurements of oxygen and carbon dioxide permeability were carried out at a temperature of 23 °C and a relative humidity of 0% and the measurements of water vapour permeability were carried out at 23°C and 90% RH. These measurements were conduct on film with different

thickness: the PLA/TiO$_2$ films have a thickness about 130μm and the PLA/ZnO and PLA/D67G films about 60 μm.

4.2.1 Oxygen permeability of PLA/TiO$_2$ nanocomposite, PLA/ZnO composite and PLA/MMT nanocomposite films

The analysis of O$_2$ permeability were carried out at 23°C and 0%RH. The tables 4.5, 4.6 and 4.7 show the values of OTR and of oxygen permeability of the PLA film and its composites and nanocomposites.

For the PLA/ TiO$_2$ systems there is a reduction of about 11% in O$_2$ permeability respect to PLA for the system PLA/5% TiO$_2$; the other compositions do not present any variation compared to PLA.

The PLA/ZnO composites present an improvement of the barrier properties. In particular we have a decrease of the permeability of about 8% for PLA/3%ZnO and 17% for PLA/1% ZnO and PLA/5% ZnO. This results can be probably ascribe to due to the homogeneous distribution of ZnO particles (see Figure 2.6.2, 2.6.3 and 2.6.4, Chapter 2).

The results, for PLA/MMT nanocomposites, show that all the compositions lead to an improvement of the barrier, in particular the system PLA /1% D67G shows a decrease of the permeability of about 21%, the samples PLA/3% D67G and PLA/5% D67G have a reduction of O$_2$ permeability about 32%, compared to pure PLA. This decrease for higher composition of clay (>1%), could be due to the increase of crystallinity found in the systems PLA/3% D67G and PLA/5% D67G; in addition to the greater number of particles present in the matrix PLA/D67G 3 and 5% do not present different permeability. On the other hand, increasing the composition the morphological analysis has shown the presence of bigger clay agglomerates (see Figure 2.9.2, Chapter 2). These agglomerates prevent a more drastic reduction of the permeability for the sample containing the 5% of MMT.

Moreover, the MMT in the matrix, especially if nanometric and submicrometric, affect the path of the O_2 gas molecules, which are forced to have a longer path in the polymeric film.

The interpretation of the results, for the composites and nanocomposites, is somewhat complex since the permeability of a composite polymer depends on numerous factors. First you need to consider the crystalline phase and the amorphous polymer. The crystalline phase is considered to be impermeable to gases and therefore the greater the crystalline fraction, the lower the permeability. Moreover, the presence of clay particles, especially if nanometric and micrometric sub, alters the path of gas molecules permeating that are forced to travel a longer path through the film. This theory proposed by Nielsen [4] presents a number of experimental deviations so that was recently proposed an alternative model [5,6] which takes into account not only the tortuous path of other factors such as the interface and the free volume of the region around the particles.

For all composites and nanocomposites these results are important considering that an inorganic phase is mixed with an organic phase. In the case where do not have a significant reduction of O_2 permeability, like for the PLA/TiO_2 nanocomposites, this is, however, a good result because the permeability of the systems is not increased compared to the permeability to the PLA.

Table 4.5 *OTR and O$_2$ permeability of PLA, PLA/2% TiO$_2$, PLA/2% mTiO$_2$, PLA/5% TiO$_2$, PLA/5% mTiO$_2$ films*

Sample	OTR (cm^3/(24hxm^2)	Permeability [(cm^3/(24hxm^2)]x(cm/bar)
PLA	144	2.24 ± 0.28
PLA/2% TiO$_2$	146	2.18 ± 0.18
PLA/2% mTiO$_2$	157	2.14 ± 0.20
PLA/5% TiO$_2$	155	1.98 ± 0.23
PLA/5% mTiO$_2$	136	2.24 ± 0.22

Table 4.6 *OTR and O$_2$ permeability of PLA, PLA/1% ZnO, PLA/3% ZnO e PLA/5% ZnO films*

Sample	OTR (cm^3/(24hxm^2)	Permeability [(cm^3/(24hxm^2)]x(cm/bar)
PLA	573	2.23 ± 0.22
PLA/1% ZnO	326	1.83 ± 0.03
PLA/3% ZnO	343	2.06 ± 0.10
PLA/5% ZnO	322	1.84 ± 0.06

Table 4.5 *OTR and O$_2$ permeability of PLA, PLA/1% D67G, PLA/3% D67G e PLA/ 5% D67G films*

Sample	OTR (cm^3/(24hxm^2)	Permeability [(cm^3/(24hxm^2)]x(cm/bar)
PLA	573	2.23 ± 0.22
PLA/1% D67G	458	1.76 ± 0.01
PLA/3% D67G	385	1.52 ± 0.03
PLA/5% D67G	380	1.52 ± 0.07

4.2.2 Carbon dioxide permeability of PLA/TiO$_2$ nanocomposite, PLA/ZnO composite and PLA/MMT nanocomposite films

Like the oxygen and water vapour barrier properties, also the carbon dioxide barrier property is of particular importance on food packaging application. The analysis of CO_2 permeability were carried out at 23 °C and 0%RH. The Tables 4.8, 4.9 and 4.10 show the values of CO_2 transmission rate (TR) and permeability of the films of PLA and nanocomposites. The results show that the PLA/TiO$_2$ systems have not an improvement of the barrier properties whereas the PLA/ZnO and PLA/D67G systems show a decreased permeability to CO_2. For PLA/ZnO composites it has a reduction of carbon dioxide permeability about 13% respect to PLA. For the PLA/D67G composites the improvements of the barrier properties is bigger. It is possible to see a decrease of carbon dioxide permeability of 14% for the nanocomposite PLA/3% D67G, 17% for PLA/5% D67G and 19% for PLA/1% D67G. Not only the best distribution of the particles but also the crystallinity increases the barrier properties of the systems.

Table 4.7 *CO$_2$TR and CO$_2$ permeability of PLA, PLA/2% TiO$_2$, PLA/2% mTiO$_2$, PLA/5% TiO$_2$, PLA/5% mTiO$_2$ films*

Sample	CO$_2$TR (cm^3/(24hxm^2))	Permeability [(cm^3/(24hxm^2)]x(cm/bar)
PLA	423	5.14 ± 0.21
PLA/2% TiO$_2$	403	5.46 ± 0.18
PLA/2% mTiO$_2$	420	5.53 ± 0.20
PLA/5% TiO$_2$	483	6.52 ± 0.15
PLA/5% mTiO$_2$	589	7.53 ± 0.18

Table 4.9 *CO$_2$TR and CO$_2$ permeability of PLA, PLA/1% ZnO, PLA/3% ZnO and PLA/5% ZnO films*

Sample	CO$_2$TR (cm^3/(24hxm^2))	Permeability [(cm^3/(24h*m^2)]x(cm/bar)
PLA	1740	8.00 ± 0.20
PLA/1% ZnO	1001	7.05 ± 0.96
PLA/3% ZnO	1031	6.96 ± 0.04
PLA/5% ZnO	1048	6.86 ± 0.26

Table 4.10 *CO$_2$TR and CO$_2$ permeability of PLA, PLA/1% D67G, PLA/3% D67G and PLA/5% D67G films*

Sample	CO$_2$TR (cm^3/(24hxm^2))	Permeability [(cm^3/(24hxm^2)]x(cm/bar)
PLA	1740	8.00 ± 0.20
PLA/1% D67G	1473	6.47 ± 0.64
PLA/3% D67G	1328	6.93 ± 0.51
PLA/5% D67G	1257	6.65 ± 0.46

4.2.3 Water vapour permeability of PLA/TiO$_2$ nanocomposite, PLA/ZnO composite and PLA/MMT nanocomposite films

Biodegradable polyesters, like PLA, are moisture sensitive [7,8], so the analysis of permeability to water vapour is of fundamental importance for developing new packaging materials. Water molecules, at different activity and temperatures, could have effect on the microbial growth and influence the shelf life of the packed products.

The analysis of the water vapour permeability were performed at 23°C and 90% RH.

The results, reported in Tables 4.11, 4.12 and 4.13, do not show significant variation for the composites and nanocomposites, and they are in agreement with literature data [7,9,10].

Table 4.11 *WTR and H_2O permeability* of *PLA, PLA/2% TiO_2, PLA/2% $mTiO_2$, PLA/5% TiO_2, TiO_2, PLA/5% $mTiO_2$ films*

Sample	WTR ($cm^3/(24hxm^2)$)	Permeability $[(cm^3/(24hxm^2)]x(cm/bar)$
PLA	26	0.31 ± 0.01
PLA/2% TiO_2	24	0.33 ± 0.01
PLA/2% $mTiO_2$	25	0.31 ± 0.01
PLA/5% TiO_2	25	0.32 ± 0.01
PLA/5% $mTiO_2$	32	0.37 ± 0.04

Table 4.12 *WTR and H_2O permeability of PLA, PLA/1% ZnO, PLA/3% ZnO e PLA/5% ZnO films*

Sample	WTR ($cm^3/(24hxm^2)$)	Permeability $[(cm^3/(24hxm^2)]x(cm/bar)$
PLA	55	0.21 ± 0.01
PLA/1% ZnO	41	0.25 ± 0.01
PLA/3% ZnO	42	0.25 ± 0.01
PLA/5% ZnO	42	0.24 ± 0.02

Table 4.7 *WTR and H_2O permeability of PLA, PLA/1% D67G, PLA/3% D67G e PLA/5% D67G films*

Sample	WTR ($cm^3/(24hxm^2)$)	Permeability $[(cm^3/(24hxm^2)]x(cm/bar)$
PLA	55	0.21 ± 0.01
PLA/1% D67G	49	0.22 ± 0.01
PLA/3% D67G	46	0.25 ± 0.01
PLA/5% D67G	44	0.25 ± 0.02

REFERENCES

[1] "Polylactide-Based Nanocomposites!" S.S. Ray and J. Ramontja, National Centre for Nano-Structured Materials, Council for Scientific and Industrial Research, Pretoria 0001, Republic of South Africa.

[2] "Effect of Molecular Weight and Crystallinity on Poly(lactic acid) Mechanical Properties" G. Perego, G.D. Cella,, and C. Bastioli. Novamont S.p.A., Via Fauser, 8, 28100 Novara, Italy.

[3] "Novel toughened polylactic acid nanocomposite: Mechanical, thermal an d morphological properties" H. Balakrishnan, A. Hassan, , M.U. Wahit, A.A. Yussuf, S. Bahri, A. Razak. Materials & Design Volume 31, Issue 7, (2010), pp. 3289–329.

[4] "Models for the permeability of filled polymer systems" LE. Nielsen J Macromol Sci Part A: Pure Appl Chem 1967; 1:929-42.

[5] GW. Beall Pinnavaia TJ, Beall GW, editors. "Polymer-clay nanocomposites" New York: Jhon Wiley & Sons Inc.; 2000. P. 267-79.

[6]"Transparent clay–polymer nano brick wall assemblies with tailorable oxygen barrier" A.Morgan, DG: Priolo, JC: Grunian. Appl Mater Interfaces 2010; 2:312-20.

[7] "Polylactides-chemistry properties and green packaging technology: a review" Ahmed, S.K. Varshney Int J Food Prop, 14 (2011), pp. 37–58.

[8] Hopfenberg HB, Stannett V. American chemical society. division of organic coatings and plastics chemistry. Permeability of plastic films and coatings to gases, vapors, and liquids. In: Proceeding of the Borden Award Symposium of the Division of Organic Coatings and Plastics Chemistry of the American Chemical Society, honoring Professor Vivian T. Stannett, Plenum Press, New York; 1974.

[9] "PLA-ZnO nanocomposite films: Water vapor barrier properties and specific end-use characteristics" R. Pantani , G. Gorrasi , G.Vigliotta M.

Murariu, P. Dubois. European Polymer Journal 49(11), (2013), pp. 3471–3482.

[10] "Tensile, water vapor barrier and antimicrobial properties of PLA/nanoclay composite films" J.W. Rhim, S.I. Homg, C.S. Ha, LWT - Food Science and Technology, (2009), pp. 612–617.

CHAPTER 5

UV-VIS SPECTROPHOTOMETRY AND DEGRADATION STUDY

5.1 UV-VISIBLE SPECTROPHOTOMETRY OF PLA/ TiO2 NANOCOMPOSITES, PLA/ZnO COMPOSITE AND PLA/MMT(Dellite 67G) NANOCOMPOSITES

PLA and PLA composite films were subjected to UV-visible spectrophotometric analysis to verify the influence that the particles of TiO_2, ZnO and MMT have on the absorption of ultraviolet and visible light. Figures 5.1.1, 5.1.2 and 5.1.3 report the transmittance percentage (%) as a function of the wavelength in the range from 200 to 850 nm. Figure 5.1.1 is for PLA/TiO_2 nanocomposite films obtained by compression moulding (thickness about 130 μm); figure 5.1.2 for PLA/ZnO composite films and the figure 5.1.3 for PLA/MMT(Dellite 67G) nanocomposite films, both obtained by calendar (thickness about 60 μm). Probably PLA film obtained by compression molding has the lowest transmittance of the PLA film obtained by calender because the first one presents more asperities on the surface. In all the figures PLA transmittance is reported as reference, considering that in fig. 5.1.1 it is measured with a film by compression moulding, whereas in 5.1.2 and 5.1.3 it is measured with a film by calender. The transmittance percentage indicates the amount of radiation transmitted by the optical medium at a given wavelength. The radiation, that is not transmitted, is reflected or absorbed by the optical medium. The smaller is the transmittance, the greater the absorption.

The transmittance values lower than 100% are due to the absence in the instrument of an integrating sphere; this sphere is able to collect the

transmitted radiation deflected respect to the direction of the incident radiation due to the asperities present on the film surface.

The figures 5.1.1, 5.1.2 and 5.1.3 underline that by increasing the amount of fillers the transmittance in the visible region decreases respect to that of PLA. This effect could be ascribed to the presence of nanoparticles and particles, which absorb energy. This phenomenon can be attributed to the agglomeration trend with respect to the fillers loading [1, 2] .

In the visible region (400-800 nm) PLA film, by compression moulding, has a transmittance of about 76% (Figure 5.1.1), whereas that by calender has transmittance of about 90% (Figure 5.1.2 and 5.1.3). The PLA transmittance starts to decrease at about 382 nm and becomes 0 at 225 nm; this saturation of the spectra at 225 nm is due to the absorbance of PLA ester groups [3].

For PLA/2% $mTiO_2$ nanocomposite film, Figure 5.1.1, the transmittance is 0% from 200 to 368 nm; then the transmittance increases slightly up to 60% (at wavelength 850nm). For PLA/2% TiO_2 nanocomposite film the transmittance is 0% from 200 to 411 nm, after this value the transmittance increases slightly up to 50% (at wavelength 850nm). For PLA/5% TiO_2 nanocomposite film the transmittance is 0% from 200 to 446 nm, after this value the transmittance increases slightly up to 40% (at wavelength 850nm) and for PLA/5% $mTiO_2$ nanocomposite film the transmittance is 0% from 200 to 498 nm, after this value the transmittance increases slightly up to 22% (at wavelength 850nm). The percentage of transmittance for PLA/TiO_2 nanocomposites has lower values than PLA, this is due to the particles which do not give transparency to the films. It is possible to note that in the visible region the curves for PLA/TiO_2 nanocomposites do not have a plateau, and also that the transmittance, from the 850nm to the UV range (< 400nm), decreases slowly compared to PLA and in particular it

decreases more slowly increasing TiO_2 amount (modified and unmodified). This action of TiO_2 nanoparticles extends the anti-UV area.

For PLA and PLA/ZnO films, Figure 5.1.2, the transmittance is 0% from 200 to 227 nm, then there is an increase of T (%) which is lowest for the composite with ZnO 5 wt% and highest for plain PLA. Analysing the spectra from 850 to 200 nm, PLA film has transmittance value of about 80-90 % up to 227 nm then it sharply decrease to zero value; for film with ZnO 1 wt% it is observed a constant decrease of transmittance in all the visible region followed by a small increase at about 385 nm and finally a sharp decrease at about 230 nm. The composite film with ZnO 3 wt% has qualitatively the same behaviour of the previous commented composite film, but with lower value of transmittance; finally, the composite film with 5 wt% of ZnO shows very low transmittance value in all the visible region, and it goes to zero in the range 227-200nm.

The lower values of transmittance shown by the composite films is due to the adsorption and reflection of the particles and agglomerates of the ZnO particles [4]. The reason why the UV-vis spectra of the films, with different percentages of ZnO, show an absorption in the region around 385nm, is due to the intrinsic capacity of the ZnO particles to absorb the UV light [5-7]. The mechanism of protection from UV rays in the polymers by the particles ZnO is based, instead, on the absorption of UV radiation and on their re-emission in the visible region avoiding the generation of heat [8].

The PLA/MMT nanocomposites curves follow the same behaviour of PLA curve, Figure 5.1.3. Analysing the spectrum from 850 to 200 nm, PLA film has transmittance value of about 80-90 % up to 227 nm. The percentage of transmittance for PLA/MMT nanocomposites has values lower than PLA, in fact, in the visible region for PLA/1% D67G the transmittance is about 85-90% and for PLA/3-5% D67G is about 75-84%. In the range 300-227

nm the transmittance decreases a bit faster than PLA, in particular when the D67G amount is more than 1%. This decrease in transmittance is related to the presence of D67G nanoparticles, because the light interacts with D67G nanoparticles and they absorb some of the energy [3].
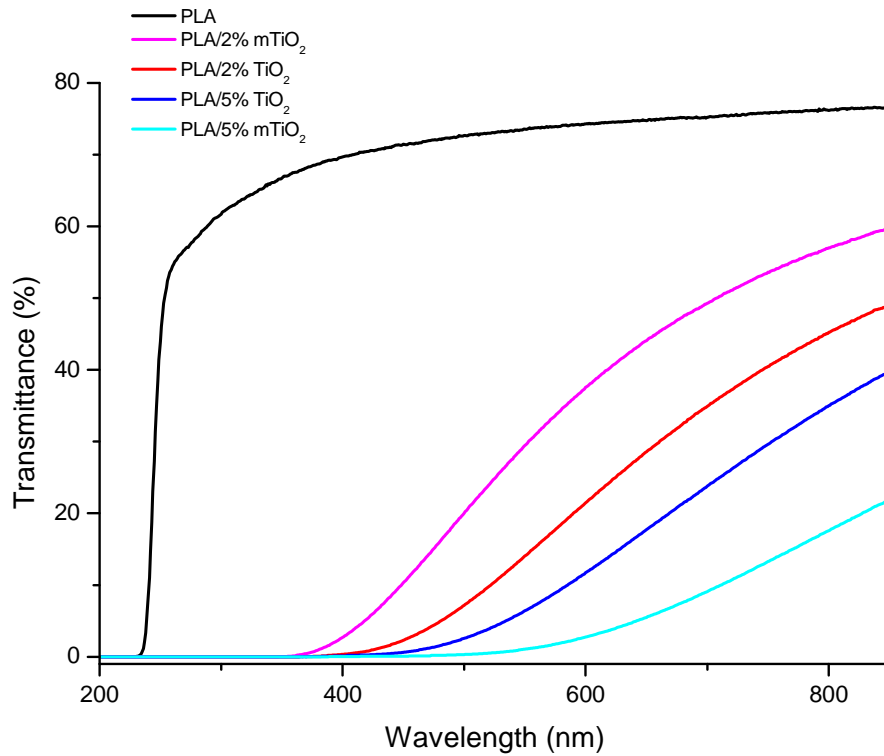

Figure 5.1.1 *UV-visible spectrum of PLA, PLA/2% TiO$_2$, PLA/2% mTiO$_2$, PLA/5% TiO$_2$ and PLA/5% mTiO$_2$ nanocomposites*
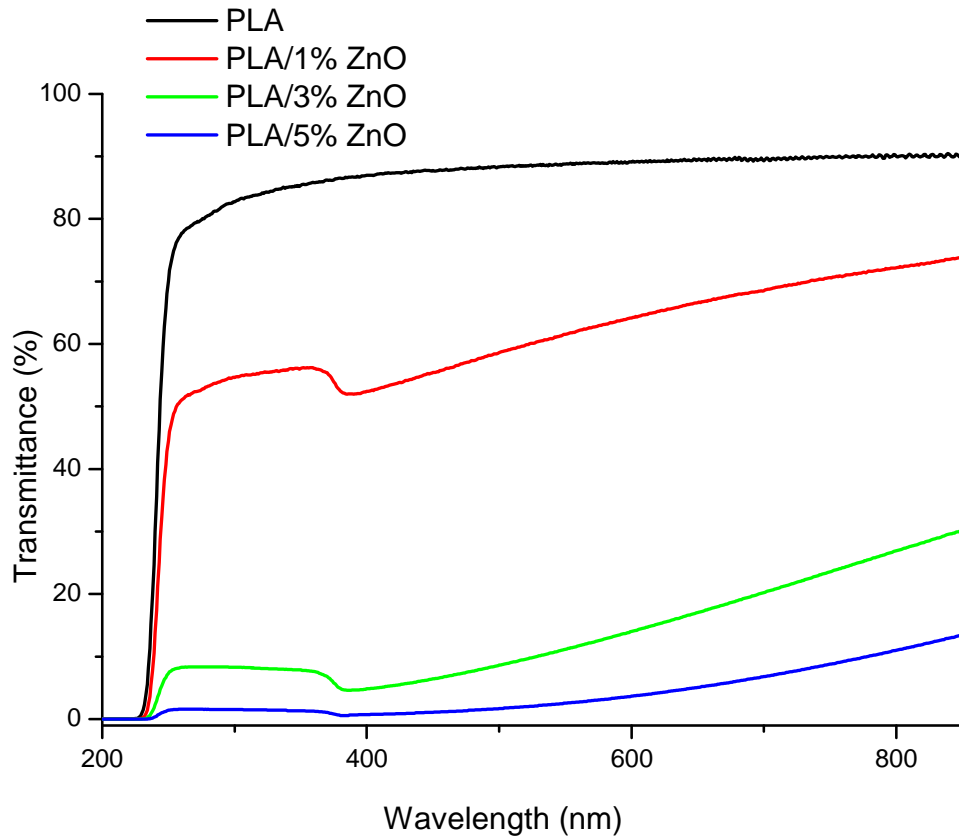
Figure 5.1.2 *UV-visible spectrum of PLA, PLA/1% ZnO, PLA/3% ZnO and PLA/5% ZnO composites.*

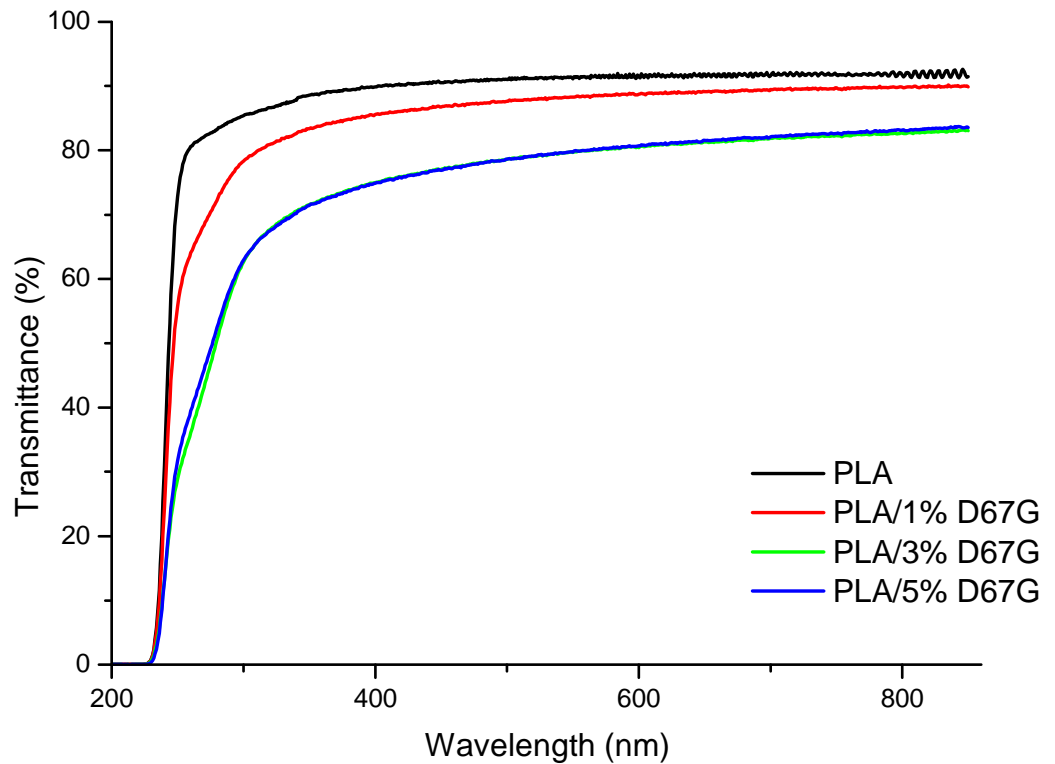***Figure 5.1.3*** *UV-visible spectrum of PLA, PLA/1% D67G, PLA/3% D67G and PLA/5% D67G nanocomposites*

5.2 UV DEGRADATION STUDY OF PLA/TiO$_2$ NANOCOMPOSITE, PLA/ZnO COMPOSITE AND PLA/MMT(Dellite 67G) FILMS

The material usefulness depends on its durability in a particular environment in which materials are used or their interaction with environmental factors [9]. Photo-oxidative (UV) degradation is the process of decomposition of the material by the action of light, which is considered as one of the primary sources of damage of polymeric substrates in ambient conditions [10]. Chemical degradation of polymers is an irreversible change and is a very important phenomenon, which affects the performance of all plastic materials in daily life and leads finally to the loss of functionality. In practice, changes in polymer properties due to chemical, physical or biological reactions resulting in bond scissions and subsequent chemical transformations are categorized as polymer degradation [10,11].

114

Recently, because of environmental concerns, the UV degradation, applied to biodegradable and biocompatible synthetic PLA, has been receiving growing attention.

Ho and Pometto [12,13] showed that the degradation of PLA plastic films was enhanced by a factor of 55–97% by UV irradiation over a period of 8 weeks. Copinet et al. [12,14] further studied the effect of simultaneously UV irradiation with relative humidity and temperature changes. Their study revealed that the degradation rate was enhanced by UV irradiation over a period of 30 days.

Although the enormous literature devoted to nanocomposites materials, only very few papers deal with the ageing of PLA-based nanocomposites [15]. So far, these studies concern nanocomposites with montmorillonite and classical polymer matrices, such as polypropylene, polyethylene and polycarbonate [11,16]. In all cases, similar conclusions are obtained, which show that the nanocomposites degrade faster than the neat polymers.

In this work, PLA systems were exposed to UV light, at 25% relative humidity and 40°C, in order to study effect of three different fillers (TiO_2, ZnO and MMT) on the degradation of PLA matrix.

5.2.1 UV degradation of PLA/TiO_2 nanocomposite films

Figure 5.2.1 reports the PLA/TiO_2 nanocomposites weight loss as a function of the UV exposure time. It clearly shows that the weight loss is significantly faster in PLA respect to that of nanocomposites. PLA degradates in about 17 days. This means that TiO_2 nanoparticles decrease the UV degradation of neat PLA. Moreover for the first 40 days of exposure, the weight losses in PLA/TiO_2 nanocomposites vary linearly and do not seem to depend significantly on the amount of TiO_2 nanoparticles (modified or not modified), as also reported in literature [17,18]. After this time, changes in the slope of PLA/2% TiO_2 and PLA/2% mTiO_2

nanocomposites are observed and at 73 days of UV exposure, PLA/2% TiO$_2$ shows a weight reduction of about 95%, PLA/2% mTiO$_2$ of about 87%, PLA/5% TiO$_2$ of about 73% and PLA/5% mTiO$_2$ of about 48%. After 73 days of UV exposure, the degradation is faster for PLA/2% TiO$_2$ respect to PLA/5%TiO$_2$ and in particular is faster when the particles are not modified.
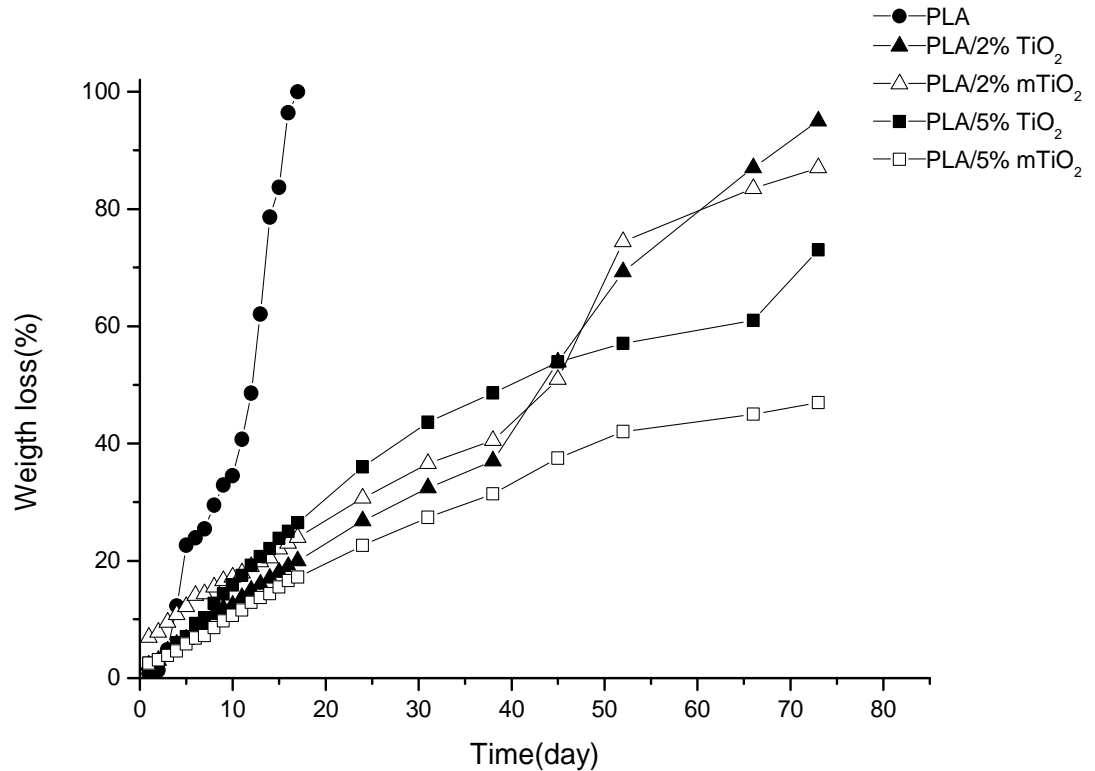

Figure 5.2.1 *Weight loss/UV irradiation time dependence for PLA, PLA/2% TiO$_2$, PLA/2% mTiO$_2$, PLA/5% TiO$_2$ and PLA/5% mTiO$_2$ films*

5.2.2 UV degradation of PLA/ZnO composite and PLA/MMT(Dellite 67G) nanocomposite films

The PLA/ZnO composites and PLA/MMT nanocomposites have similar behavior, Figure 5.2.2 and 5.2.3 respectively. In both cases, the neat PLA degrades faster than PLA loaded with ZnO and D67G and the degradation is almost completed in 21 days.

Figure 5.2.2 shows that PLA starts to degrade faster than PLA/ZnO composites already after the first days of UV exposure. The weight loss as a function of time is lower increasing the amount of ZnO particles in the composites. For example after 14 days of UV exposure the PLA has a weight loss of about 80%, PLA/1% ZnO of about 36%, PLA/3% ZnO of about 23% and PLA/5% ZnO of about 12%.

Figure 5.2.3 shows that PLA and PLA/MMT nanocomposites have the same weight loss in the first 2 days of UV exposure. After this period PLA starts to degrade faster than PLA/MMT nanocomposites. In particular after 15 days of UV exposition the PLA has a weight loss of about 80%, PLA/1% D67G of about 75%, PLA/3% D67G of about 65% and PLA/5% D67G of about 45%.
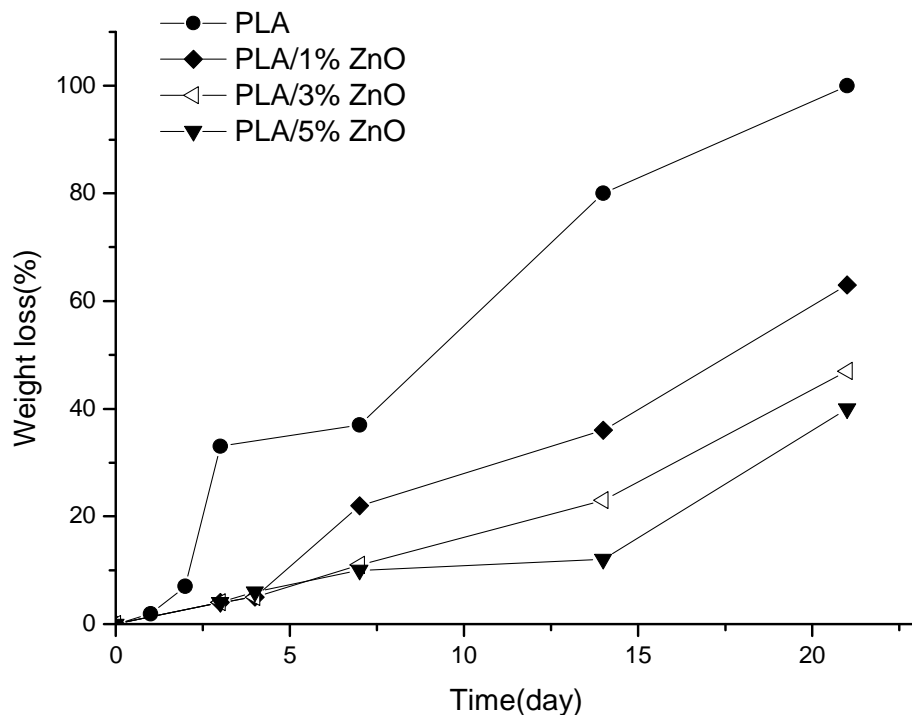

Figure 5.2.2 *Weight loss/UV irradiation time dependence for PLA, PLA/1% ZnO, PLA/3% ZnO and PLA/5% ZnO*
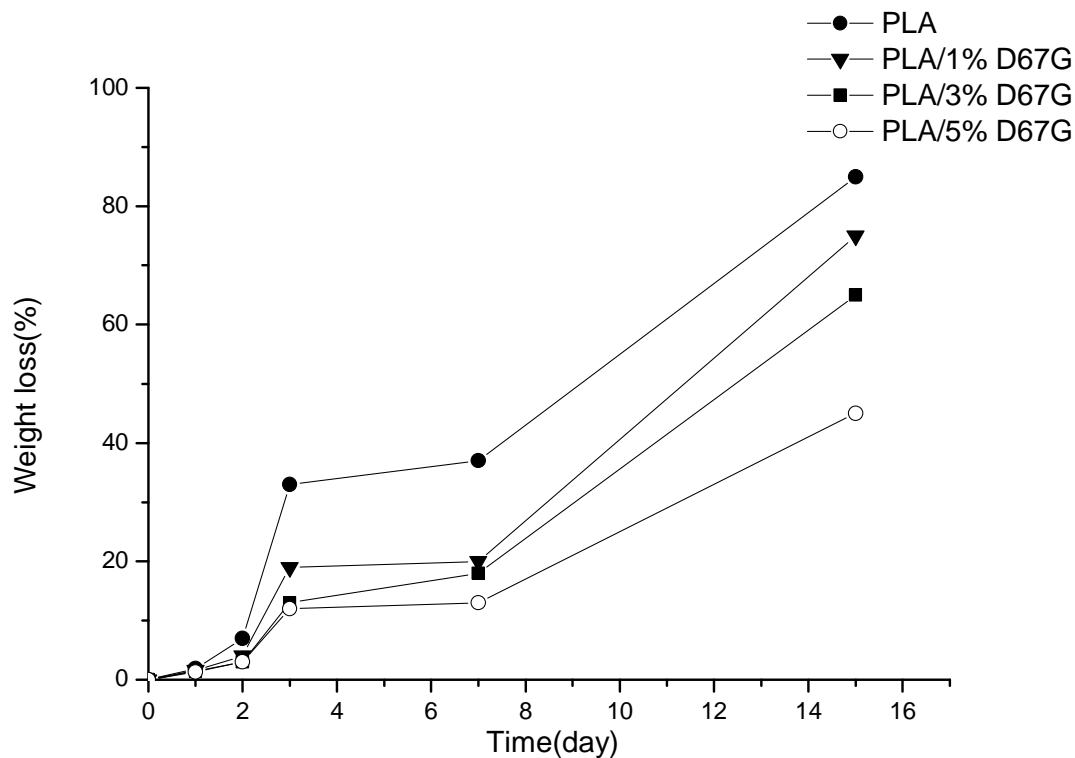
Figure 5.2.3 *Weight loss/UV irradiation time dependence for PLA, PLA/1% D67G, PLA/3% D67G and PLA/5% D67G*

Comparing the three systems is possible to observe that PLA/TiO$_2$ films reach the 50% of degradation after 40 days of UV exposure, PLA/ZnO composites and PLA/MMT nanocomposites reach the same degradation after 21 and 12 days respectively. This means that the UV degradation is faster for PLA/MMT nanocomposites than that of PLA/ZnO and PLA/TiO$_2$. The slowest UV degradation is observed for PLA/TiO$_2$ nanocomposites.

Moreover, in the PLA/ZnO and PLA/MMT films the amount of fillers influences the UV degradation: by increasing the particle amount the degradation process proceeds faster. This kind of results is different from some results reported in literature : Buzarovska found that the UV degradation is faster in the composites than in PLA and Nakayama et al. have reported that the degrees weight loss in the PLA matrix owing to UV

irradiation did not depend on the amount of added functionalized TiO$_2$ nanoparticles [17,18].

5.2.3 ATR Spectroscopy on PLA/TiO$_2$ nanocomposite, PLA/ZnO composite and PLA/MMT(Dellite 67G) nanocomposite films after UV degradation

PLA and PLA composite films were exposed to UV radiation to verify the effect of particles on PLA photodegradation. The UV irradiation produces the formation of degradation products, which lead to evolution of new peaks in the ATR spectra. These peaks were investigated by ATR spectroscopy in the range from 4000 to 400 cm^{-1} , at different time of UV exposure.

5.2.3.1 ATR Spectroscopy on PLA and PLA/TiO$_2$ films after 0, 3 and 14 days of UV degradation

Figure 5.2.4 shows the FTIR-ATR absorbance spectra, in the range 4000-400 cm^{-1}, of UV irradiated PLA films after 0, 3 and 14 days of UV degradation. For PLA, after 0 days of UV exposure, the spectrum shows a strong absorbance band at 1748 cm^{-1}, attributed to the stretching vibrations of amorphous carbonyl groups [19]. The other observed bands, positioned at 1455 and 1380 cm^{-1}, are due to the CH$_3$ asymmetric and symmetric deformations. The strong absorption band located at 1186 cm^{-1} is due to C-O-C stretching mode. After the UV degradation it is observed formation of new bands. The infrared analysis of PLA photooxidation shows (Figure 5.2.4) in the hydroxyl region a broad absorption band with a maximum at 3500 cm^{-1} that corresponds to products such as hydroperoxides or alcohols [20]; the second absorption band is a narrow band with a maximum at 1843 cm^{-1} and it is attributed to anhydride groups [20-23]; and the

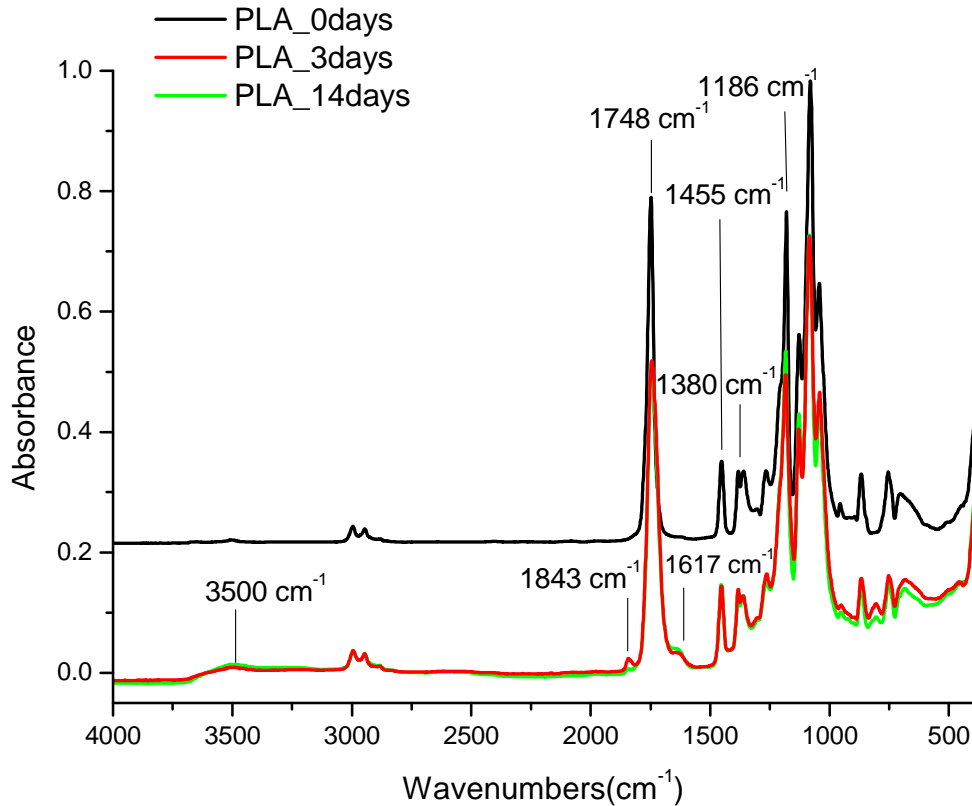formation of absorption band with a maximum at 1617 cm^{-1} that can be ascribed to the stretching of the C=O.

Figure 5.2.4 *FTIR-ATR spectra of UV irradiated PLA films after 0, 3 and 14 days of UV degradation.*

As reported by Bocchini et al. [3] reported photooxidation radical mechanism of PLA, as it is proposed here, Figure 5.2.5. Photooxidation usually begins by radical formed from impurities by UV-irradiation or thermal decomposition. The reaction with higher probability is the abstraction of tertiary hydrogen from PLA chain with the formation of a tertiary radical P• (1). This radical can react with oxygen to form a peroxide radical (2), which may easily abstract another hydrogen from a tertiary carbon with the formation of an hydroperoxide and the initial radical P• (3). Then, the hydroperoxide undergoes photolysis (4) with the

formation of the HO• and a PO• radical that can further evolve by β-scission (5). Taking into account the stability of the different fragments the most probable β-scission appears to be the (5b) reaction, leading to the formation of anhydride groups [1].
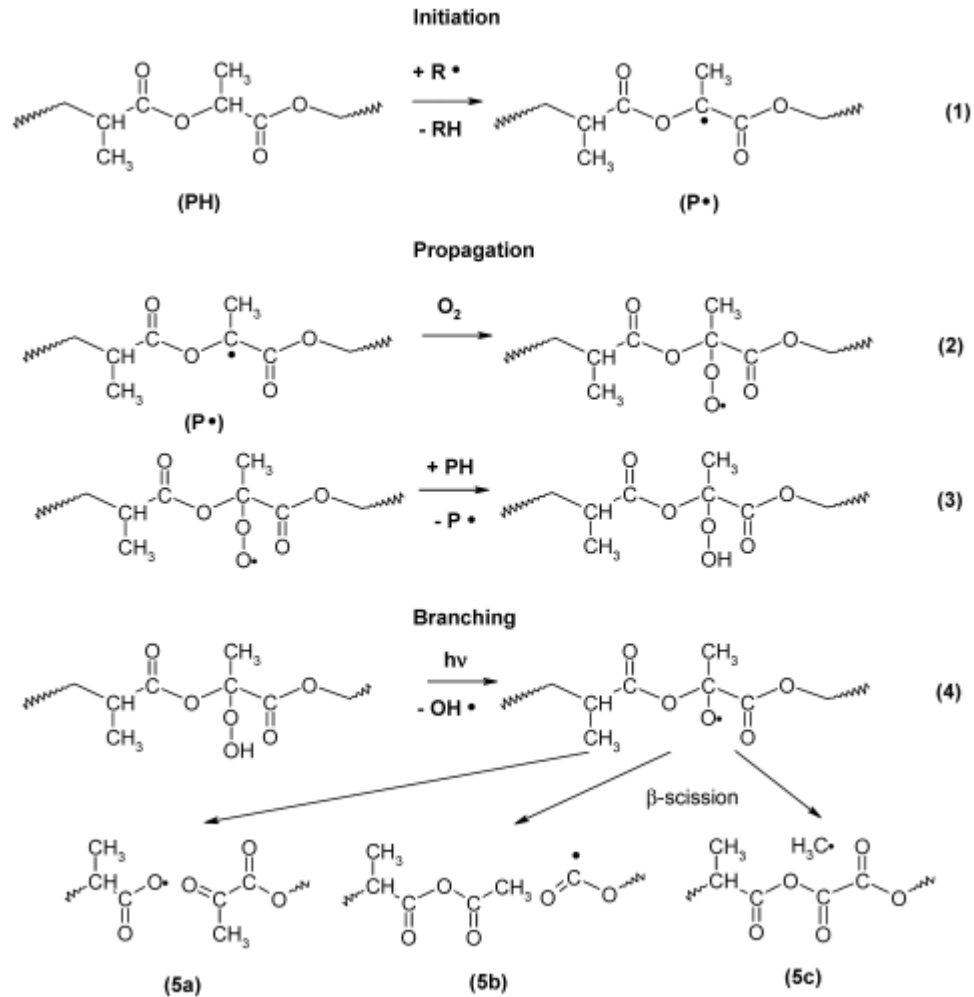

Figure 5.2.5 *Radical oxidation process of irradiated PLA sample: Hydroperoxide chain propagation and formation of anhydrides by photolysis of hydroperoxide*

Figure 5.2.6, 5.2.7, 5.2.8 and 5.2.9 show the FTIR-ATR absorbance spectra, in the range 2000-1000 cm^{-1}, of UV irradiated PLA/TiO$_2$ nanocomposite films after 0, 3, 14 and 30 days of UV degradation. The

spectrum was obtained from 4000 to 400 cm^{-1}, but it is shown here only the range 2000-1000 cm^{-1} where the effects of UV degradation are detectable. The infrared analysis of PLA/TiO$_2$ nanocomposite films photooxidation shows the presence of a band with a maximum at 1843cm^{-1}, attributed to the formation of anhydride groups [23]. It is also possible to note that the PLA/TiO$_2$ nanocomposite films do not show other typical degradation peak of PLA, indicating that the TiO$_2$ nanoparticles inhibit the formation of hydroperoxides or alcohols, carboxylic salt and primary amide group. The inhibition of PLA degradation is independent of TiO$_2$ nanoparticles (modified or not), and of their amount and of the UV exposure time.
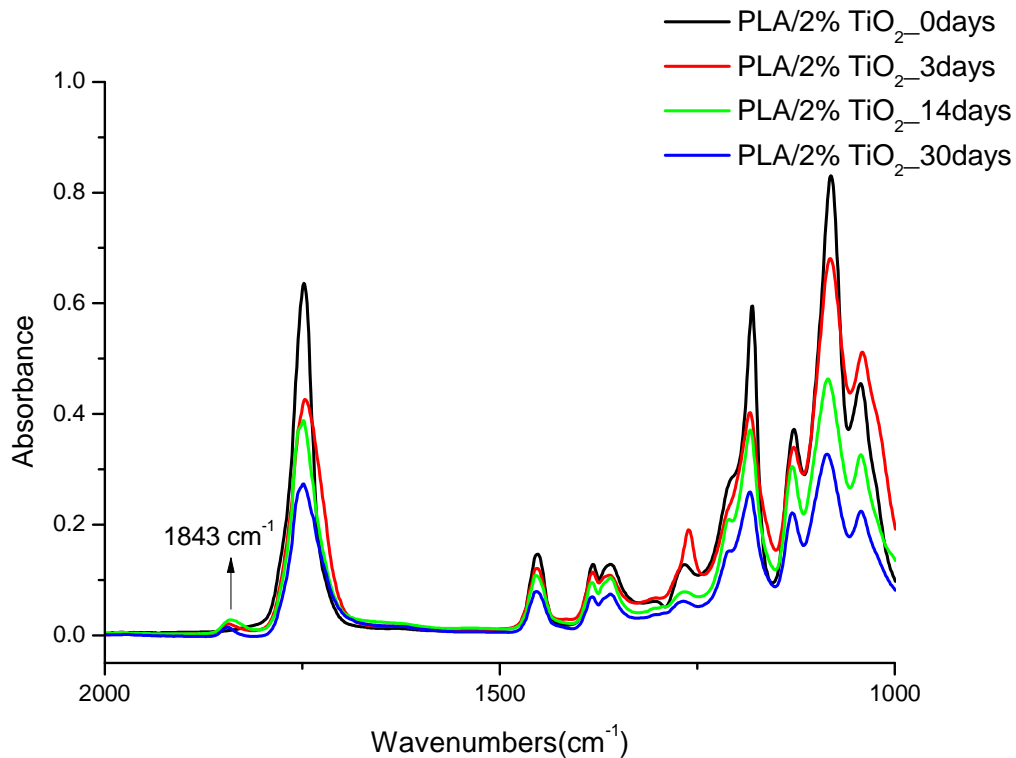

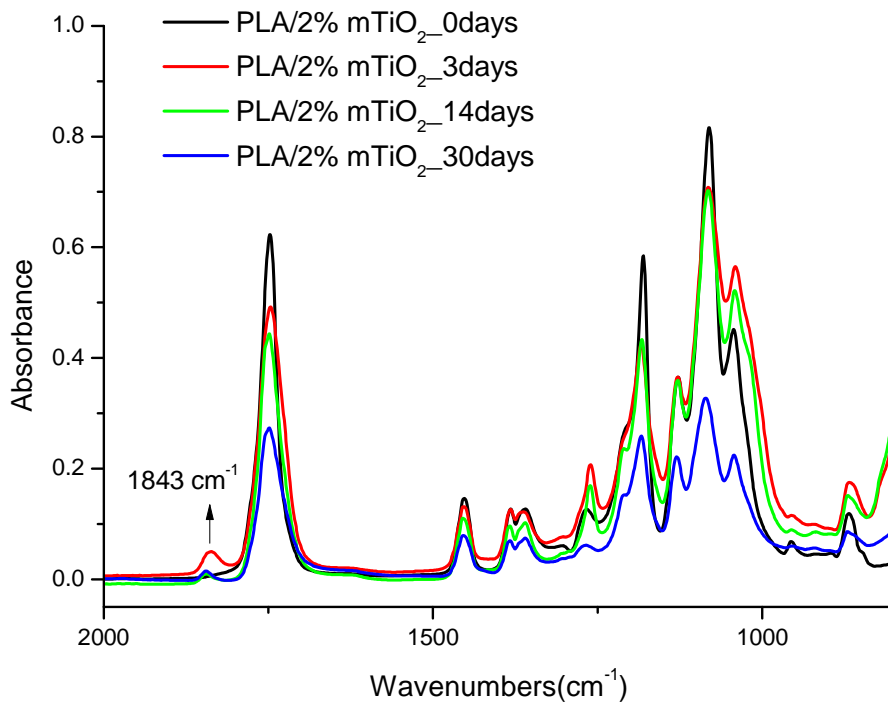***Figure 5.2.6*** *FTIR-ATR spectra of UV irradiated PLA/2% TiO$_2$ nanocomposite films 0, 3, 14 and 30 days of UV degradation.*

Figure 5.2.7 *FTIR-ATR spectra of UV irradiated PLA/2% mTiO$_2$ nanocomposite films 0, 3, 14 and 30 days of UV degradation.*

Figure 5.2.8 *FTIR-ATR spectra of UV irradiated PLA/5% TiO$_2$ nanocomposite films 0, 3, 14 and 30 days of UV degradation*

123

Figure 5.2.9 *FTIR-ATR spectra of UV irradiated PLA/5% mTiO₂ nanocomposite films 0, 3, 14 and 30 days of UV degradation.*
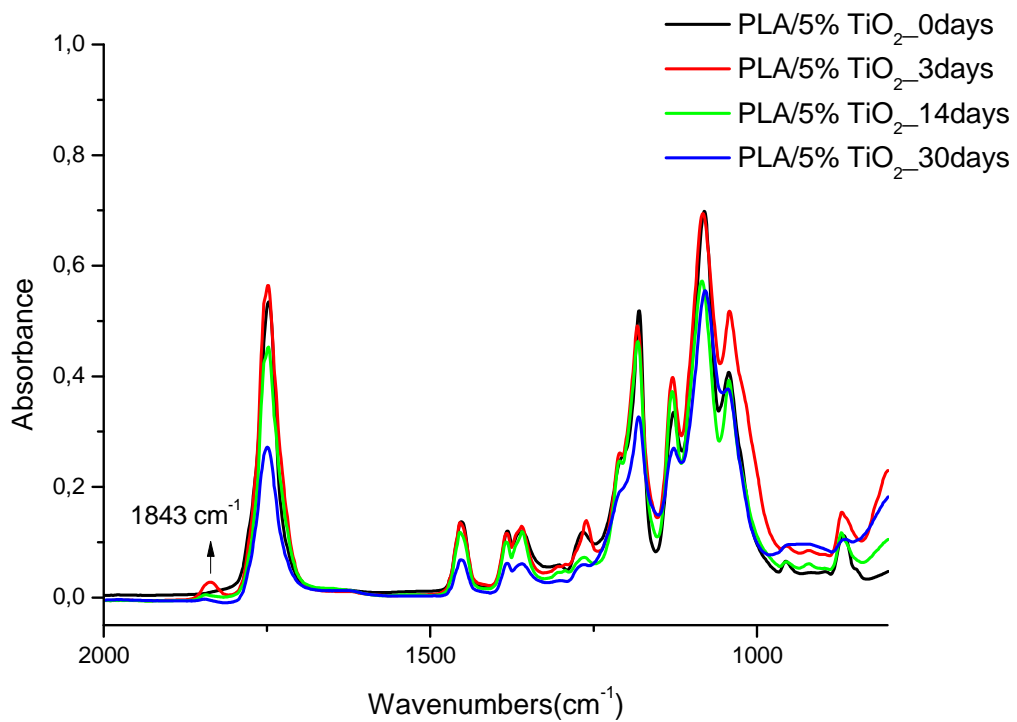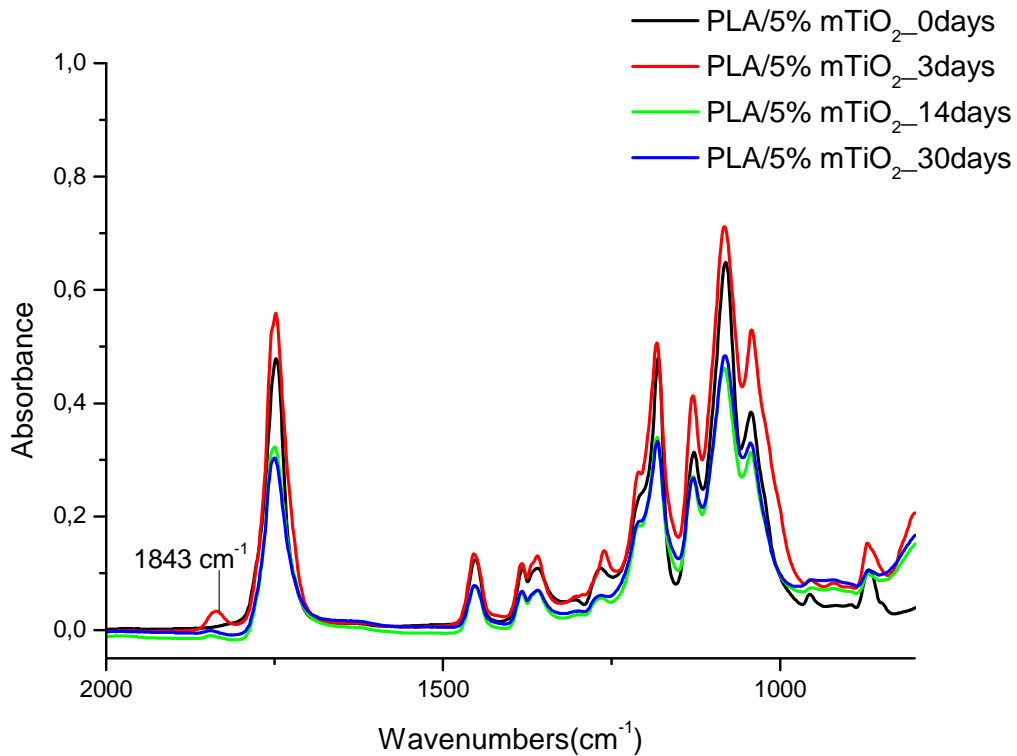
5.2.3.2 ATR Spectroscopy on PLA and PLA/ZnO composite films after 0, 3, 14, 21 days of UV degradation

Figure 5.2.10 shows the FTIR-ATR absorbance spectra, in the range 4000-400 cm⁻¹, of UV irradiated PLA films (by calender) after 0, 3 and 14 days of UV degradation. It possible to observe that the calendar films and compression moulding films of PLA have the same UV degradation behavior (see subparagraph 5.2.1.1 Chapter 5).
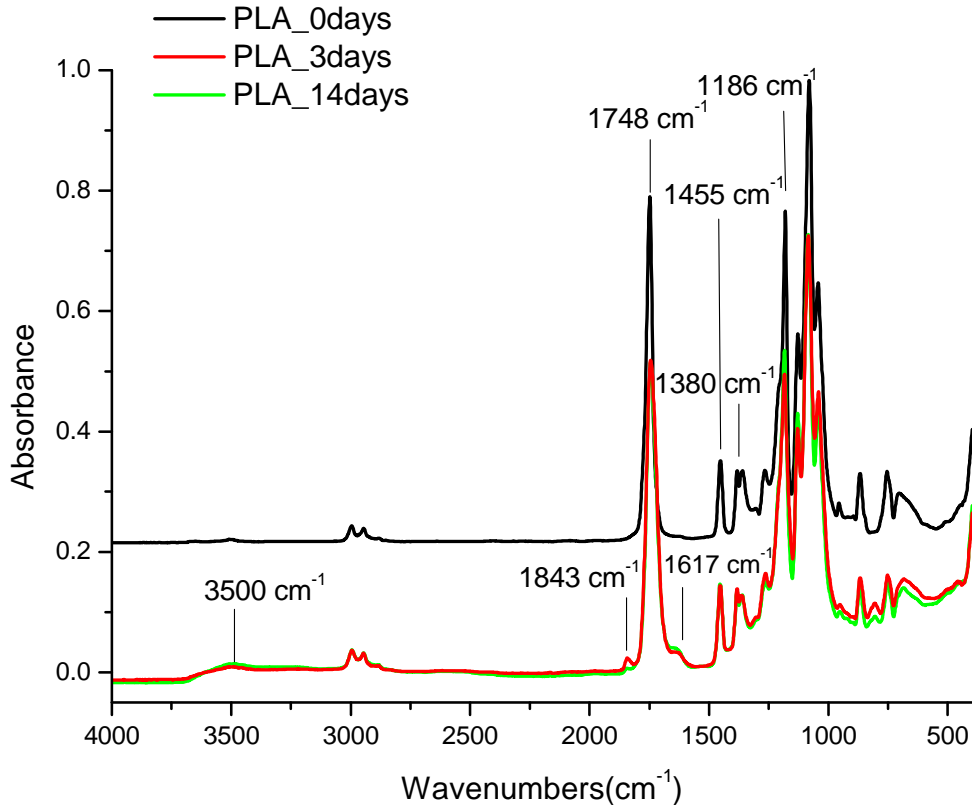
Figure 5.2.10 *FTIR-ATR spectra of UV irradiated PLA films after 0, 3 and 14 days of UV degradation.*

Figures 5.2.11, 5.2.12 and 5.2.13 show the FTIR-ATR absorbance spectra, in the range 4000-1600 cm^{-1}, of PLA/ZnO composite films exposed for 0, 3, 14 and 21 days at UV irradiation. The IR analysis of the PLA/ZnO composites during photo-oxidation also presents the formation of the three absorption bands with maxima at 3500, 1845 and 1617 cm^{-1} as observed in the case of pristine PLA (Figure 5.2.10). This finding indicates that the same PLA oxidation photoproducts are formed in the presence of ZnO particles. However, one can observe a dramatic difference in terms of photoproduct concentrations because under identical exposure times the absorbance measured at 1617 cm^{-1} is considerably more intense for the PLA/ZnO composites than for the PLA. In particular, this band increases with the amount of ZnO content in the composites and with the UV

exposure time. The increasing of that band could be attributed to the possible interaction between the ZnO particles and the active products of PLA photo-degradation.

Figure 5.2.11 *FTIR-ATR spectra of UV irradiated PLA/1% ZnO composite films after 0, 3,14 and 21 days of UV degradation*

Figure 5.2.12 *FTIR-ATR spectra of UV irradiated PLA/3% ZnO composite films after 0, 3,14 and 21 days of UV degradation*
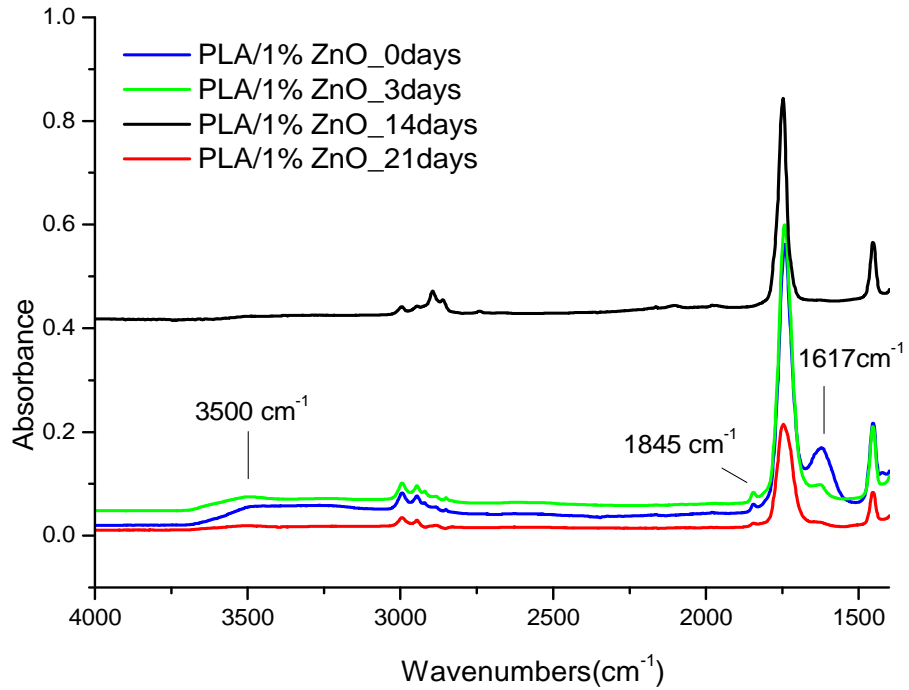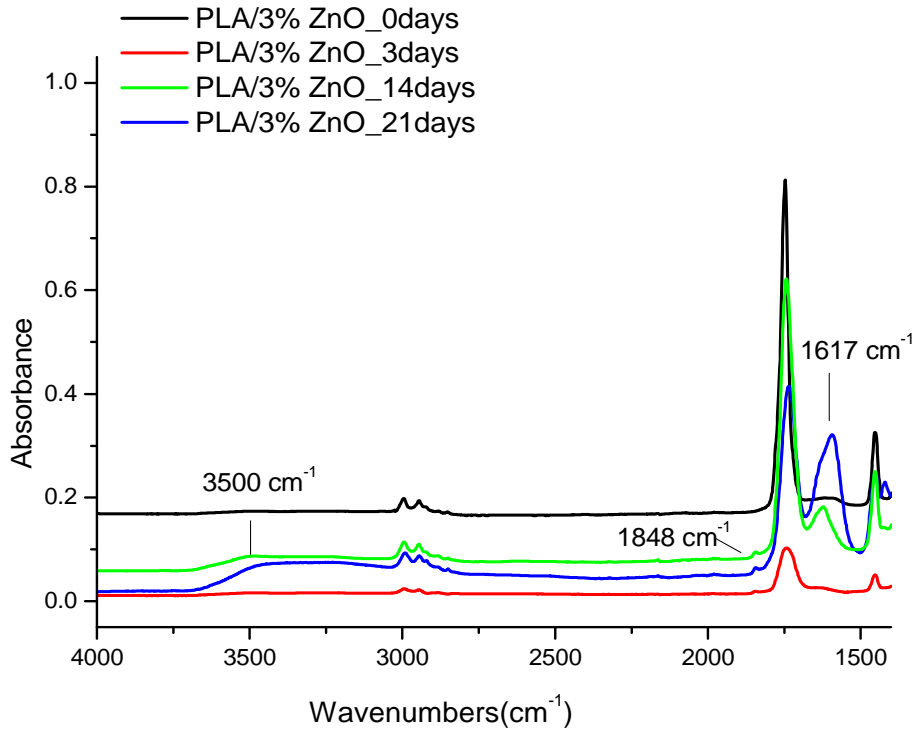

Figure 5.2.13 *FTIR-ATR spectra of UV irradiated PLA/5% ZnO composite films after 0, 3,14 and 21 days of UV degradation*

5.2.3.3 ATR Spectroscopy on PLA and PLA/MMT(Dellite 67G) nanocomposite films after 0, 3, 7 and 14 days of UV degradation

Figure 5.2.14 shows the FTIR-ATR absorbance spectra, in the range 4000-400 cm^{-1}, of UV irradiated PLA films (by calender) after 0, 3, 7 and 14 days of UV degradation. It possible to observe that the calendar films and compression moulding films of PLA have the same UV degradation behavior (see subparagraph 5.2.1.1 Chapter 5).
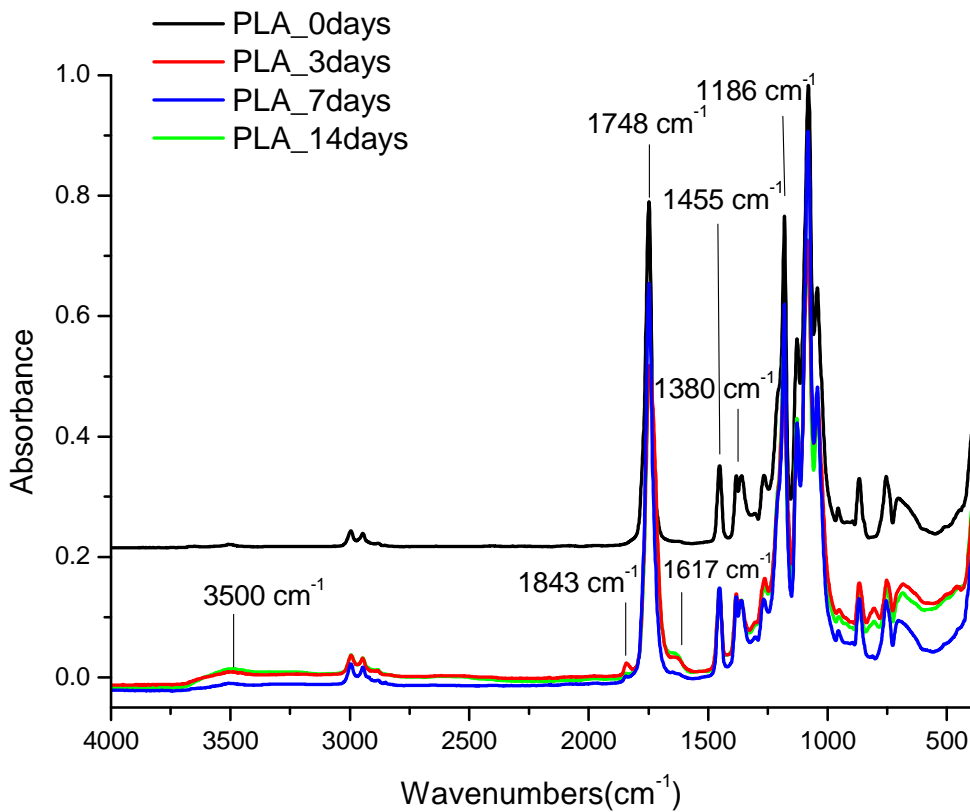
Figure 5.2.14 *FTIR-ATR spectra of UV irradiated PLA films after 0, 3, 7 and 14 days of UV degradation*

Figures 5.2.15, 5.2.16 and 5.2.17 show the FTIR-ATR absorbance spectra, in the range 4000-1400 cm^{-1}, of UV irradiated PLA/MMT nanocomposite films after 0, 3 , 7 and 14 days of UV degradation. The IR analysis of the PLA/MMT nanocomposites during photo-oxidation also presents the formation of the three absorption bands with maxima at 3500, 1843 and 1617 cm^{-1} as observed in the case of pristine PLA (Figure 5.2.10). This observation indicates that the same PLA oxidation photoproducts are formed in the presence of MMT nanoparticles.
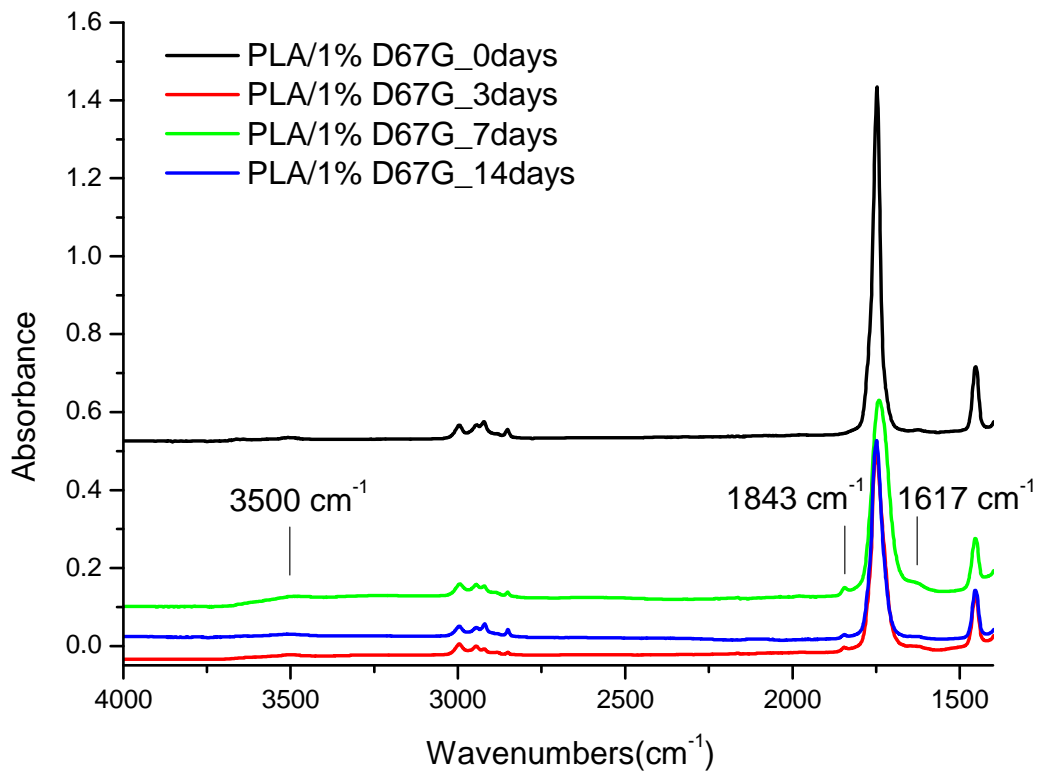
Figure 5.2.15 *FTIR-ATR spectra of UV irradiated PLA/1% D67G nanocomposite films after 0, 3, 7 and 14 days of UV degradation*
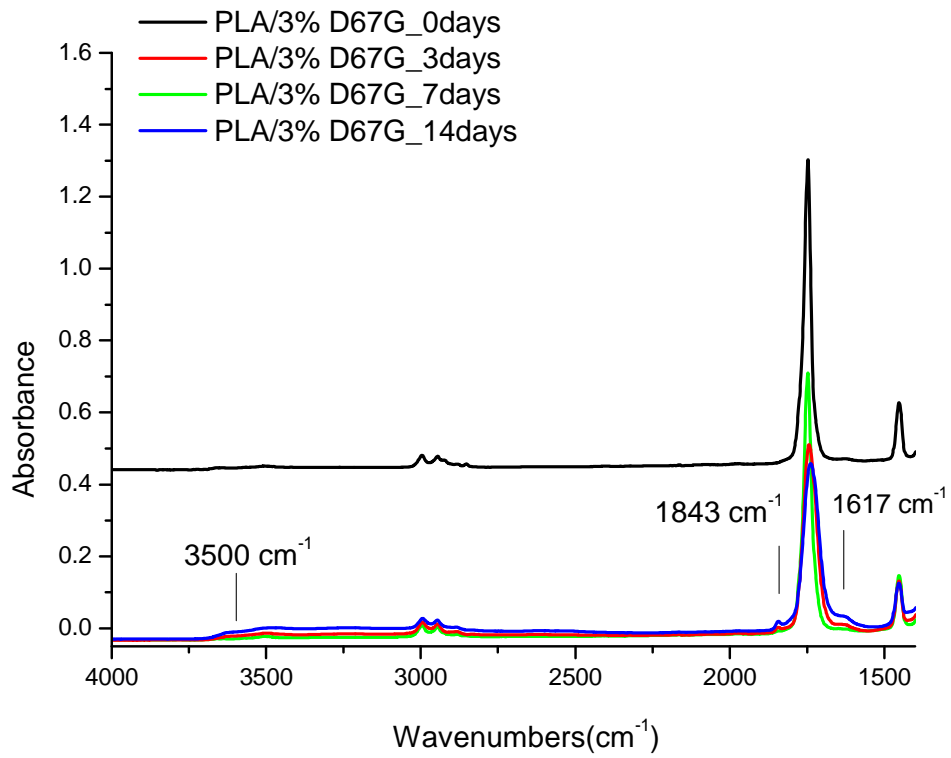
Figure 5.2.16 *FTIR-ATR spectra of UV irradiated PLA/3% D67G nanocomposite films after 0, 3, 7 and 14 days of UV degradation*
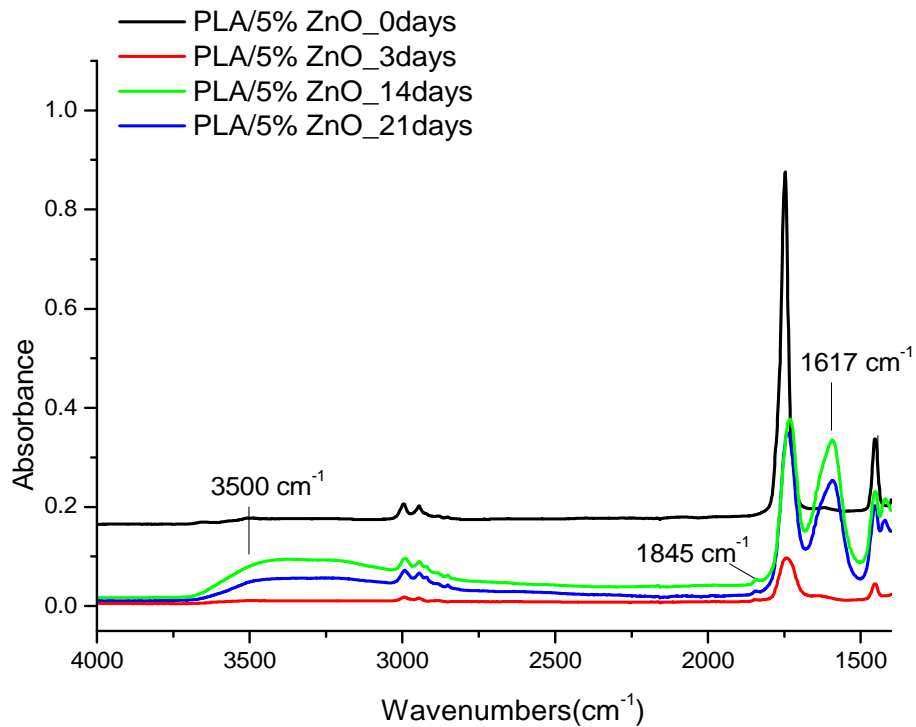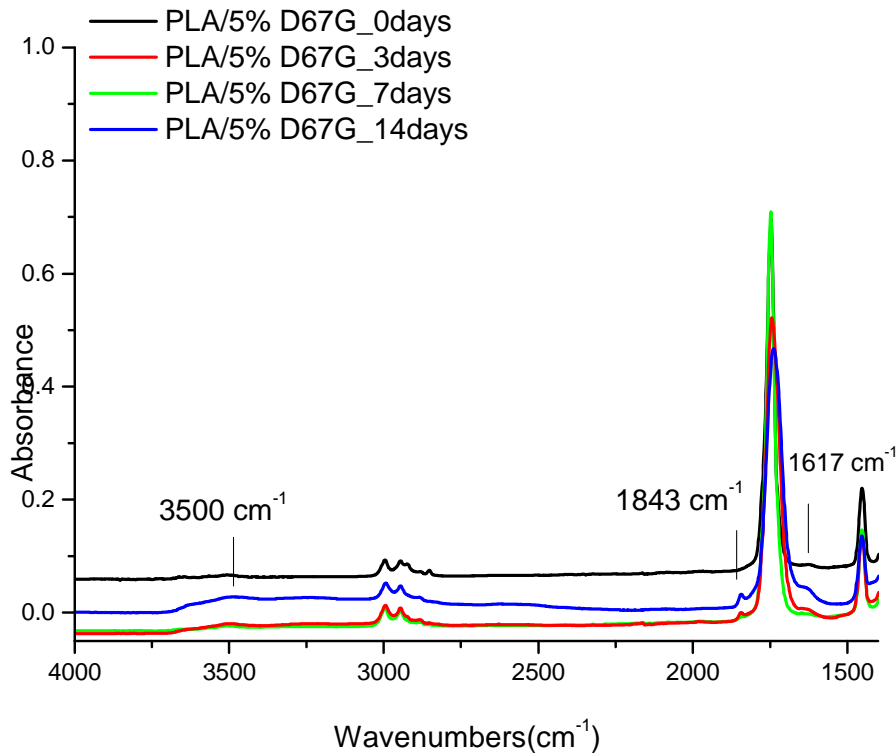
Figure 5.2.17 *FTIR-ATR spectra of UV irradiated PLA/5% D67G nanocomposite films after 0, 3, 7 and 14 days of UV degradation*

5.3 HYDROLYTIC DEGRADATION OF PLA/TiO$_2$ NANOCOMPOSITE, PLA/ZnO COMPOSITE AND PLA/MMT(Dellite 67G) NANOCOMPOSITE FILMS

The hydrolytic degradation of PLA is a well-known process. It happens mainly in the bulk of the material and not from its surface [24,25]. The hydrolytic chains cleavage proceeds preferentially in amorphous regions, leading therefore to an increase of the polymer global crystallinity [26]. This explains the much faster hydrolysis rate of the amorphous P(D,L-LA) compared to semicrystalline P(L,L-LA). The formation of lactic acid oligomers, which directly follow from chain scission, increases the carboxylic acid end groups concentration in the medium. The carboxylic functions

are known to catalyse the degradation reaction. In conclusion, the hydrolytic degradation of PLA is a selfcatalysed and self-maintaining process [27]. Such mechanisms can be affected by various factors, such as chemical structure, molar mass and its distribution, purity, morphology, shape and history of the specimen, as well as the conditions under which the hydrolysis is conducted [28,29].

Neat PLA, nanocomposites and composites were put in contact with 1M NaOH solution, at 37°C (see Chapter 1). Figure 5.3.1, 5.3.2 and 5.3.3 report the weight losses versus solution contact time for PLA/TiO_2 , PLA/ZnO and PLA/MMT respectively.

5.3.1 Hydrolytic degradation of PLA/TiO_2 nanocomposite films

Figure 5.3.1 shows the weight loss of PLA and PLA/TiO_2 nanocomposite films as a function of solution contact time. PLA/TiO_2 nanocomposites films exhibited higher weight loss as a function of time than neat PLA. This result is in agreement with that reported by Buzarovska in literature [18]. It can be observed that nanocomposites containing modified TiO_2 nanoparticles degrade faster than the nanocomposites containing not modified TiO_2 nanoparticles. In particular PLA/5% mTiO_2 nanocomposite is fully degraded after 300 min; while at the same time (300min) PLA/5% TiO_2 displays a weight loss of 79%, PLA/2% mTiO_2 of 71%, PLA/2% TiO_2 of 69% and neat PLA of 46%.

From the results, it could be concluded that the hydrolytic degradation time of PLA nanocomposite films can be widely controlled by TiO_2 content [18].
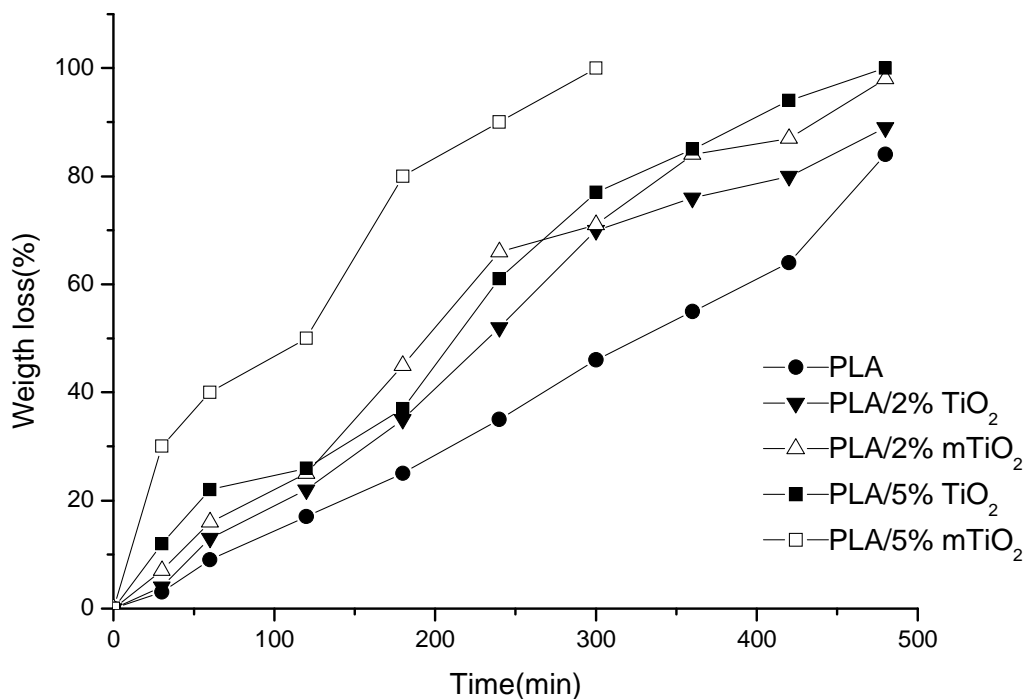
Figure 5.3.1 *Weight loss (%)-time dependence (in 1 M NaOH) for PLA, PLA/2% TiO₂ ,*
PLA/2% mTiO₂, PLA5% TiO₂ and PLA/5% mTiO₂ nanocomposites.

5.3.2 Hydrolytic degradation of PLA/ZnO composite films

Figure 5.3.2 shows the weight loss of PLA and PLA/ZnO composites films as a function of exposed time in hydrolytic solution.

The PLA produced by calender has different degradation respect the PLA produced by compression molding, used for the PLA/TiO$_2$ system; this is due to the different methods to produce films and to their different thickness, lower for PLA produced by calender. In particular PLA produced by calender has hydrolytic degradation faster than PLA produced by compression molding.

 PLA hydrolytic degradation is slow respect the PLA/ZnO composites. For all the composites, the degradation is very slow in the first 10 minutes, but it suddenly increases after that time.

After 30 minutes, for example, PLA has loss 12% in weight, whereas: PLA/1% ZnO has loss 38% in weight, PLA/3% ZnO has loss 36% and PLA/5% ZnO 28%. This means that ZnO particles decrease the degradation time of PLA but that by increasing the amount of ZnO particles the required time for hydrolytic degradation increases and that the hydrolytic degradation time of PLA composite films can be widely controlled by ZnO content [30].
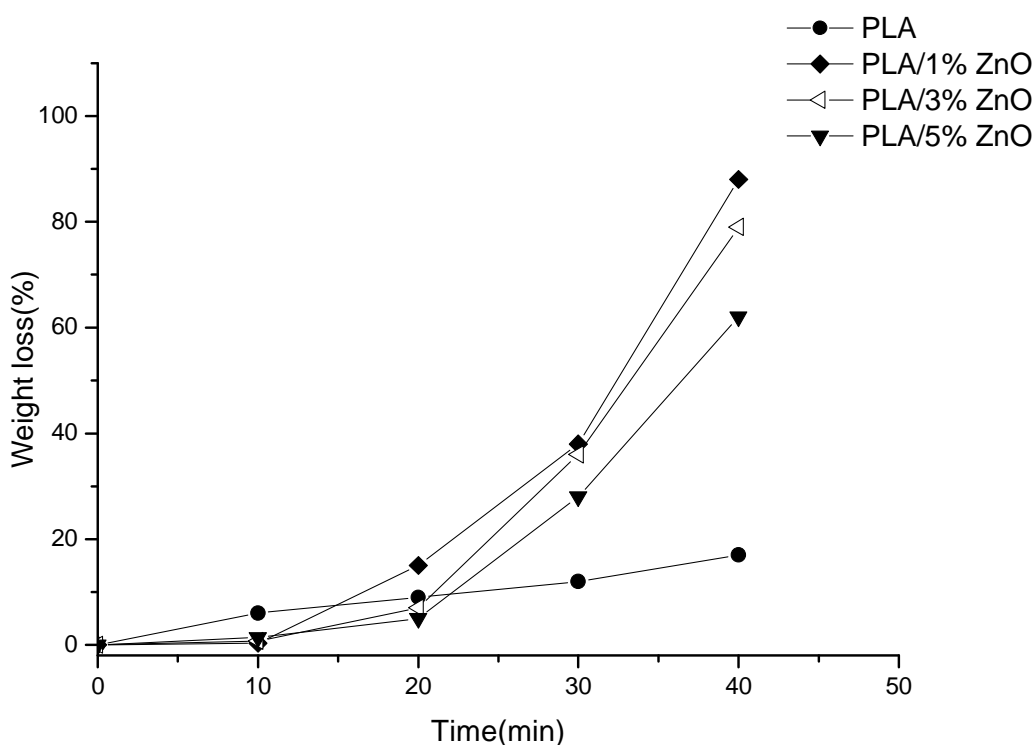
Figure 5.3.2 *Weight loss (%)-time dependence (in 1 M NaOH) for PLA, PLA/1% ZnO, PLA/3% ZnO and PLA/5% ZnO composites*

5.3.3 Hydrolytic degradation of PLA/MMT(Dellite 67G) nanocomposite films

Figure 5.3.3 shows the weight loss of PLA and PLA/MMT nanocomposites films as a function of exposed time in hydrolytic test. In the first 10 minutes the PLA and PLA/MMT nanocomposites show almost the same

weight loss; increasing the contact time of samples with hydrolytic solution the behaviors are completely different. The hydrolytic degradation goes slowly for PLA than for PLA/MMT nanocomposites; linear trend can be observed in the relation between weight loss and exposure time in the early stage of degradation. At 30 minutes, the weight loss of neat PLA is 12%, for PLA/1% D67G is 22%, for PLA/3% D67G is 33% and for PLA/5% D67G is 29%. The PLA/3% D67G shows the higher weight loss respect PLA/1% D67G because has a bigger amount of MMT and respect PLA/5% D67G because PLA/3% D67G is better exfoliated (see TEM, Chapter2). The hydrolytic degradation for PLA/MMT nanocomposites proceeds more slowly than neat PLA; in particular increasing the amount of MMT nanoparticles the time of hydrolytic degradation decreases and if the nanoparticles in the matrix are intercalated, or better exfoliated, reducing the amount of MMT nanoparticles is possible decrease the time of hydrolytic degradation of the system PLA/MMT [14].
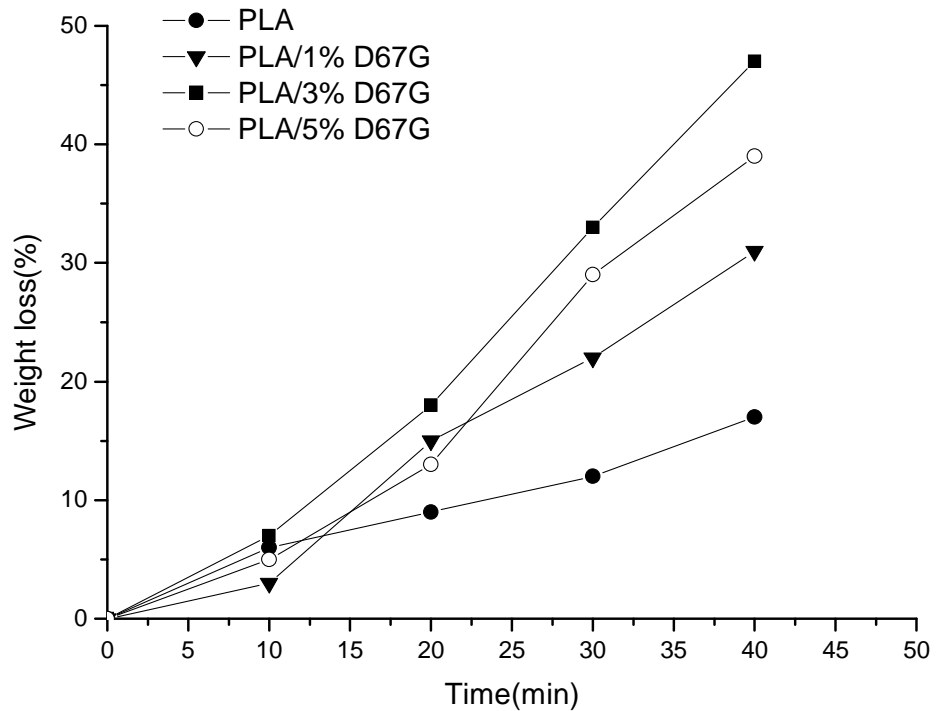
Figure 5.3.3 *Weight loss(%)/time dependence (in 1 N NaOH) for PLA, PLA/1% D67G, PLA/3% D67G and PLA/5% D67G nanocomposites*

It is possible conclude that ZnO particles decrease better the time of hydrolytic degradation of PLA nanocomposites respect MMT nanoparticles; while TiO_2 nanoparticles increase significantly that time. Hydrolytic degradation time of PLA composite films can be widely controlled by nanoparticles and particles content.

5.4 ENZYMATIC DEGRADATION OF PLA/TiO₂ NANOCOMPOSITE, PLA/ZnO COMPOSITE AND PLA/MMT(Dellite 67G) NANOCOMPOSITE FILMS

In 1981, Williams first reported that hydrolysis of PLA is catalyzed by proteinase K from *Tritirachium album* [31,32]. Thereafter, microbial degradation of PLA has been studied extensively [33,34]. Intensive studies

on biodegradation of PLA by using proteinase K have clarified the main factors affecting the biodegradability.

Proteinase K preferentially hydrolyzes poly(L-lactide) (PLLA) rather than poly(D-lactide) (PDLA), and the rate of enzymatic hydrolysis of PLA depends on its stereochemical composition [35-39]. Crystallinity of PLA also strongly affects the degradation rate [35-37,40-42]. Proteinase K hydrolyzes predominantly amorphous region of PLA and hardly the folding chains in the crystalline region, so that the hydrolysis rate decreased with increasing crystallinity of PLA [35-36,40-42]. Degradability also depends on molecular weight of PLA, [39] crystalline size, [41] and polymer blending [39,42-48]. Although the effects of properties of PLA materials on biodegradability have been studied extensively as mentioned above, interactions between PLA materials and proteinase K have been remained unclear [31].

Moreover the study of enzymatic degradation of PLA composites and nanoomposites is only in an early stage of research.

PLA, nanocomposites and composites were put in contact with Proteinase K solution at 37°C (see Chapter 1). Figure 5.4.1, 5.4.2 and 5.4.3 report the weight loss versus time of solution contact for (PLA/TiO$_2$, PLA/ZnO and PLA/MMT) respectively.

5.4.1 Enzymatic degradation of PLA/TiO$_2$ nanocomposite films

Figure 5.4.1 shows weight loss after contact of PLA and PLA/TiO$_2$ nanocomposites films in proteinase K solutions at 37°C. The weight losses in the first 4h for PLA and for PLA/TiO$_2$ nanocomposites are similar then the samples start to differentiate their behavior: the weight loss is faster increasing the TiO$_2$ amount in the composites and it results independent on the modification of the titanium oxide. Therefore it can be concluded that a

dominant factor, determining the PLA enzymatic degradation, is the increasing of filler content.
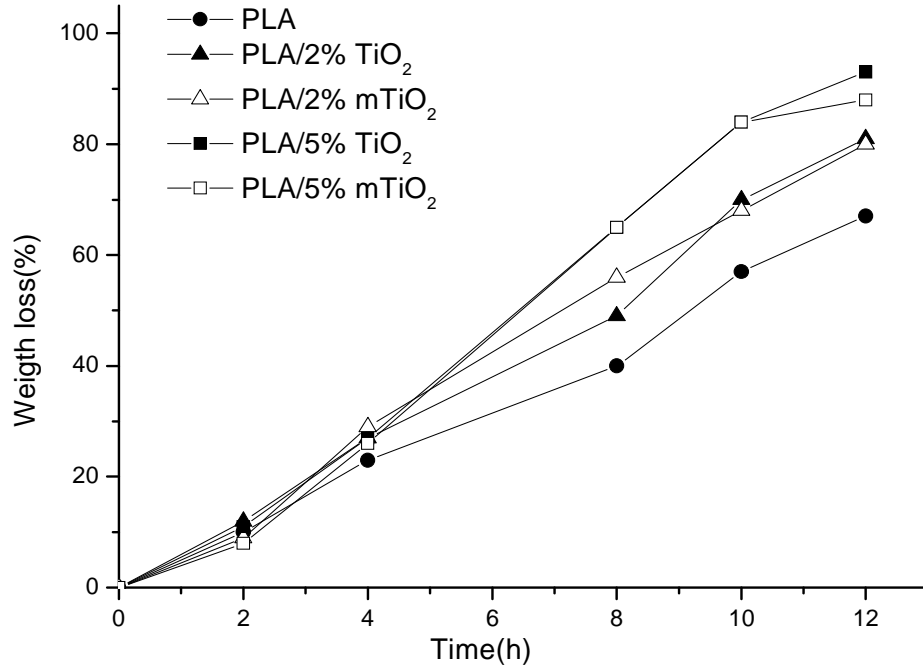
Figure 5.4.1 *Weight loss of PLA, PLA/2% TiO$_2$, PLA/2% mTiO$_2$, PLA5% TiO$_2$ and PLA/5% mTiO$_2$ nanocomposite films during the enzymatic degradation at 37°C*

5.4.2 Enzymatic degradation of PLA/ZnO composite films

Figure 5.4.2 shows weight loss after contact of PLA and PLA/ZnO composites films in proteinase K solutions at 37°C.

PLA is completely degraded after 12 days. The PLA/ZnO composites show the some behavior at different concentration of ZnO particles and their degradation is similar to that of PLA. After 12 days of preteinase K solution contact the weight loss of PLA/5% ZnO is almost the same of neat PLA, about 99.7%, for PLA/3% ZnO the loss is about 94% and for PLA/1% ZnO is about 85%.
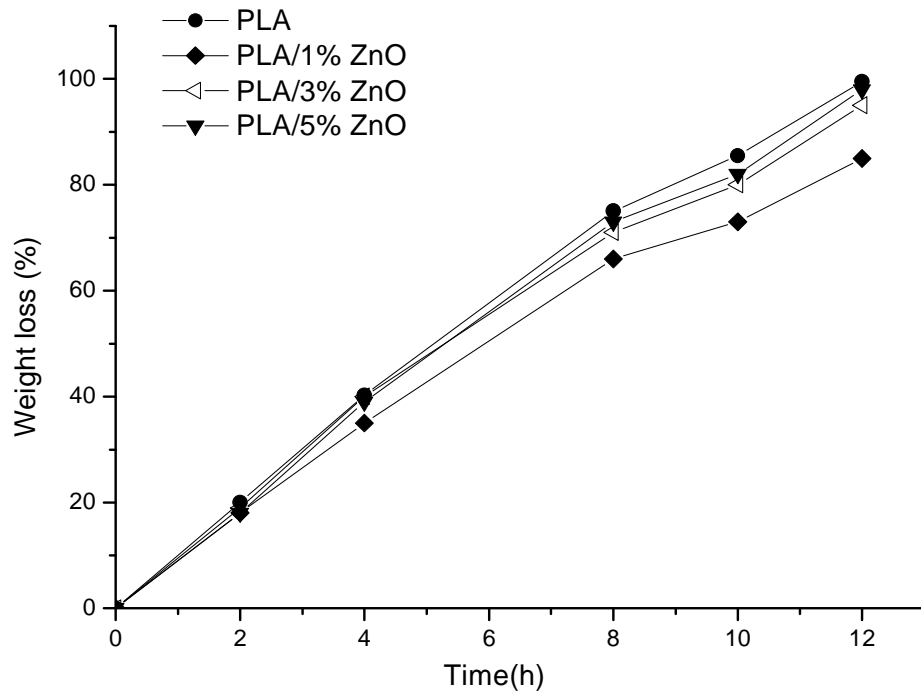
Figure 5.4.2 *Weight loss of PLA, PLA/1% ZnO , PLA/3% ZnO and PLA5% ZnO composite films during the enzymatic degradation at 37°C*

5.4.3 Enzymatic degradation of PLA/MMT(Dellite 67G) nanocomposite films

Figure 5.4.3 shows weight loss after contact of PLA and PLA/MMT nanocomposites films in proteinase K solutions at 37°C. Again, PLA is completely degraded after 12 days. PLA/1% D67G degrades faster than PLA/3% D67G and PLA/5% D67G, which have similar behaviour. After 12 days of preteinase K solution contact PLA/1% D67G has a weight loss about 89%, PLA/3% D67G about 66% and PLA/5% D67G about 69%. So increasing the amount of MMT nanoparticles the weight loss decreases.
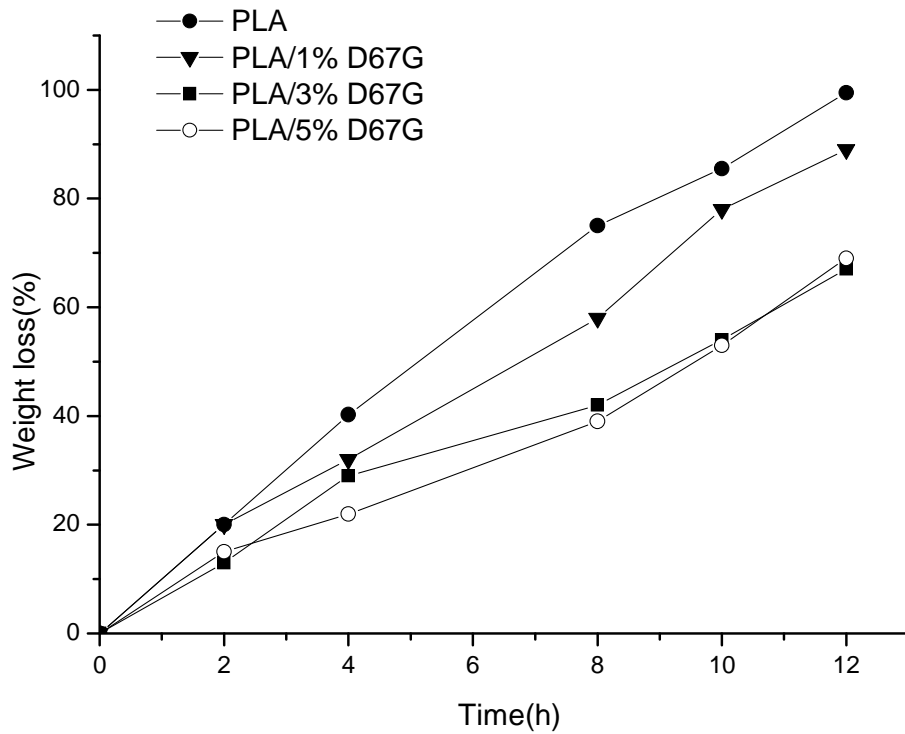
Figure 5.4.3 *Weight loss of PLA, PLA/1% D67G , PLA/3% D67G and PLA5% D67G nanocomposite films during the enzymatic degradation at 37°C*

In conclusion the enzymatic degradation is faster for PLA/TiO$_2$ nanocomposites respect neat PLA, while for PLA/ZnO and PLA/MMT is slower. In all the system the weight loss is function of the filler amount.

5.5   ISOTHERMAL   DEGRADATION   OF   PLA/TiO$_2$ NANOCOMPOSITE, PLA/ZnO COMPOSITE AND PLA/MMT(Dellite 67G) NANOCOMPOSITE FILMS

5.5.1 Isothermal degradation of PLA/TiO$_2$ nanocomposite films
Figures 5.5.1 A, B and C show the TGA measurements performed under isothermal conditions, up to 40 minutes, at 200, 220 and 240°C for PLA and PLA/TiO$_2$ nanocomposites.

After 40 min of treatment at 200°C there is no significant weight loss for PLA and the four composites. The small differences are inside the experimental error (Figure 5.1 A).
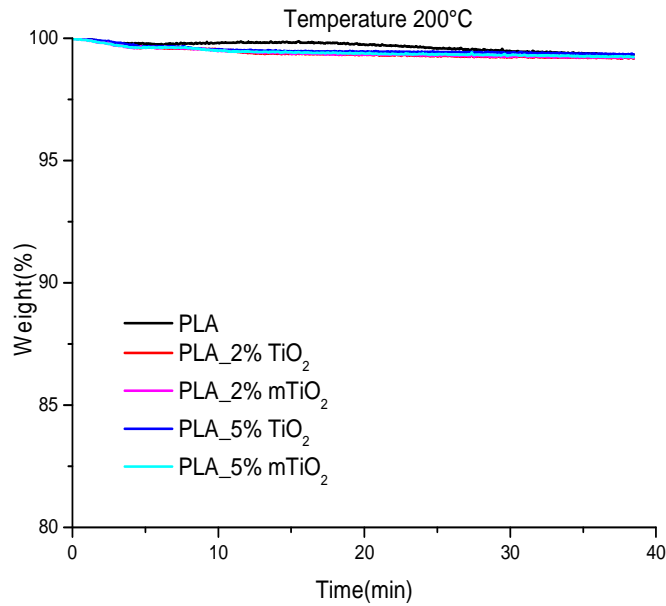
A
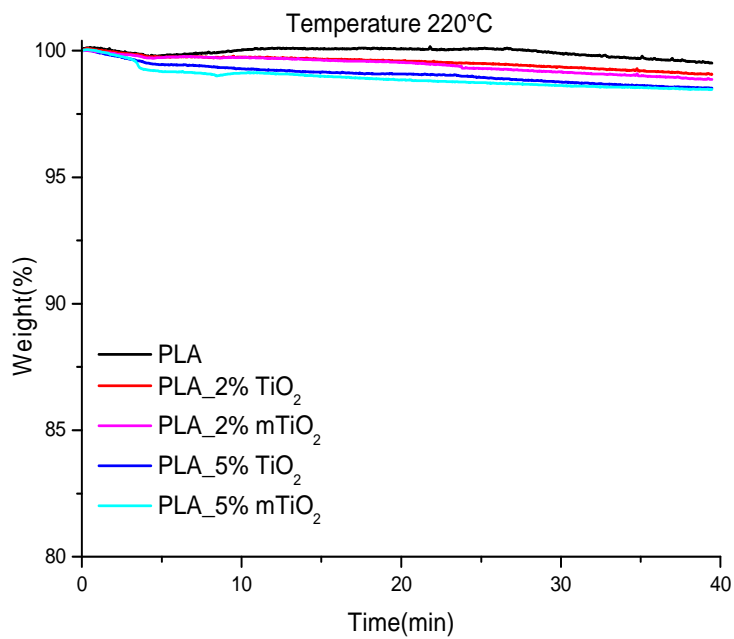
B
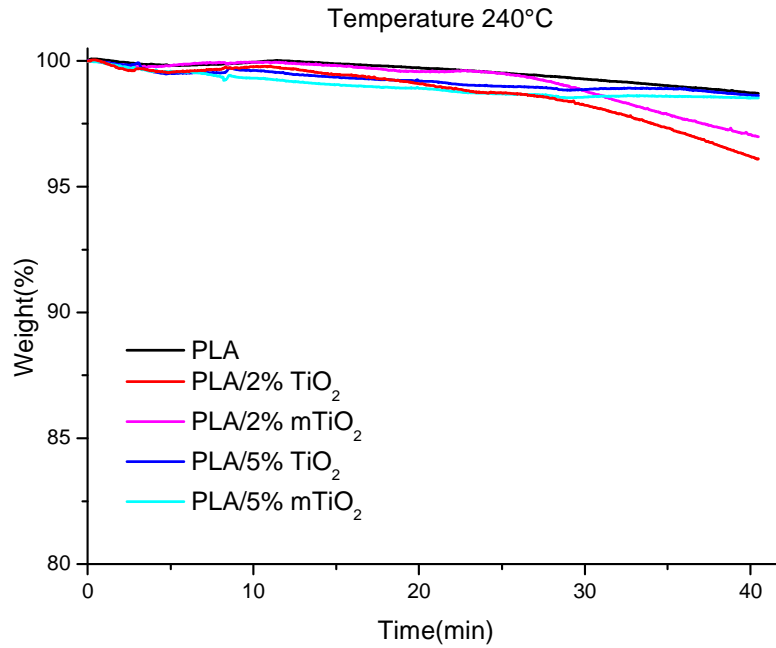
C

Figure 5.5.1 *TGA under isothermal conditions (under air) of PLA, PLA/2% TiO₂ ,*
PLA/2% mTiO₂, PLA5% TiO₂ and PLA/5% mTiO₂ nanocomposite films at (A) 200°C,
(B) 220°C, (C) 240°C

At the end of the 40 min of treatment at 220°C the weight loss for PLA is
0.5%, about 1% for the nanocomposites with 2%TiO_2 and 1.5% for the
nanocomposites with 5%TiO_2, independently of modification (Figure 5.5.1
B).

At 240°C (Figure 5.5.1 C), after the 40 min of treatment, the weight loss
for PLA and the two nanocomposites with 5%TiO_2 is about 1.5%, whereas
it is about 3.5% for the nanocomposites with 2%TiO_2, independently of
modification.

5.5.2 Isothermal degradation of PLA/ZnO composite films
Figures 5.5.2 A, B and C show the TGA measurements performed under
isothermal conditions at 200, 220 and 240°C, respectively, for PLA and

PLA/ZnO composites. ZnO particles induce the degradation of PLA and hence the weight loss.

For all the three temperatures, weight loss for the PLA and the four composites up to about 15 min is not found. At higher time, the degradation induces the weight loss which results to be function of ZnO content and temperature. In particular at 200°C the weight loss at 40 minutes is: 2% for neat PLA, 1% for PLA/1% ZnO, 7% for PLA/3% ZnO and 9% for PLA/5% ZnO; at 220°C and at 40 minutes the weight loss is: 2% for neat PLA, 10% for PLA/1% ZnO, for 36% PLA/3% ZnO and 50% for PLA/5% ZnO; at 240°C and at 40 minutes the weight loss is: 18% for neat PLA, 80% for PLA/1% ZnO, 93% for PLA/3% ZnO and 94% for PLA/5% ZnO.
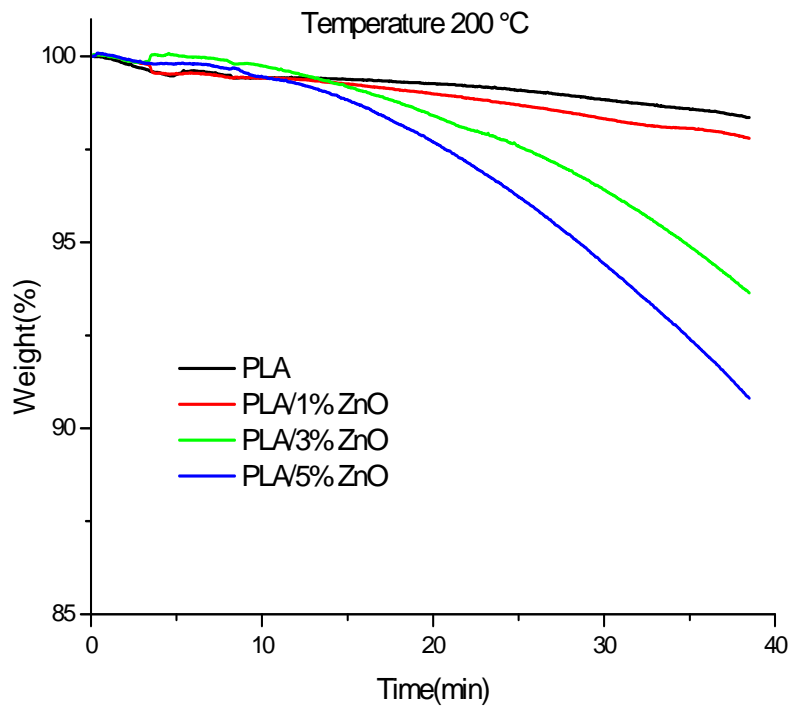
A
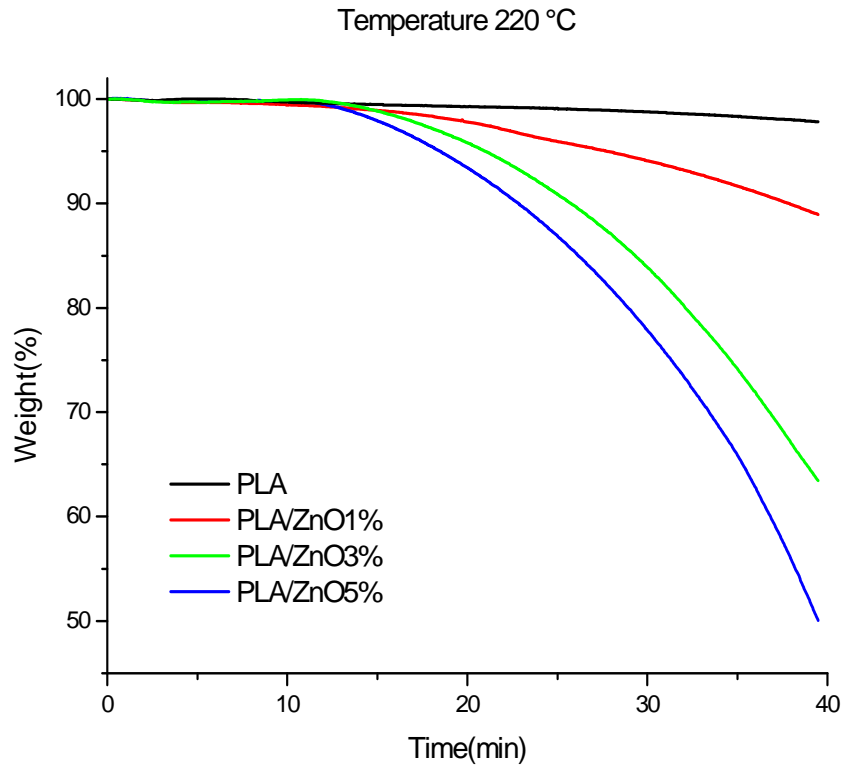
B
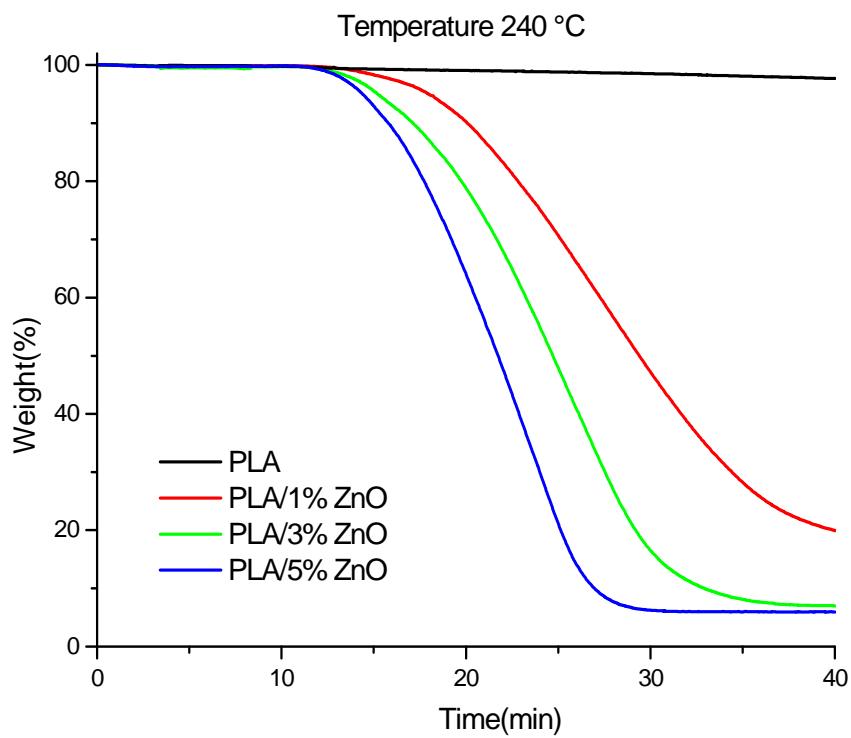
C

Figure 5.5.2 *TGA under isothermal conditions (under air) of PLA, PLA/1% ZnO, PLA/3% ZnO and PLA/5% ZnO composite films at (A) 200 °C, (B) 220°C, (C) 240°C*

5.5.3 Thermal degradation of PLA/MMT(Dellite 67G) nanocomposite films

Figures 5.5.3 A, B and C show the TGA measurements performed under isothermal conditions at 200, 220 and 240°C respectively for PLA and its composites with MMT (Dellite67G).
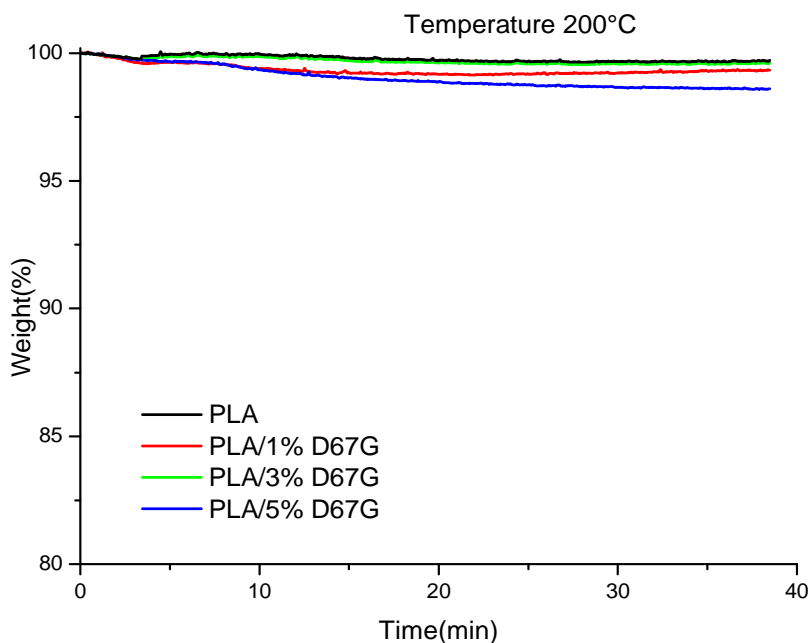
A
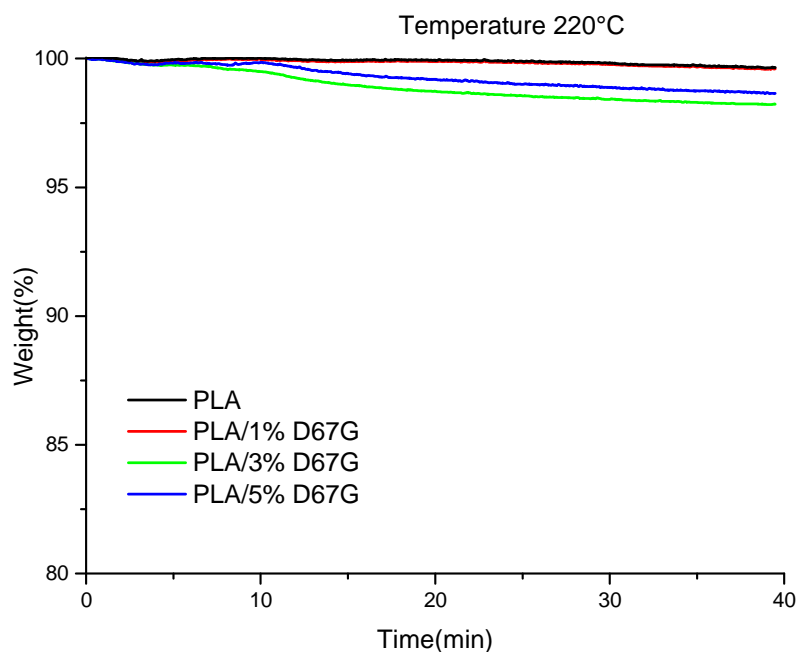
B
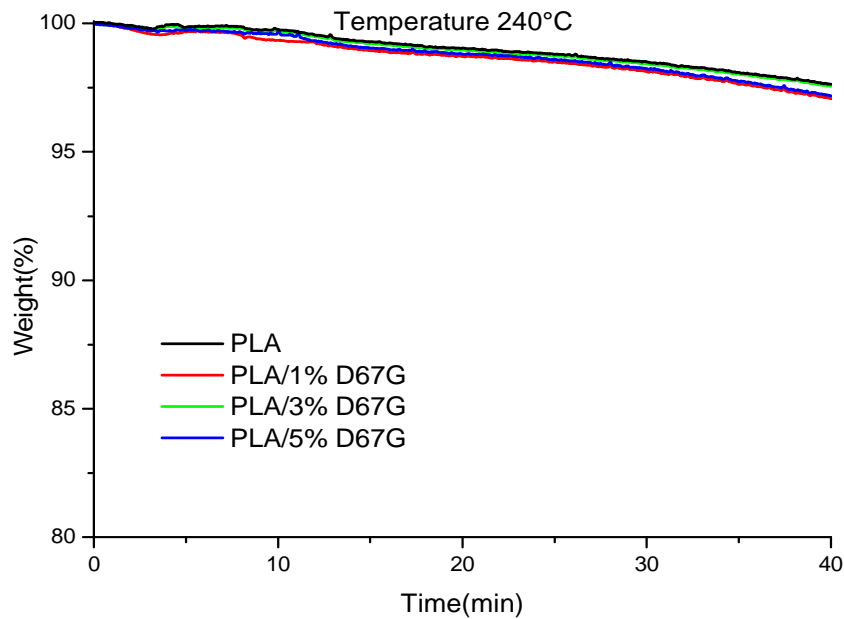
C

Figure 5.5.3 *TGA under isothermal conditions (under air) of PLA, PLA/1% D67G, PLA/3% D67G and PLA/5% D67G nanocomposite films at (A) 200°C, (B) 220°C, (C) 240°C*

For these systems and at each of the three temperatures, the PLA and the nanocomposites display the same degradation behavior. The differences in weight loss among the four samples are less than 1%, that is, the PLA thermal degradation is not affected by the presence of MMT nanoparticles. The degradation rate seems to be similar at 200 and 220°C, but faster at 240°C.

This study underlines that the presence of ZnO is able to speed up the isothermal degradation of PLA in a way that is function of the ZnO amount and of the temperature, whereas TiO_2 and D67G do not result to influence significantly the degradation of PLA , at least up to the limit of time (40min) investigated.

REFERENCES

[1] "Morphology, mechanical and optical properties of transparent BR/clay nanocomposites", S. Wang, Y. Zhang, W. Ren, Y. Zhang, H. Lin, Polym. Test., 24,(2005), pp. 766–774.

[2] "Effect of nanoclay on optical properties of PLA/clay composite films", H.M. Cele, V. Ojijo, H. Chen, S. Kumar, K. Land, T. Joubert, M.F.R. de Villiers, S.S. Ray, Polymer Testing, 36, (2014), pp. 24–31.

[3] "Polylactic Acid and Polylactic Acid-Based Nanocomposite Photooxidation" S. Bocchini , K. Fukushima , A. Di Blasio , A. Fina , A. Frache , F. Geobaldo, *Biomacromolecules*, 11 (11), (2010), pp 2919–2926.

[4] "Transparent nanocrystalline ZnO films prepared by spin coating", M. Berber, V. Bulto, R. Kliβ, H. Hahn, Scripta Materials 53(5), (2005), pp. 547-551.

[5] "Effect of particle morphology on the properties of polypropylene/nanometric zinc oxide (PP/nanoZnO)" O. Hui Lin, H. Md Akil, and S. Mahmud, , Received 16 April 2009; accepted 9 July 2009.

[6] "Zinc oxide : properties and application" H.E. Brown, 1976, International lead and Zinc organization inc. , New York.

[7] "Degradation studies of polyolefins incorporating transparent nanoparticulate zinc oxide UV stabilizers" A. Ammala, A.J. Hill, P. Meakin, S.J. Pas and T.W. Turney, , Journal of Nanoparticle Research 4 (2002), pp. 167–174.

[8] "Functional behaviour of polypropylene/ZnO–soluble starch nanocomposites" S. Chandramouleeswaran, S. T. Mhaske, A. A. Kathe, P. V. Varadarajan, V. Prasad, N.Vigneshwaran.

[9] "Photo-stabilization of EPDM–clay nanocomposites: effect of antioxidant on the preparation and durability" Sunil P. Lonkar, A. Pratheep

Kumar and Raj Pal Singh, Polymers for advanced technologies, Polym. Adv. Technol. 2007; 18: 891–900.

[10] "Mechanistic implications of plastics degradation" B. Singh, N. Sharma, Polymer Degradation and Stability 93,(2008), pp. 561-584.

[11] "Biopolymers: Reuse, Recycling, and Disposal" M. Niaounakis, Elsevier, 2,(2013), pp.84.

[12] "Preparation, characterization, and properties of TiO_2/PLA nanocomposites by in situ polymerization" W. Zhuang, Jing Liu, J. Hua Zhang[1],B.Xing Hu, J. Shen Polymer Composites 30(8), (2009), pp. 1074–1080.

[13] "Degradation of Polylactic Acid (PLA) Plastic in Costa Rican Soil and Iowa State University Compost Rows" Kai-Lai G. Ho, Anthony L. Pometto III, Arnoldo Gadea-Rivas, Jorge A. Briceño, Augusto Rojas, Journal of environmental polymer degradation, 7(4),(1999), pp. 173-177.

[14] "Effects of ultraviolet light (315 nm), temperature and relative humidity on the degradation of polylactic acid plastic films" A. Copinet, C. Bertrand , S. Govindin , V. Coma , Y. Couturier , Chemosphere., 55(5), (2004), pp.763-73.

[15] H.O. Zhou, T.J. Shi, H.L. Wang, L.F. Di, and J.Z. Wang, Polym. Mater. Sci. Eng., (2006), 22, pp. 220 .

[16] "Poly(lactic acid) degradation in soil or under controlled conditions" A. Torres,S.M. Li,S. Roussos, and M. Vert, J. Appl. Polym. Sci., (1996), 62, 2295.

[17] "Preparation and characterization of poly(L-lactic acid)/TiO2 nanoparticle nanocomposite films with high transparency and efficient photodegradability" N. Nakayama, T. Hayashi, Polymer Degradation and Stability 92 (2007) , pp. 1255-1264.

[18] "Biodegradable poly(L-lactic acid)/TiO$_2$ nanocomposites: Thermal properties and degradation" A. Buzarovska and A. Grozdanov Journal of Applied Polymer Science (2012), 123 (4), pp. 2187–2193.

[19] "Comparison of miscibility and structure of poly (3-hydroxybutyrate-co-3-hydroxyhexanoate)/poly (l-lactic acid) blends with those of poly (3-hydroxybutyrate)/poly (l-lactic acid) blends studied by wide angle X-ray diffraction, differential scanning calorimetry, and FTIR microspectroscopy" T. Furukawa, H. Sato, R. Murakami, J. Zhang, I. Noda, S. Ochiai, Y. Ozaki, Polymer (2007) 48 (6), 1749-1755.

[20] "Photochemical Behavior of Polylactide/ZnO Nanocomposite Films" S. Therias , J. Larché , P. Bussière , J. Gardette ,M. Murariu , and P. Dubois, Biomacromolecules, (2012) , 13(10) 3283-3291.

[21] "Polylactic acid and Polylactic acid-based nanocomposites S. Bocchini, K. Fukushima, A. Di Blasio, Biomacromolecules (2010), 11, pp. 2919– 2926.

[22] "Photooxidation of polylactide/calcium sulphide composites" M. Gardette, S. Therias, J. L. Gardette, M. Murariu, Ph. Dubois, Polym. Degrad. Stab.(2011), 96, pp. 616– 623

[23] "Spectra of carbonyl compounds of all kinds (factors affecting carbonyl group frequencies). In Course Notes on the Interpretation of Infrared and Raman Spectra"; D. W. Mayo, F. A. Miller, R. W. Hannah (Eds), John Wiley & Sons, Inc.: New York, (2003); pp 179-204.

[24] "Polylactide/montmorillonite nanocomposites: study of the hydrolytic degradation" M.-A. Paula , C. Delcourta , M. Alexandrea , Ph. Dege´e a , F. Monteverdeb , Ph. Dubois Polymer Degradation and Stability 87 (2005), pp. 535-542.

[25] "Hydrolytic degradation of devices based on poly(DL-lactic acid) size-dependence" I. Grizzi, H. Garreau, S. Li,M. Vert, Biomaterials (1995),16:305–11.

[26] "Aliphatic polyesters: abiotic and biotic degradation and degradation products" M. Hakkarainen, Adv Polym Sci (2001);157:113– 38.

[27] "Properties and morphology of poly(L-lactide)" and "Effects of structural parameters on long-term hydrolysis of poly(L-lactide) in phosphate-buffered solution" H. Tsuji,Y. Ikada, Polym Degrad Stab (2000);67:179–89.

[28] "Biodegradation of aliphatic polyesters" S. Li,M. Vert In: Scott G, Gilead D editors. Degradable polymers: principles and applications. London: Chapman & Hall; (1995), pp. 43–87.

[29] "Present and future of PLA polymer" M. Vert, G. Schwach,J. Coudane, Mater Sci e Pure Appl Chem (1995);A32(4):787–96.

[30] "Key factors for tuning hydrolytic degradation of polylactide/zinc oxide nanocomposites" S. Benali, S. Aouadi, A.L. Dechief, M. Murariu, P. Dubois Nanocomposites 1, Issue 1 (2015), pp. 51-61.

[31] "Enzymatic Degradation of Poly(L-lactide) Film by Proteinase K: Quartz Crystal Microbalance and Atomic Force Microscopy Study" K. Yamashita , Y.   Kikkawa ,K.   Kurokawa   and Y.   Doi, Biomacromolecules, 2005, 6 (2), pp. 850–857.

[32] "Enzymatic hydrolysis of polylactic acid" Williams, D. F. Eng. Med. 1981, 10, 5.

[33] "Polylactide stereochemistry: effect on enzymic degradability" M. S. Reeve , S.P.   McCarthy , M.   J.   Downey , R.   A.   Gross Macromolecules, 1994, 27 (3), pp 825–831.

 [34]   In Biopolymers, 4, Polyesters, Tsuji, H.; Doi, Y., Steinbüchel, A., Eds.; Wiley-VCH Verlag GmbH: Weinheim, Germany, 2002; p 129.

[35]   "Biodegradation of poly(l-lactide)" Y. Tokiwa, A. Jarerat, Biotechnol. Lett. (2004), 26, pp. 771.

[36] "Enzymatic degradability of poly (lactide): effects of chain stereochemistry and material crystallinity" R. T. MacDonald, S. P. McCarthy, R. A. Gross, Macromolecules (1996), 29, 7356.

[37] "Influence of Crystallinity and Stereochemistry on the Enzymatic Degradation of Poly(lactide)s" Li, S.; McCarthy, S. Macromolecules 1999, 32, 4454.

[38] "Enzymatic degradation of stereocopolymers derived from L-, DL- and meso-lactides" Li, S.. Tenon, M.; Garreau, H.; Braud, C.; Vert, M. Polym. Degrad. Stab. (2000), 67, 85.

[39] "Enzymatic hydrolysis of poly(lactide)s: effects of molecular weight, L-lactide content, and enantiomeric and diastereoisomeric polymer blending" H. Tsuji, S. Miyauchi, Biomacromolecules (2001), 2, 597.

[40] "Effects of physical aging, crystallinity, and orientation on the enzymatic degradation of poly(lactic acid)" H. Cai, V. Dave, R. A. Gross, S. P. J McCarthy,. Polym. Sci., Part B: Polym. Phys. (1996),34, 2701.

[41] "Enzymatic hydrolysis of poly (lactide) s: effects of molecular weight, L-lactide content, and enantiomeric and diastereoisomeric polymer blending" H. Tsuji, S. Miyauchi, Polym. Degrad. Stab. 2001, 71, 415.

[42] "Poly(L-lactide): 7. Enzymatic hydrolysis of free and restricted amorphous regions in poly(L-lactide) films with different crystallinities and a fixed crystalline thickness" H. Tsuji, S. Miyauchi,Polymer 2001, 42, 4463.

[43] "Biodegradable polymer blends of poly(lactic acid) and poly(ethylene glycol)" M. Sheth, R. A. Kumar, V. Davé, R. A. Gross, S. P. J. McCarthy, Appl. Polym. Sci. 1997,66, 1495.

[44] "Separation and Enzymatic degradation of blend films of poly(L-lactic acid) and cellulose." M. Nagata, F. Okano, W. Sakai, N. J. Tsutsumi, Polym. Sci., Part A: Polym. Chem. 1998,36, 1861.

[45] "Blends of aliphatic polyesters: V non-enzymatic and enzymatic hydrolysis of blends from hydrophobic poly(L-lactide) and hydrophilic poly(vinyl alcohol)" H. Tsuji, S. Miyauchi, Polym. Degrad. Stab. 2001, 71, 403.

[46] " Miscibility and biodegradability of blends of poly(lactic acid) and poly(vinyl acetate)" A. M. Gajria, V. Davé, R. A. Gross, S. P. McCarthy, Polymer 1996, 37, 437.

[47] "Enzymatic degradation of poly(epsilon-caprolactone)/poly(DL-lactide) blends in phosphate buBer solution" Z. Gan, D. Yu, Z. Zhong, Q. Liang, X. Jing, Polymer 1999, 40, 2859.

[48] "Selective enzymatic degradations of poly(L-lactide) and poly(epsilon-caprolactone) blend films" L. Liu, S. Li, H. Garreau, M. Vert, Biomacromolecules 2000, 1, 350.

[49] "Porous Biodegradable Polyesters, 3. Preparation of Porous Poly(ε-caprolactone) Films from Blends by Selective Enzymatic Removal of Poly(L-lactide)" H. Tsuji, T. Ishizaka, Macromol. Biosci. 2001, 1, 59.

CHAPTER 6

ANTIBACTERIAL PROPERTIES

6.1 ANALYSIS OF ANTIBACTERIAL PROPERTIES OF PLA/TiO$_2$ NANOCOMPOSITE FILMS

TiO$_2$ is the most commonly used semiconductor photocatalyst. The photocatalytic properties, activated by UV-A irradiation, have been utilized in various environmental applications to remove contaminants from both water and air [1-4]. A wealth of information on TiO$_2$ photocatalytic inactivation of bacteria has been acquired over the last 20 years [5,6]. TiO$_2$ can kill both Gram-negative and Gram-positive bacteria, although Gram-positive bacteria are less sensitive due to their ability to form spores [6]. More recently, nano-sized TiO$_2$ was also reported to kill viruses including poliovirus 1 [7], hepatitis B virus [8], Herpes simplex virus [9], and MS2 bacteriophage [10]. The concentration of TiO$_2$ usually required to kill bacteria varies between 100 and 1000 ppm, depending on the size of the particles and the intensity and wavelength of the light used [6].

Inactivation of bacteria with TiO$_2$ nanoparticles offers a number of advantages: i) TiO$_2$ is non hazardous and inexpensive; ii) the UV content of solar light (about 5%) is sufficient to activate the TiO$_2$ for the production of reactive oxygen species (ROS) and OH radicals, which are the primary factors in the inactivation of bacteria [11-13].

The antibacterial activity of the sole TiO$_2$ powder has been tested in order to confirm its bactericidal effect against E. Coli when exposed to UV light. Two solution composed by 10 ml of bacterial solution + 10 mg of TiO$_2$ (powder) were prepared. One of them is exposed to the UV light. A lamp of 6W is placed at 11 cm from the solution for 30 minutes. Moreover, in order to verify if UV light is able to act as bactericidal against E. Coli, the sole bacterial solution is exposed to the lamp light (also, the bacterial

solution not exposed to UV light is considered as reference). The bacterial solution was prepared according to the method described in Chapter 1. All the solutions, after spreading on petri disks were incubated at 35°C and the colony numbers counted.

The results of this experiment are shown in Table 6.1. From the table it is clear that TiO_2 powder displays great antibacterial activity against E. Coli if activated by UV lamp (reduction of 100% after 30 minutes, where as only 27% if not activated). Moreover the E.Coli growth is not affected by UV radiation (reduction of 0% of bacterial solution after 30 minutes independently from its exposure to UV light).

Table 6.1 Reduction (%R) of E. Coli in contact with TiO_2 powder for 30 minutes and in presence of UV

Sample	%R (t=0')	%R (t=30')
(10ml bacterial solution+ 10 mg TiO_2) exposed to UV light	0	99.99 ± 0.01
(10ml bacterial solution+ 10 mg TiO_2) not exposed to UV light	0	27.05 ± 0.01
10ml bacterial solution exposed to UV light	0	0
10ml bacterial solution not exposed to UV light	0	0

Verified the TiO_2 powder antibacterial activity against E. Coli when activated by UV light, antibacterial tests on PLA and PLA/TiO_2 nanocomposite films have been performed by following the procedure written in Chapter 1. In the phase of contact of the films with the bacterial solution the samples are exposed to the UV light. Again, the UV exposure

was realized with a lamp of 6W placed at 11 cm from the solution for 30 minutes. In Figure 6.1.1 is shown the histogram of the bacterial concentration of E. coli (CFU / ml) as a function of compositions and of the contact time between the bacterial solution and the film (30 minutes). Table 6.2 shows the percentage (%) reduction of E. Coli at different contact time calculated from the equation given in Chapter 1.

Table 6.2 Reduction (%R) of E. Coli in contact with PLA and PLA/TiO$_2$ nanocomposites for 30 minutes and in presence of UV

Sample	%R (t=0')	%R (t=30')
PLA	0	0
PLA/2% TiO$_2$	0	20.22 ± 0.01
PLA/2% mTiO$_2$	0	19.03 ± 0.01
PLA/5% TiO$_2$	0	25.10 ± 0.01
PLA/5% mTiO$_2$	0	24.00 ± 0.01
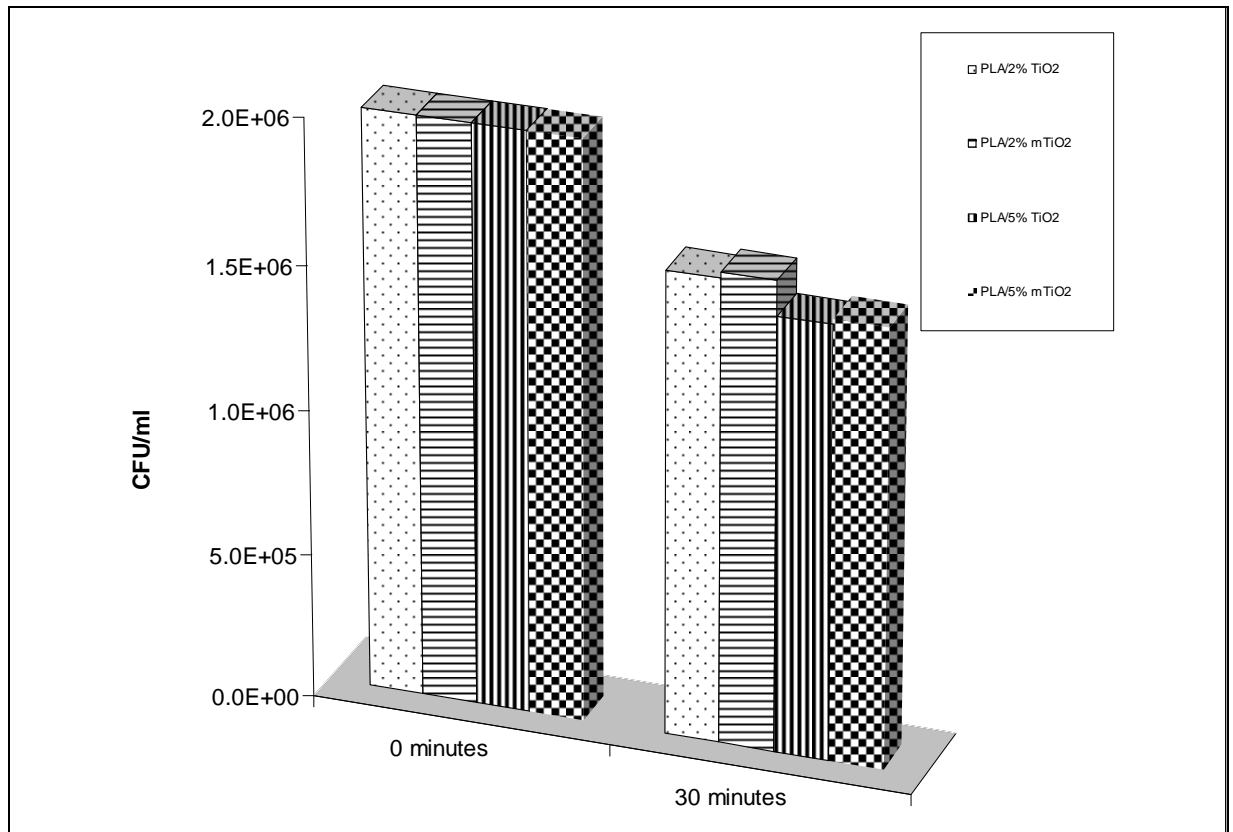
Figure 6.1.1 Effect of time and filler content on the antibacterial activity against E.Coli for PLA/TiO$_2$ nanocomposite films

From table 6.2, it is clear that the percentage reduction of E. Coli colonies after 30 min of exposure to UV light is about 23% for all the PLA/TiO$_2$ nanocomposites, insufficient value to define the films as antimicrobial.

The low antimicrobial activity for PLA/TiO$_2$ films after 30 min can be attributed to the fact that the majority of the nanoparticles are completely embedded in the polymer matrix (as shown in the SEM micrographs in the Chapter 2) and therefore there are very few particles on the film surface that can be activated by UV radiation.

6.2 ANALYSIS OF ANTIBACTERIAL PROPERTIES OF PLA/ZnO COMPOSITE FILMS

ZnO particles are known for their antibacterial activity and recent studies confirm their efficacy as antimicrobial agents, even in thermoplastic

156

polymers [14-17]. From these studies emerged important results: the ZnO particles exhibit antimicrobial activity against bacteria that are resistant to high temperatures and pressures; the antibacterial activity is dependent on the surface area and the concentration, while the crystalline structure and shape of the particles have little influence; the treatment at higher temperature of the ZnO particles has a significant effect on the antibacterial activity. Despite this, the mechanism of antimicrobial activity is fully clarified: according to Sawai et al [14], the formation of hydrogen peroxide is able to destroy the cell membrane; according to Stoimenov et al [18] ZnO particles link through chemical bonds to the bacterial membrane and cause the formation of electrostatic forces that damage the cell membrane itself.

Anyway, the most creditable hypothesis is the formation of reactive oxygen species even if it is not yet entirely clear how these species are produced [19].

In Figure 6.2.1 it is shown the histogram of the bacterial concentration of E. Coli (CFU/ml) as a function of the contact time between the bacterial solution and the film (1 , 24, 48 hours and 5 days) and compositions. Table 6.3 shows the percentage (%) reduction of E. Coli at different contact time. The concentration of the initial bacterial solution is $2x10^6$ CFU/ml. After 1 hour of contact no change in concentration is observed for any of the samples. After 24h of contact, significant decrease of bacterial concentration is found only for the PLA/5% ZnO sample (%R= 99.99); after 2 days, the bacterial concentration for the two composites with 1 and 3% of ZnO is further decreased, but the values of %R are still far 99.99; the tests done after 5 days of contact indicate that %R is finally equal 99.99.

A visual method for observing a biocide effect of ZnO particles is shown in Figures 6.2.2 and 6.2.3. In Figure 6.2.2 the bacterial growth of E. Coli, after 24 hours of contact between the solution and PLA, is well evident on

the Petri dish. At same contact time, no bacterial growth is instead observed for PLA/5% ZnO composite (Figure 6.2.3).

Table 6.3 Reduction (%R) of E. Coli in contact with PLA and PLA/ZnO composite films for 1, 24, 48 hours and 5 days

Sample	%R (t=1 h)	%R (t=24 h)	%R (t=48 h)	%R (t=5 days)
PLA	0	0	0	0
PLA/1% ZnO	0	42.41 ± 0.01	76.22 ± 0.01	99.99 ± 0.01
PLA/3% ZnO	0	57.04 ± 0.01	82.80 ± 0.01	99.99 ± 0.01
PLA/5% ZnO	0	99.99 ± 0.01	99.99 ± 0.01	99.99 ± 0.01
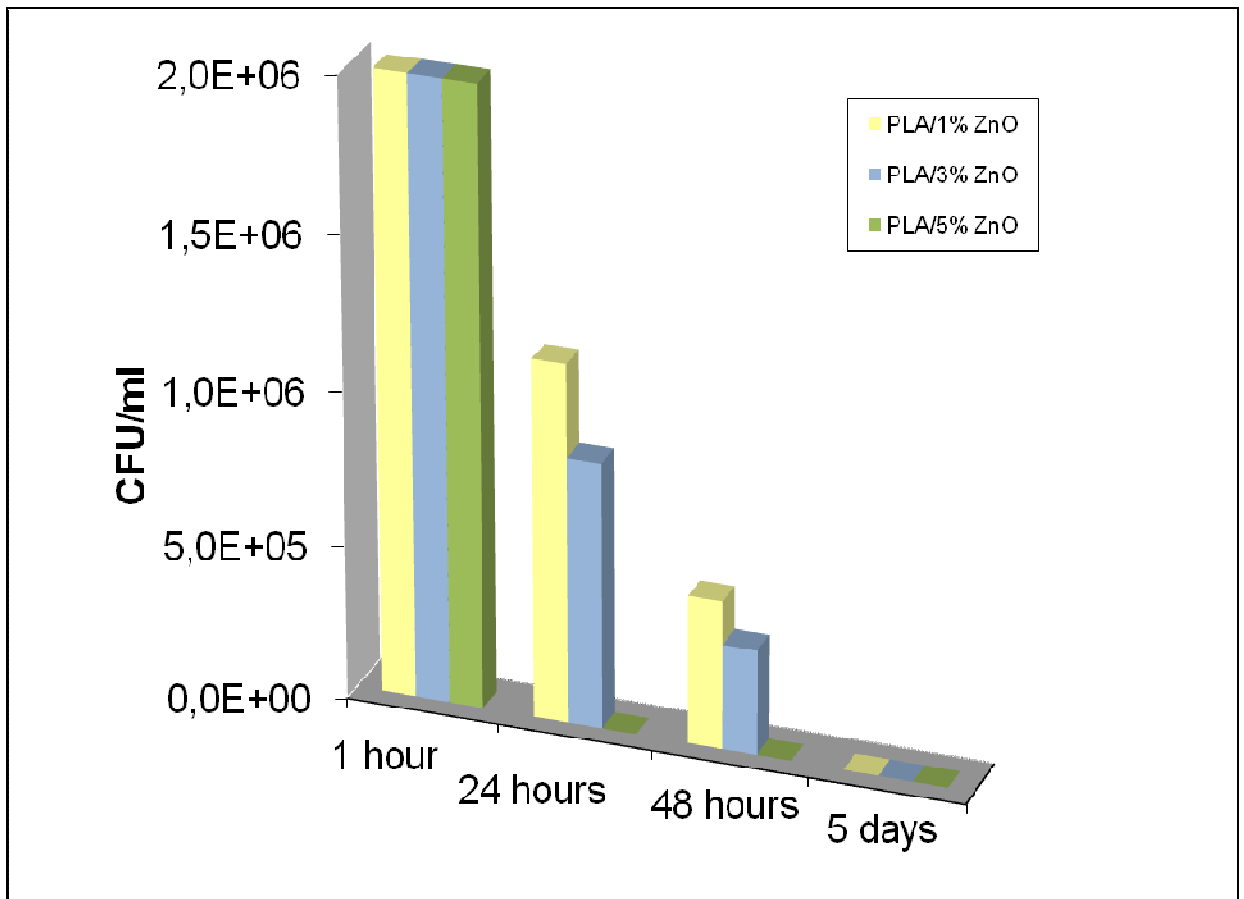
Figure 6.2.1 Effect of time and filler content on the antibacterial activity against E. Coli for PLA/ZnO composite films

These results clearly indicate that the antibacterial activity against E. Coli of PLA/ZnO composites increases by increasing contact time and ZnO content.

Figure 6.2.2 *Bacterial growth of E. Coli after 24 h of contact between PLA (control) and the solution*
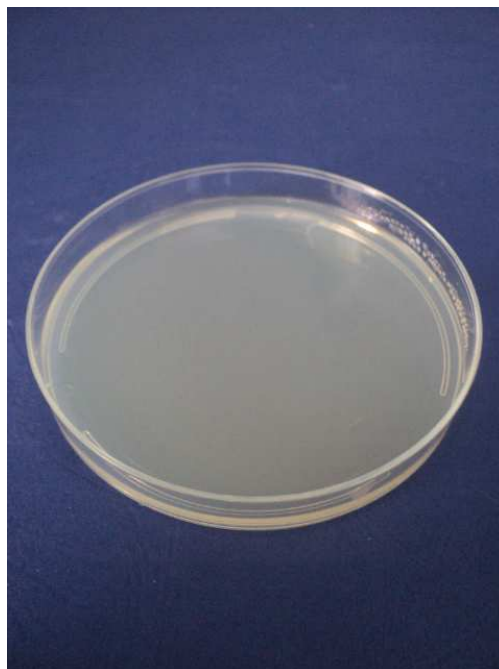
Figura 6.2.3 *Bactericidal effect of the system PLA/5% ZnO after 24 h of contact with the solution*

6.3 ANALYSIS OF ANTIBACTERIAL PROPERTIES OF PLA/MMT(Dellite 67G) NANOCOMPOSITE FILMS

Rhim et al. [20] reported that some nanocomposite films prepared with certain organically modified nanoclay had a strong antimicrobial function against both Gram-positive and Gram-negative bacteria. They postulated that the antimicrobial function of nanocomposite films could be attributed to the quaternary ammonium groups of organically modified clays. Table 6.4 shows the percentage reduction of E. Coli concentration after different contact time of bacterial solution with PLA and PLA/MMT films. In Figure 6.3.1 it is shown the histogram of the bacterial concentration of E. coli (CFU/ml) as a function of the contact time between the bacterial solution and the film (1, 24, 48 hours and 5 days) and compositions.

The results show a decrease of the bacterial concentration by increasing the amount of MMT. PLA/3% D67G film presents the highest E.coli reduction (80%) after 5 days. This antibacterial reduction is probably caused by the quaternary salt ammonium presents on the MMT nanoparticles surface, as found in literature. The higher % reduction found for PLA/3% D67G respect PLA/5% D67G nanocomposites is probably due to its intercalated structure, as shown by the TEM micrographs (see Chapter 2). The intercalation exposes higher MMT specific surface to the bacterial solution contact, increasing the bactericidal effect.

Anyway, the % reduction found in this experiment is not sufficient to state that PLA/MMT nanocomposites have antibacterial activity.

Table 6.4 Reduction (%R) of E. Coli in contact with PLA and PLA/ MMT nanocomposite films for 1, 24, 48 hours and 5 days

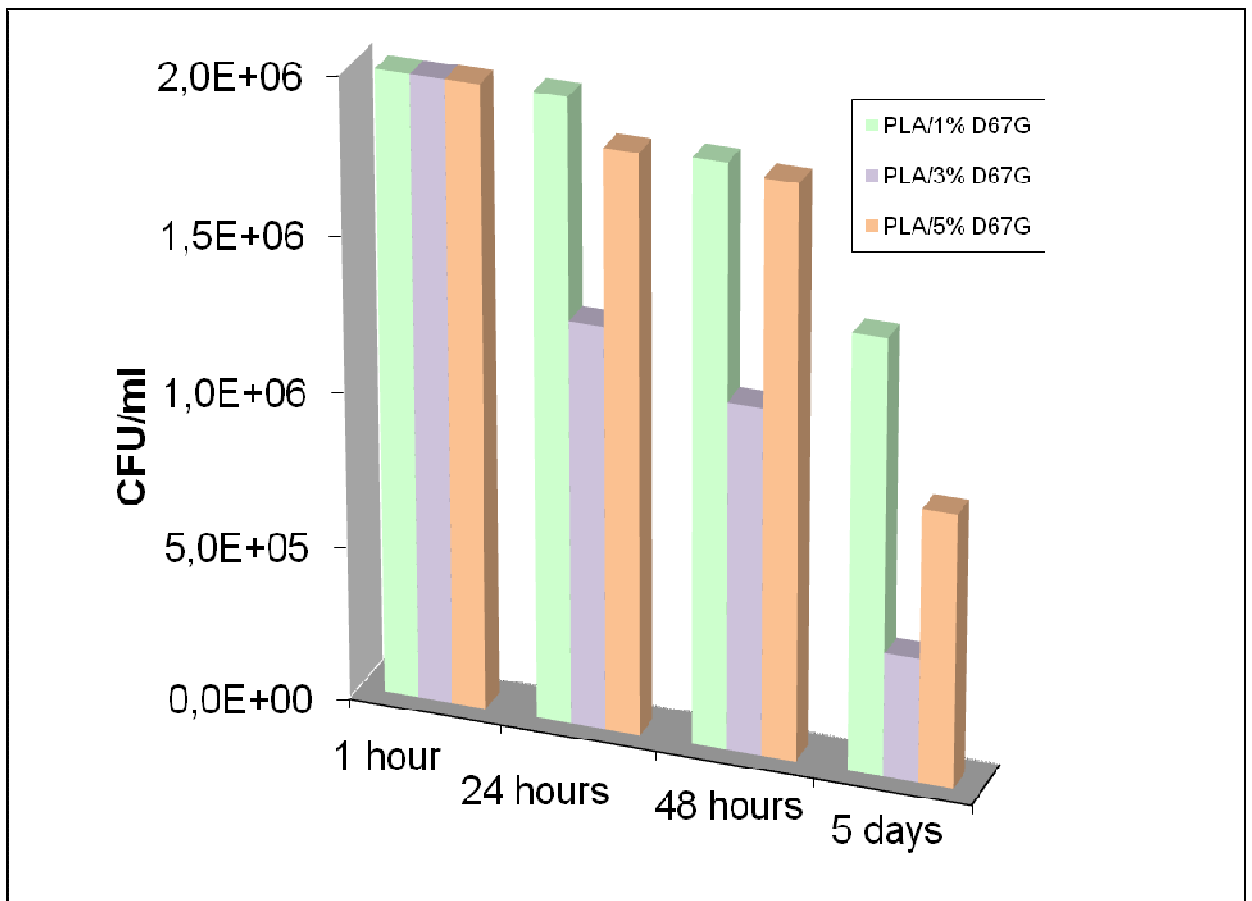| Sample	%R (t=1 h)	%R (t=24 h)	%R (t=48 h)	%R (t=5 days)
PLA	0	4.02 ± 0.01	7.02 ± 0.01	21.20 ± 0.01
PLA/1% D67G	0	0	6.50 ± 0.01	30.03 ± 0.01
PLA/3% D67G	0	35.00 ± 0.01	44.08 ± 0.01	80.02 ± 0.01
PLA/5% D67G	0	7.05 ± 0.01	8.02 ± 0.01	55.75 ± 0.01

Figure 6.3.1 Effect of time and filler content on the antibacterial activity against E.Coli for PLA/MMT nanocomposite films

REFERENCES

[1] "Antimicrobial nanomaterials for water disinfection and microbial control: Potential applications and implications" Qilin Li, Shaily Mahendra, Delina Y. Lyon, Lena Brunet, Michael V. Liga, Dong Li, Pedro J.J. Alvarez Water Research Volume 42, Issue 18, November 2008, Pages 4591–4602.

[2] "A practical demonstration of water disinfection using TiO_2 films and sunlight" S. Gelover, L.A. Gómez, K. Reyes, M.T. Leal Water Res., 40 (2006), pp. 3274–3280.

[3] "TiO_2/UV: single stage drinking water treatment for NOM removal?" C.A. Murray, E.H. Goslan, S.A. Parsons J. Environ. Eng. Sci., 6 (3) (2007), pp. 311–317.

[4] "Photocatalytic surface reactions on indoor wall paint" T. Salthammer, F. Fuhrmann Environ. Sci. Technol., 41 (18) (2007), pp. 6573–6578.

[5] "Photoelectrochemical sterilization of microbial cells by semiconductor powder" T. Matsunaga, R. Tomoda, T. Nakajima, H. Wake FEMS Microbiol. Lett., 29 (1–2) (1985), pp. 211–214.

[6] "Bactericidal activity of TiO_2 photocatalyst in aqueous media: toward a solar-assisted water disinfection system" C. Wei, W.Y. Lin, Z. Zainal, N.E. Williams, K. Zhu, A.P. Kruzic, R.L. Smith, K. Rajeshwar Environ. Sci. Technol., 28 (5) (1994), pp. 934–938.

[7] "Photocatalytic inactivation of coliform bacteria and viruses in secondary wastewater effluent" R.J. Watts, S. Kong, M.P. Orr, G.C. Miller, B.E. Henr Water Res., 29 (1995), pp. 95–100.

[8] "Photocatalysis effect of nanometer TiO_2 and TiO_2-coated ceramic plate on Hepatitis B virus" L. Zan, W. Fa, T.P. Peng, Z.K. Gong, J. Photochem. Photobiol. B. Biol., 86 (2) (2007), pp. 165–169.

[9] "Photocatalytic effect of TiO$_2$ films on viruses and bacteria" P. Hajkova, P. Spatenka, J. Horsky, I. Horska, A. Kolouch, Plasma Process. Polym., 4 (2007), pp. S397–S401.

[10] "Different inactivation behavior of MS-2 phage and Escherichia coli in TiO$_2$ photocatalytic disinfection" M. Cho, H. Chung, W. Choi, J. Yoon, Appl. Environ. Microbiol., 71 (1) (2005), pp. 270–275.

[11] "Growth and Some Enzymatic responses of E. Coli to Photocatalytic TiO$_2$" by A. Erdem, D. Cha and C.P. Huang; Nanoscience and Nanotechnology: Environmental and Health Impacts, (2008), 13, pp. 319-340.

[12] "Developing and testing method for antibacterial efficacy on TiO2 photocatalytic products" J. Y. Kim, C. H. Park, J.Y. Yoon, Environmental Engineering Research (EER),(2008), 13/3, pp. 136-140.

[13] "Study of antibacterial activity of nonhydrolitic synthesized TiO$_2$ against E. Coli, P. Aeruginosa and S. Aureus" H. Hitkova, A. Stoyanova , N. Ivanova, M. Sredkova , V. Popova , R. Iordanova , A. Bachvarova-Nedelcheva, Journal of Optoelectronics and Biomedical Materials Vol. 4 Issue 1, January - March 2012, p. 9 – 17.

[14] "Quantitative evaluation of antifungal activity of metallic oxide powders (MgO, CaO and ZnO) by an indirect conductimetric assay" J. Sawai, Yoshikawa, T. J. Appl. Microbiol., 2004, 96, 803.

[15] "Adsorption and growth inhibition of bacteria on carbon materials containing zinc oxide" O. Yamamoto, K. Nakakoshi,T. Sasamoto, H. Nakagawa, Miura, K. Carbon, 2001, 39, 1643.

[16] " Toxicological Impact Studies Based on Escherichia coli Bacteria in Ultrafine ZnO Nanoparticles Colloidal Medium" R. Brayner, R. Ferrari-lliou, N. Brivois, S. Djediat, M. F. Benedetti, F. Fiévet Nano Lett., 2006, 6, 866.

[17]"Effect of lattice constant of zinc oxide on antibacterial characteristics" O. Yamamoto, M. Komatsu, J. Sawai, Z. Nakagawa J. Mater. Sci.-Mater. M., 2004, 15, 847.

[18] "Metal Oxide Nanoparticles as Bactericidal Agents" Peter K. Stoimenov , Rosalyn L. Klinger , George L. Marchin , and Kenneth J. Klabunde *Langmuir*, 2002, 18 (17), pp 6679–6686.

[19] "Antibacterial activity of ZnO nanorods prepared by a hydrothermal method" K.H. Tam, A.B. Djurišic, C.M.N. Chan, Y.Y. Xi, C.W. Tse, Y.H. Leung, W.K. Chan, F.C.C. Leung, D.W.T. Au Thin Solid Films, 2008, 516, 6167.

[20] "Preparation and characterization of chitosan-based nanocomposite films with antimicrobial activity" J.W. Rhim, S.I. Hong, H.M. Park, P.K. Ng, J Agric Food Chem. 2006 Aug 9;54(16):5814-22.

CONCLUSIONS

The aim of this work was to develop new films based on PLA for applications in the food packaging with improved properties such as barrier, mechanical, UV properties, antibacterial activity by adding TiO_2 nanoparticles (modified by plasma treatment, and not modified), particles of ZnO (obtained by spray pyrolysis process) and nanoparticles of MMT (modified by dimethyl dihydrogenated tallow ammonium) to the polymer matrix. Structural and morphological characterizations were performed, followed by a study on the PLA composites degradation.

PLA was mixed with the TiO_2 powder with a mixer, two formulations were prepared by using both modified and unmodified TiO_2 nanoparticles: 2wt% and 5wt%. PLA/TiO_2 films were produced by compression moulding.

The PLA/ZnO composites and PLA/MMT(Dellite 67G) nanocomposites were prepared by mixing the components from the melt using a twin-screw extruder. In order to improve the dispersion of the filler within the PLA matrix, two masterbatches were prepared, in particular PLA/ZnO 80/20 wt% and PLA/Dellite67G 80/20 wt%; then to each of them PLA was added in such quantity to obtain the final compositions with 1, 3 and 5% by weight of ZnO and MMT (Dellite67G).

The pure components and samples were characterized by WAXD, TEM, ATR, SEM, DSC, TGA, UV-visible spectroscopy, mechanical, barrier and antibacterial properties. Moreover, it was also carried out a study on degradation by using different degradation source UV light, hydrolytic, enzymatic and isothermal medium.

- PLA/TiO_2 and PLA/ZnO films are amorphous, this means that PLA crystallization process is not influenced by TiO_2 (modified and unmodified)

and ZnO particles. PLA /3% D67G and PLA /5% D67G have a very low crystallinity of about 4% and 8%, respectively.

- Morphological analysis highlighted important results. For all the PLA/TiO$_2$ compositions, it can be observed that the nanoparticles dispersion and distribution is homogeneous, moreover, the TiO$_2$ nanoparticles (both modified or not) are perfectly embedded in the matrix. In all the PLA/ZnO samples the ZnO particles are fairly distributed in the polymer matrix with an average size of about 1.2 μm. This result can be regarded as good considering the nature inherently incompatible between the organic and the inorganic phase and the natural tendency of particles of sub-micrometer and nanometer size to agglomerate because of their high surface energy. In the PLA/MMT system, it is possible to highlight two aspects: the first is that the process of extrusion and subsequent calendering was able to create a good dispersion of the filler in the PLA matrix, the second is that nanocomposites present intercalation: it is most effective in the composite PLA/3% D67G in which the distance between the clay layers is higher than that of other composites. It is known from the literature that in order to maximize the properties of a polymer / clay nanocomposite it is necessary to obtain an exfoliated morphology. For these reasons, studies are in progress to select the best composition (addition of an additional compatibilizer) and the best process conditions for realizing an exfoliated nanocomposite.

- The different fillers do not influence the cold crystallization process and the melting behaviour of PLA and do not alter the glass transition temperature of the polymer amorphous phase.

- The thermal stability of the composite varies with the nanoparticle nature: it increases significantly with TiO$_2$ nanoparticles, in particular if modified; it decreases adding ZnO particles; it is not found significant variations with

the addition of D67G, except for the PLA/3% D67G nanocomposite for which a slight increase of stability is present.

- The tensile tests show that the addition of TiO_2, ZnO and MMT particles causes an increase of deformation at break (ε_b) parameters, except for PLA/5% ZnO and PLA/5% MMT. The elongation at yield point (ε_y) is not strongly influenced by addition of the particles.

   The parameters at strength (σ_y and σ_b) are slightly affected by the presence of clay and TiO_2 for all compositions; contrarily they increase by increasing ZnO particles, especially in transverse direction.

   The Young's modulus increases with the addition of clay and ZnO for all compositions, but decreases with TiO_2 addition.

   For PLA/TiO_2 systems, it has been found an increase of the toughness respect to PLA, in particular the toughness doubles for the samples with 5% of TiO_2 (modified and unmodified) and it triples for the samples with 2% of TiO_2 (modified and unmodified).

- The composites show a decrease of oxygen permeability compared to PLA. The amount of O_2 permeability reduction depends on the different particle used.

   PLA/TiO_2 systems have not an improvement of the CO_2 barrier properties whereas the PLA/ZnO and PLA/D67G systems show a decrease in CO_2 permeability.

   The results for water vapour barrier properties do not show significant variation for the composites and nanocomposites, and they are in agreement with literature data.

- PLA/TiO_2 nanocomposites do not present antibacterial activity against E.coli after 30 minutes of exposure to UV light. This can be attributed to the fact that the majority of the nanoparticles are completely embedded in the polymer matrix and therefore there are very few particles on the film surface that can be activated by UV radiation.

PLA/ZnO composites present bactericidal activity against E.Coli, in particular, at time t = 24 hours the concentration of E.coli is decreased, respectively, by 99.9, 57.04 and 42.41% for the samples PLA/5% ZnO, PLA/3% ZnO and PLA/1% ZnO.

PLA/MMT nanocomposites show a decrease of the bacterial concentration by increasing the amount of MMT. PLA/3% D67G film presents the highest E.coli reduction (80%) after 5 days. This antibacterial reduction is probably caused by the quaternary salt ammonium presents on the MMT nanoparticles surface, as found in literature. The higher % reduction found for PLA/3% D67G respect PLA/5% D67G nanocomposites is probably due to its intercalated structure.

- PLA/TiO$_2$ films absorb UV radiation up to 500 nm by increasing the TiO$_2$ content. The films containing ZnO show an absorption in the region around 385 nm, confirming the screening effect of ZnO to UV radiation reported in the literature, contrarily the PLA/MMT nanocomposites do not absord UV- radiation.

- The UV degradation study shows that PLA degrades faster than composites. PLA film obtained by compression molding degraded completely in about 17 days, while the PLA obtained by calender in 21 days. The weight loss as a function of time is lower by increasing the amount of particles in the polymer matrix. Moreover, by comparing the three systems, the degradation rate is the following: PLA/MMT > PLA/ZnO > PLA/TiO$_2$.

The PLA/ZnO composite and PLA/MMT nanocomposite films during photo-oxidation degraded by following the same mechanism of PLA, whereas, PLA/TiO$_2$ nanocomposite films seem to degrade with a different mechanism from PLA. PLA/TiO$_2$ system does not present all the typical degradation peaks of PLA, this can be attributed to the inhibiting action of TiO$_2$ nanoparticles on PLA UV degradation.

- The hydrolytic degradation of PLA produced by calender is faster than that of PLA obtained by compression moulding. Moreover PLA/TiO$_2$, PLA/ZnO and PLA/MMT films exhibit degradation faster than PLA. For PLA/TiO$_2$ nanocomposites, the degradation is faster by increasing the nanoparticles amount. Modified nanoparticles speed up the degradation respect to the unmodified one.

  For PLA/ZnO composite films, the degradation is faster decreasing the ZnO particles amount. Finally for PLA/MMT nanocomposite films, PLA/3% D67G degrades faster than other compositions. By comparing the three systems, the degradation rate is the following: PLA/ZnO> PLA/MMT > PLA/TiO$_2$.

- The enzymatic degradation for PLA/TiO$_2$ nanocomposites is faster than PLA, while for PLA/ZnO and PLA/MMT is slower. In all the systems the weight loss is function of the filler amount. No difference in the degradation rate of different composites can be revealed.

- The presence of ZnO is able to speed up the isothermal degradation of PLA in a way that is function of ZnO amount and temperature. TiO$_2$ and MMT do not influence significantly the degradation of PLA (at least up to the limit of time, 40min, investigated in this work).

  In conclusion, this work was designed to evaluate the possibility to employ PLA based composites/nanocomposites for food packaging application and to evaluate their degradation times. The results are surely satisfactory for all the systems; in particular, PLA/ZnO composite films show good mechanical and barrier properties and excellent antibacterial properties against E.Coli. For its characteristics, among these three studied systems, PLA/ZnO is the best system to employ in the food packaging field.